Microbial Effects on Physico-Mechanical and Microstructural Properties of Commercial Portland Cements

Onesmus Mulwa Munyao (MSc.)

I84/37352/2017

A Thesis Submitted in Fulfillment of the Requirements for the Award of the Degree of Doctor of Philosophy (Chemistry) in the School of Pure and Applied Sciences of Kenyatta University

July, 2022

DECLARATION

This thesis is my original work and has not been presented for a degree or other award at any other institution

Onesmus Mulwa Munyao

Department of Chemistry

Kenyatta University

Signature …… Date ……...

We confirm that the candidate successfully completed the work reported in this thesis under our supervision

Prof. Joseph Karanja wa-Thiong'o

Department of Chemistry

Kenyatta University

Signature …… Date ……...

Prof. Jackson Wachira Muthengia

Department of Physical Sciences

University of Embu

Signature …… Date ……...

DEDICATION

The work is in honour of my spouse Faith Nzilani with profound appreciation for her endless love and prayers. To our amazing children, Faith Nthoki and Fritz Munyao who have always been a great source of joy in our lives. To my dear parents, Daniel Munyao and Jenifer Nzoki for their immeasurable love, support and prayers.

ACKNOWLEDGEMENTS

I will forever remain indebted to my supervisors, Prof. Joseph Karanja wa- Thiong'o of Kenyatta University and Prof. Jackson Wachira Muthengia of University of Embu. It is through their academic counselling, technical guidance, timely response and positive criticism that saw me through this work. I owe the success of this work to them. I greatly thank the African Development Bank in collaboration with the Ministry of Education, Science & Technology for the PhD scholarship award. I wish to express my sincere appreciation to Prof. Karen Scrivener of École Polytechnique Fédérale de Lausanne, Switzerland, for the full funding and granting me an opportunity to attend, participate and learn the best cement research practices at the Laboratory of Construction Materials at École Polytechnique Fédérale de Lausanne - Switzerland during the 5th doctoral school. Many thanks go to Prof. John Provis of University of Sheffield, United Kingdom, for awarding me the PhD grant to attend the 74th Rilem week and present a paper during the 40th Cement and Concrete Conference at the University of Sheffield, UK.

My special thanks go to Prof. Romano Mwirichia of University of Embu, whose guidance on culturing of bacteria is well acknowledged. I also sincerely appreciate the management of Savannah Cement Ltd- Kenya for the support granted to me to undertake the studies. Further, I extend my appreciation to the Ministry of Mining and Petroleum- Kenya, United States International University, Africa- Kenya and the University of Pretoria, South Africa, for offering me an opportunity to carry out various cement tests in their laboratories. I sincerely thank all the technical staff and colleagues from Kenyatta University and University of Embu for the gratifying research experiences you offered me. Lastly, I humbly thank the Almighty God for His eternal Love, Protection and Grace over my life. May His Holy name be glorified. Amen.

TABLE OF CONTENTS

LIST OF TABLES

LIST OF FIGURES

LIST OF PLATES

LIST OF ABBREVIATIONS, SYMBOLS AND ACRONYMS

Cement Chemical Nomenclature and Symbols

H = H_2O	Water
C = CaO	Calcium Oxide
F = Fe_2O_3	Iron (III) Oxide
S = SiO_2	Silicon Dioxide
M = MgO	Magnesium Oxide
N = N_2O	Sodium Oxide
K= K_2O	Potassium Oxide
$\overline{S}$ = SO_3	Sulphur Tri Oxide
CH = $Ca(OH)_2$	Calcium Hydroxide
A = Al_2O_3	Aluminium Oxide
C_3S = $3CaO.SiO_3$	Tricalcium Silicate
C_2S = $2CaO.SiO_2$	Dicalcium Silicate
C_3A = $3CaO.Al_2O_3$	Tricalcium Aluminate
C_4AF = $4CaO.Al_2O_3.Fe_2O_3$	Tetracalcium Aluminoferrite
$C_6A\overline{S}_3H_{32}$ = $3CaO.Al_2O_3.3CaSO_4.32H_2O$	Ettringite
$C\overline{S}H_2$ = $CaSO_4.2H_2O$	Gypsum
C-S-H	Calcium Silicate Hydrate
C-A-H	Calcium aluminate hydrate

Abbreviations and Acronyms

WC	Water - Cement Ratio
ASTM	American Standards for Testing and Materials
ANOVA	Analysis of variance
ISO	International Organization for Standardization
Cement Mortar	Mortar made from either PPC or OPC
KEBS	Kenya Bureau of Standards
EAS	East African Standards
XRD	X-ray Diffraction
SEM	Scanning Electron Microscopy
XRF	X-ray Fluorescence
FTIR	Fourier Transform Infrared
LOI	Loss on ignition
IR	Insoluble Residue
MICC	Microbially induced concrete corrosion
MPa	Mega Pascal
OD	Optical Density
S. novella	*Starkeya novella*
T. intermedius	*Thiobacillus intermedius*
A. thiooxidans	*Acidithiobacillus thiooxidans*
OPC	Ordinary Portland Cement
OPC H-H	OPC mortar cast with distilled water as both mixing and curing media

OPC TI-H	OPC mortar cast with *Thiobacillus intermedius* bacteria solution as the mixing media and cured in distilled water
OPC TI-TI	OPC mortar cast using *Thiobacillus intermedius* bacteria solution as both the mixing and curing media
OPC AT-H	OPC mortar cast with *Acidithiobacillus thiooxidans* bacteria solution as the mixing media and cured in distilled water
OPC AT-AT	OPC mortar cast with *Acidithiobacillus thiooxidans* bacteria solution as both the mixing and curing media
OPC SK-H	OPC mortar cast with *Starkeya novella* bacteria solution as the mixing water and cured in distilled water
OPC SK-SK	OPC mortar cast with *Starkeya novella* bacteria solution as both the mixing and curing media
PPC	Portland Pozzolana Cement
PPC H-H	PPC mortar cast with distilled water as both mixing and curing media
PPC TI-H	PPC mortar cast with *Thiobacillus intermedius* bacteria solution as the mixing media and cured in distilled water
PPC TI-TI	PPC mortar cast using *Thiobacillus intermedius* bacteria solution as both mixing and curing media
PPC AT-H	PPC mortar cast with *Acidithiobacillus thiooxidans* bacteria solution as the mixing media and cured in distilled water
PPC AT-AT	PPC mortar cast with *Acidithiobacillus thiooxidans* bacteria solution as both mixing and curing media

PPC SK-H	PPC mortar cast with *Starkeya novella* bacteria solution as the mixing water and cured in distilled water
PPC SK-SK	PPC mortar cast with *Starkeya novella* bacteria solution as both mixing and curing media

ABSTRACT

Structures made using cement are prone to deterioration over time. Majority of structural failures have been attributed to inappropriate concrete mix designs, poor engineering designs, substandard aggregates, mixing water and sand. While many studies have focused on use of alternative cementitious materials to improve on the durability of existing Ordinary Portland cement (OPC), little attention has been given to microbial influence on concrete durability. This study investigated the influence of *Thiobacillus intermedius*, *Starkeya novella* and *Acidithiobacillus thiooxidans* bacteria on physico-mechanical and microstructural properties of selected Kenyan made cements. Commercial Ordinary Portland Cement (OPC) and Portland Pozzolana Cement (PPC) were used to cast the mortar prisms. The control mortar prisms were prepared using distilled water whereas the bacteria solutions were utilized as mix water, curing medium or a combination of two. The test cements were further subjected to 1.5 % sulphuric acid solution as a curing media. Physical characterization of both control and bacterial test cement pastes was carried out to determine normal consistency, setting time and soundness. Compressive strength was determined at 2^{nd}, 7^{th}, 28^{th}, 56^{th} and 90^{th} day of curing. XRD and FTIR were used to characterize the hydration products of the test mortars after curing for 28 days. Scanning Electron Microscopy (SEM) was carried out to study the surface morphology of the hydrated cement mortars after curing for 28 days. Both control and bacterial mortar prisms were subjected to accelerated chloride and sulphate ingress test after curing for 28 days. Apparent Diffusion Coefficients (D_{app}) were estimated from the solutions to Fick's Second Law of Diffusion. Results showed conformity of physical characteristics of control and microbial cement pastes to Kenya cement standards. The compressive strength however decreased significantly for all the bacterial prepared mortar prisms. OPC exhibited the highest strength decrease of 33.5% at 90^{th} day of curing when mixed and cured in *Starkeya novella* bacteria solution. SEM analysis showed extreme erosion of hydration products with formation of deleterious expansive ettringite crystals for the bacterial prepared mortars in the pore matrices. Control mortar prisms exhibited systematic formation of hydration products within the pore system. Mortars prepared with bacteria solutions as mixing water exhibited pronounced ingress of chloride and sulphate ions. OPC SK-SK mortars exhibited chloride and sulphate apparent diffusion coefficients (D_{app}) of 8.2995×10^{-10} m^2/s and 1.3562×10^{-9} m^2/s respectively. There was increased water absorptivity in the microbial mortars. OPC SK-SK registered the highest water absorptivity of 72.75%. The exposed mortar prisms in 1.5% sulphuric acid solution exhibited low compressive strength at all curing ages with OPC demonstrating the highest decrease in compressive strength of 73.56% at 90^{th} day of curing. Results from this study show that the selected bacteria commonly present in sewer systems play a vital role in deteriorating cement-based materials. This reduces the service life and the durability of the exposed cement structures with time. The work recommends development of remedial methods to prevent the bacteria attack on concrete and mortar structures placed in sewer and other aggressive environments.

CHAPTER ONE

INTRODUCTION

1.1 Background

Cement is described as second topmost utilized building constituent on earth after water (Krishnapriya *et al.,* 2015). Its distinctive properties such as flexible application in a wide range of environments and high compressive strength makes it the most ideal construction material (Munyao *et al.,* 2020c). Enormous volumes of concrete and mortar are used across the world in erection of buildings, bridges, sewer systems and railway lines among other structures (Munyao *et al.,* 2019; Haifen *et al.,* 2015).

Concrete and mortar made structures are susceptible to deterioration during their service life. Concrete structures are susceptible to deterioration as a result of chemical, physical and mechanical effects. Chemical effects like acid corrosion, contribute significantly to the shortening of the lifetime of concrete structures (Beddoe and Hilbig, 2009). The majority of concrete structural failures have been attributed to the entry of aggressive external elements such as carbon dioxide, sulphate and chloride ions (Niloofar *et al.*, 2019; Sumit *et al.,* 2019; Emilio *et al.,* 2008).

Biodeterioration of concrete or mortars also results from secondary products such as biogenic acids formed by bacteria that cause degradation in concrete or mortar. In countries with warm climates, deteriorated sewer collecting systems have a considerable influence on public health and environmental safety (Guadalupe *et al.,* 2010). In sewer pipes and sewage treatment facilities, hydrogen sulfide gas, moisture and oxygen promote the formation of biogenic acid (sulphuric acid), which deteriorates the structure via a process known as microbially induced concrete

corrosion (MICC) (Robert *et al.,* 2002; Islander *et al*., 1991). In some instances, the microbial attack may result in a reduction of the estimated service life of concrete structures to fewer than ten years (Jensen, 2009).

Degradation of cement- based materials through MICC has a vast commercial impact globally. This is because most of wastewater treatment plants, sewage lines and structures in chemically aggressive areas are made up of cement (Shiping *et al.,* 2010). Generally, the influence of microbes on concrete deterioration is facilitated by the microbial production of mineral and/or organic acids, which degenerates the concrete matrix and hence weakens the concrete structure (Rigby, 2010). Yamanaka *et al.* (2002) observed that specific environmental conditions perform critical function in accelerating concrete biodeterioration.

The activities of degrading microorganisms in concrete and mortar-built structures play a vital role in accelerating other damaging processes such as corrosion of the rebar through chloride ingress (Tahereh *et al.,* 2017). This is common in marine areas or in structures subjected to deicing salts (Glass and Buenfeld, 2000). Corrosion of the reinforcement bars lead to loss of structural integrity, which culminates to structural failure (Emilio *et al.,* 2008). The attack on the concrete and mortar surface by the acid generated from the microbial activities is more pronounced and deleterious. This is because the microorganisms uninterruptedly release the corrosive acid on the exposed concrete surfaces and hence weakening the concrete constituents (Rogers *et al.*, 1996).

Formation of thin invisible biofilms on the surface of cement-based structures by some microorganisms trigger the deleterious effect and hence compromise on the integrity of such

structures (Escadeillus *et al.,* 2007). Some bacteria species especially *Thiobacillus* have been reported to have destructive properties on concrete structures (Okabe *et al.,* 2007; Nica *et al.,* 2000). According to Roberts *et al.* (2002), these bacteria thrive very well in sewage systems and hence any cement-based structure erected near sewage systems is prone to biodeterioration.

Biodeterioration of concrete structures does not occur in freshly placed concrete due to high pH of cement (Sand *et al.,* 1987). As a result of the carbonation process and hydrogen sulfide neutralization in the sewer systems, the pH of the placed concrete is gradually reduced (Zhang *et al.,* 2008; Nielsen *et al.,* 2005; Lahav *et al.,* 2004; Matos and Arires, 1995). Sulphur-oxidizing bacteria oxidize the unstable hydrogen sulphide to form biogenic sulphuric acid (Satoh *et al.,* 2009; Vollertsen *et al.,* 2008; Zhang *et al.,* 2008). Biogenic sulphuric acid formed reacts with portlandite to form additional gypsum. The aluminate phase of the cement further reacts with gypsum to form ettringite, which is an expansive crystalline material (O'Connell *et al.,* 2010; Saricimen *et al.,* 2003). The resultant gypsum and ettringite weakens concrete structures (Cwalina, 2008).

The expense of maintaining concrete structures owing to microbial deterioration is often underestimated as microorganisms frequently speed up processes that would take place at a slower rate in their absence. Every year, billions of dollars are spent on infrastructure maintenance and repair due to biodeterioration (Sanchez- Silva and Rosowsky, 2008). Microbial degradation has a significant effect on not only the longevity and integrity of concrete structures, but environmental and public safety issues are also a concern since hazardous gases like hydrogen sulphide are produced (Grengg *et al.,* 2017). Notwithstanding the considerable work done previously, biodeterioration of concrete and mortar structures remain a major threat on the durability of

cement-based materials. In addition to lack of comprehensive information regarding biodeterioration, there has been no agreed methods to commendably assess the problem (Min *et al.,* 2020). This work investigated the influence of *Thiobacillus intermedius, Starkeya novella* and *Acidithiobacillus thiooxidans* bacteria on performance of commercial OPC and PPC.

1.2 Statement of the Problem

Poor craftsmanship, sloppy structural designs and inconsistencies in the quality of aggregates, sand and mixing water have all contributed to the collapse of cement-based infrastructures in developing countries like Kenya. There has been minimal or no consideration on the effects of external factors such as microorganisms found in the concrete environment. Concrete structures placed in microbial rich environments may be, subjected to microbial attack. Microbial activities in such environment may affect the properties of the placed concrete /mortar structure. The effect may be physical, mechanical and/ or microstructural leading to reduced service life of the concrete/mortar structure.

1.3 Justification of the Study

Structures constructed with cement are prone to deterioration over the course of their lifespan. Majority of these failures are due to substandard construction and craftsmanship, inadequate structural design, foundation instability and unexpected loads. While the reduction of the concrete service life may be through physical and mechanical deterioration influences, the chemical influences such as acid induced corrosion are among the major features that reduce the life cycle of concrete. Chemical and physical processes that contribute to structural failures include water leaching, alkali aggregate reactions, sulphate and chloride attack, freeze-thaw cycling and

corrosion of the reinforcing bars. Structural failures have been reported to cause death and property loss in Kenya as well as other countries across the world.

While substantial research on the durability of cementitious materials has been undertaken in Kenya (Munyao, 2015; Ngui, 2015; Mutitu, 2013; Muthengia, 2009), there has been no substantial work done on microbial contribution on concrete performance. Microbial involvement on structural performance has been a challenge to assess over a long time due to the versatility of the involved microbial species and the flexibility of the diverse microbial inhabitants. According to Bettina et *al.* (2016), the structural integrity of a building is greatly dependent on the assessment of the durability of cementitious materials and concrete.

National rules and standards have given minimal regard to concrete biodeterioration. Chapter 4 of the American Institute of Code Requirements for Environmental Structures (ACI 350-06) specifies the durability requirements for the concrete mixtures based on their exposure conditions. The Design Guide for Durable Concrete Structures-Bulletin d'information 182 of the Comite Euro-International du Beton (CEB) defines biodeterioration as the mechanical or chemical effects of biological processes on concrete whereas the Kenyan cement standard neither defines nor describes biodeterioration as a threat to structural durability.

Research into the impact of bacteria on cement mortar and concrete is thus critically needed in Kenya. This work is expected to contribute to the understanding of the effect of biodegrading bacteria on structural failures. This may enhance development of mitigation measures to constrain structural failures due to microbial attack and improve on the life span of cement- based materials.

1.4 Null Hypothesis

Thiobacillus intermedius, Starkeya novella and Acidithiobacillus thiooxidans bacteria have no significant effect on physico-mechanical and microstructural properties of commercial Portland cements.

1.5 Objectives

1.5.1 General Objective

To investigate the microbial effects on physico-mechanical and microstructural properties of commercial Portland cements.

1.5.2 Specific Objectives

i. To determine the chemical and phase composition of commercial OPC and PPC.
ii. To investigate the effect of *Thiobacillus intermedius*, *Starkeya novella* and *Acidithiobacillus thiooxidans* on normal consistency, setting time and soundness of commercial OPC and PPC pastes.
iii. To investigate the effect of the selected bacteria on compressive strength performance of commercial OPC and PPC mortars.
iv. To investigate the effect of the selected bacteria on microstructure of hydrated mortars of selected commercial OPC and PPC.
v. To analyze the water absorptivity and extend of chloride and sulphate ions ingress on mortars of OPC and PPC when exposed to the selected test bacteria.

1.6 Scope and Limitation

Collapse of cement-made structures in Kenya has become a serious challenge in the building and construction industry. Notwithstanding the efforts made to ensure that durability of placed concrete and mortar structures is guaranteed, failures in areas such as septic tanks and underground water collection points remains a threat. Most of concrete and mortar failures have been associated with external ingress of materials such as sulphates and chlorides. While studies on biodeterioration have pointed that some bacteria can cause significant failures of placed cement-made structure, this area has not attracted much attention.

This work sought to investigate the effect of *Thiobacillus intermedius*, *Starkeya novella* and *Acidithiobacillus thiooxidans* bacteria present in most of the sewer areas on performance of commercial Portland cements. The degrading effect of the selected bacteria on the commercial cements was monitored on compressive strength behaviour of the cast mortars with the bacteria, setting time and soundness pastes prepared with the bacteria solutions. Further the change in microstructure of the hydrated mortars made with the bacteria was attributed to the bacteria effect. The concentration of each test bacteria was only monitored during the initial culturing of the bacteria before mixing with the test cement.

1.7 Significance of the Study

Structures made with cement either inform of mortar or concrete are perceived to be durable. This is due to the characteristic nature of Portland cement to gain high strength after placement and its flexibility to be placed in virtually all environments. During its service life, concrete-based structures are subject to degradation either through chemical or physical processes. Collapse of buildings in Kenya has been a serious problem in the recent days. Most of these failures have been

associated with many factors among them poor structural designs, poor workmanship and poor quality of associated materials such as aggregates, sand and mixing water.

Structural failures due to microbial influence has not been considered as a contributing factor in collapse of buildings in Kenya. While the Kenyan cement standard neither defines nor describes the contribution of microorganisms on structural failures, some of the known degrading bacteria are commonly present in soils and find their way into the mixing water sources during construction or on the existing structures like sewerage systems. This work will help establish the contribution of some selected degrading bacteria on the performance of the commercial Portland cements with a view of recommending proper mitigation measures.

CHAPTER TWO

LITERATURE REVIEW

2.1 Portland Cement

Principally, Portland cement is the powdered product of Portland cement clinker. According to Kenya cement standard (KS EAS 18-1), Portland cement is defined as a finely ground inorganic material which when mixed with water sets and hardens by means of hydration process. Portland cement is a hydraulic binder and the most common used building material across the world (Munyao *et al.,* 2019; Henk *et al.,* 2010, Rao *et al.,* 2004). BS EN 197-1 (2011) and KS EAS 18-1 (2017) broadly describes 27 types of cements derived from Portland clinker. Calcium silicates, calcium aluminates and calcium ferrites from Portland clinker form the main composition of Portland cement (Bhatty *et al.,* 2004).

The process of manufacturing Portland clinker encompasses the burning of homogenous calcareous and siliceous raw materials in a rotary kiln at high temperatures of above 1350° C (Arthur, 2019). The resultant products (clinker phases) form the main composition of Portland cement (Trevor, 2016). Equation 2.1 -2.5 illustrates the temperature ranges of principal chemical reactions involved in the kiln (Arthur, 2019).

$$CaCO_3 \xrightarrow{800\ ^\circ C - 900\ ^\circ C} CaO + CO_2 \qquad 2.1$$

$$2CaO + SiO_2 \xrightarrow{800\ ^\circ C - 900\ ^\circ C} (CaO)_2.SiO_2 \qquad 2.2$$

$$3CaO + Al_2O_3 \xrightarrow{900\ ^\circ C - 1300\ ^\circ C} (CaO).Al_2O_3 \qquad 2.3$$

$$4CaO + Al_2O_3 + Fe_2O_3 \xrightarrow{900\ ℃ -1300\ ℃} (CaO)_4.Al_2O_3.Fe_2O_3 \quad 2.4$$

$$CaO + (CaO)_2.SiO_2 \xrightarrow{>1300\ ℃} (CaO)_3.SiO_2 \quad 2.5$$

The high temperatures facilitate sintering of the material, which further partially fuses to form nodular shaped material commonly referred to as Portland clinker (Newman and Cho, 2003). The resultant Portland clinker phases and the approximate percentage in mass are summarized in table 2.1 (Hewlett, 2003). These phases play a vital role in defining the physical and mechanical properties of Portland cement (Munyao, 2015).

Table 2.1 Typical Composition of Portland Clinker

Phase	**Chemical Formula**	**Mineral Name**	**Cement Nomenclature**	**Typical Range in % by mass**
Tricalcium Silicate	$3CaO.SiO_2$	Alite	C_3S	45 -65
Dicalcium Silicate	$2CaO.SiO_2$	Belite	C_2S	10- 25
Tricalcium aluminate	$3CaO.Al_2O_3$	Aluminate	C_3A	5 -12
Tetracalcium Aluminoferrite	$4CaO.Al_2O_3.Fe_2O_3$	Ferrite	C_4AF	5-15

The estimation of Portland Clinker phases follows a mathematical formulation developed by Robert H. Bogue (Bogue, 1929). While recent studies have shown that advanced XRD equipment's can be used in most cement quality control laboratories to measure the clinker mineralogy, Bogue calculation remains the most dependable method to estimate the clinker phases

from the chemical analysis. Equations 2.6 – 2.9 shows the Bogue mathematical model used in calculating/ estimating the composition of the Portland Clinker phases (Lea, 2004).

$$C_3S = 4.07\ (CaO) - 7.60\ (SiO_2) – 6.72\ (Al_2O_3) – 1.43\ (Fe_2O_3) – 2.85\ (SO_3) \quad 2.6$$

$$C_2S = 2.87\ (SiO_2) – 0.754\ (3CaO.SiO_2) \quad 2.7$$

$$C_3A = 2.65\ (Al_2O_3) – 1.69\ (Fe_2O_3) \quad 2.8$$

$$C_4AF = 3.04\ (Fe_2O_3) \quad 2.9$$

In the production of Ordinary Portland Cement, Portland clinker is ground together with 5% gypsum in either ball mill or vertical roller mill (KS EAS 18:1-2017). The addition of gypsum ($C\overline{S}H_2$) controls the flash setting of cement mortar/ concrete, improves workability during placement and lowers the rate of drying shrinkage (Trevor, 2016; Hawkins *et al.*, 2003). According to Tsamatsoulis and Nicolakakos (2013), the optimization of sulphate content in cement further defines the strength development of mortar and/ or concrete. Table 2.2 and 2.3 summarizes the typical chemical and phase composition of Ordinary Portland Cement (OPC) respectively (Trevor, 2016; Neville, 2011).

Table 2.2 Chemical Composition of Ordinary Portland Cement

Oxide Composition	**% w/w Composition**
CaO	63 - 65
SiO_2	20 - 22
Al_2O3	5 - 6
Fe_2O_3	3 - 4
MgO	1 - 2
SO_3	2 - 3.5
$K_2O + Na_2O$	0.2 - 0.6

Table 2.3 Phase Composition of Ordinary Portland Cement

Cement Phase	**% by Mass**	**Role / Effect on Cement Activity**
C_3S	55 - 60	Responsible for early strength development of cement (1-7 days)
C_2S	15 - 25	Responsible for late strength development (28 days and beyond)
C_3A	8 -12	Responsible for early strength development (1- 2 days)
C_4AF	9 -15	Gives cement colour

2.2 Mechanism of Portland Cement Hydration

The resultant reaction between water and non-hydrated cement or one of its constituents, commonly referred to as cement hydration, results in chemical and physico-mechanical changes that cause the cement to set and harden (James and Ivan, 2019). The loss of cement paste plasticity and subsequent conversion into a solid material is referred to as setting whereas the development of cement strength of the prepared mortar and/or concrete is referred to as hardening (James and Ivan, 2019).

When placed in high humid areas, partial hydration of cement may occur resulting in reduced physical and mechanical properties. This is the reason why cement must be kept in a dry place before placement and/or application (KS EAS 18-1 2017). According to BS EN 197-1 (2011) and KS EAS 18-1 (2017), water-cement ratio of 0.5 is recommended for a complete hydration of cement mortar. Portland cement hydration involves reaction chains between specific clinker phases, gypsum as hydrated calcium sulphate ($C\bar{S}H_2$) and water. These reactions proceed concurrently and sequentially at different rates while influencing each other in complex ways. The major phases and compounds involved includes Alite (C_3S), Belite (C_2S), Aluminate (C_3A), Ferrite (C_4AF), free lime, alkali sulfates (Na_2SO_4 and K_2SO_4) and calcium sulphate in the form of dihydrate, hemihydrate or anhydrite interground with clinker and mixing water (Peter and Martin, 2019).

The dissolution rate of clinker phases and $C\bar{S}H_2$ controls the initial hydration process. As the hydration process progresses, nucleation and crystal growth of the formed hydrate phases control the hydration. Further, the rate of hydration is, controlled by the diffusion rate of water and

dissolved ions (Juilland *et al.,* 2010). The hydration of Portland cement paste at ambient temperatures follows a series of stages categorized as pre-induction, induction, acceleration and post-acceleration periods (Peter and Martin, 2019).

2.2.1 Pre-Induction Period

The pre-induction period occurs within the first minutes after mixing cement with water. When cement is exposed to water, the ionic species present in the cement dissolves into the liquid phase leading to formation of hydrate phases. Alkali sulphates available in the cement dissolve fully within seconds contributing K^+, Na^+ and SO_4^{2-} ions. The dissolution of calcium sulphate occurs to saturation hence contributing Ca^{2+} and extra SO_4^{2-} ions. The dissolving of C_3S occurs easily hence, allowing the precipitation of calcium silicate hydrate phase at the surface of the cement particle. Since the CaO/ SiO_2 ratio of the formed hydrate is lower than that of C_3S, the hydration of C_3S is linked with an increase of Ca^{2+} and OH^- concentration in the liquid phase. While the silicate phases infiltrate the liquid phase simultaneously with Ca^{2+} and OH^-, their concentration remains very low. According to James and Ivan (2019), the portion of C_3S hydrated in the pre-induction stage is estimated to be between 2-10 %.

The dissolution of C_3A phase and subsequent reaction with ions of calcium and sulphate in the liquid phase results in formation of ettringite (AFt). An additional AFt is formed from the reaction of C_4AF phase in the same way as C_3A. The formed AFt precipitates at the surface of the cement particles. The quantity of C_3A hydration in the pre-induction stage depends on the cement type and is estimated to range between 5 - 25% (Juilland *et al.,* 2010). At this stage, Al^{3+} concentration in the liquid phase remains very low. In this period, the contribution of βC_2S is insignificant in

formation of C-S-H, calcium ions and hydroxyl ions in the liquid phase. Continual development of hydration products on cement particle surface slows down fast hydration reaction and as such, a barrier is formed between the non-hydrated material and the bulk solution (Tang *et al.*, 2017). This occurrence causes a proliferation in the concentration of dissolved ions in the liquid phase on instantaneous contact with the non-hydrated material to values closer to the theoretical solubilities of anhydrous compound (James and Ivan, 2019).

2.2.2 Induction Period

The induction period, also referred to as dormant period, occurs within the first few hours of cement hydration. After a brief burst of rapid hydration, the general rate of hydration drops substantially for a period of a few hours. This stage is characterized by sluggish hydration of all clinker phases (Över, 2012). In this stage, calcium hydroxide (CH) concentration in the liquid phase reaches the maximum limit and gradually begins to reduce whereas the SO_4^{2-} concentration remains constant as the portion consumed in the formation of AFt is substituted by dissolution of additional amounts of calcium sulphate (Zeng *et al.*, 2012). According to Young *et al.* (1977), the termination of induction period and the initiation of the main reaction is mainly due to the nucleation of the ‘second- stage’ C-S-H phase from the bulk liquid.

2.2.3 Acceleration Period

The acceleration period occurs within 3 – 12 hours after mixing cement with water. The hydration growth accelerates afresh and is managed by the nucleation and the growth of the resultant products (Scrivener *et al.*, 2015). The secondary acceleration of the C_3S results in formation of the ‘second- stage’ C-S-H (Scrivener *et al.*, 2015). A significant amount of βC_2S undergoes hydration

in this stage. Further, the crystalline portlandite (CH) precipitates from the liquid phase resulting in decline in Ca^{2+} ion concentration in the liquid phase (Huang *et al.*, 2017). The gypsum inter-ground with the cement inform of hydrated calcium sulphate ($C\bar{S}H_2$) dissolves entirely leading to reduction of SO_4^{2-} concentration ions in the liquid phase. This is because of AFt formation as well as due to the adsorption of SO_4^{2-} on the surface of the formed C-S-H (James and Ivan, 2019).

2.2.4 Post-Acceleration Period

According to Scrivener *et al.* (2015), the rate of hydration declines gradually in post acceleration stage as the quantity of unreacted materials drops. The rate of hydration process in this stage is thus controlled through diffusion. The continued hydration of C_3S and βC_2S results in continued formation of C-S-H. The involvement of βC_2S to this process increases with time and as a result, the rate at which extra calcium hydroxide is formed decreases. As a result, the AFt phase formed in previous stages of hydration begins to react in a through-solution reaction with additional C_3A and C_2 (A, F) generating monosulphates (Juilland *et al.*, 2010).

Water-cement ratio plays a vital role in determining the extent of Portland cement hydration. With initial high water-cement ratio, the hydration process continues until all the cement particles are exhausted. Nonetheless, the residue of large cement particles may persist even in mature pastes. When the water-cement ratio is low, the hydration reaction may not proceed to completion. This may be caused by the presence of substantial quantities of non-reacted materials (Scrivener *et al.*, 2015). Upon the completion of the hydration process, an ageing of the hydrated material may possibly occur. The ageing process is characterized by an additional poly-condensation of

tetrahedral SiO_4, which is present, and an increase of the average SiO_4 chain length in the C-S-H phase formed (Chen and Odler, 1992).

2.3 Degradation of Cement-Based Structures

When correctly designed, placed and cured, concrete remains the intrinsic durable material. However, during its service life, concrete and/ or mortar is subject to physical and /or chemical attack upon exposure in various environments. The nature of attack may target the cement, the rebar or the aggregates ultimately leading to the reduced service life of such cement-based structures (Lea, 2004).

2.3.1 Physical Attack

2.3.1.1 Freezing and Thawing

Concrete structures placed in extreme cold areas lose their mechanical properties due to freeze and thaw cycles (Zeinab and Tamer, 2018). According to Vimal (2009), concrete failure due to freeze and thaw is caused by pressure generated by the expansion of water. Freezing and thawing is common in areas, which experience severe winter seasons such as parts of Asia, North America and countries in North Europe (Vimal, 2009). This mode of concrete failure can be prevented by use of air entraining chemical admixtures (Ian *et al.*, 2019).

2.3.1.2 Salt Crystallization

When concrete and mortar come in contact with water, either mixing water, curing water or runoff water with significant amounts of dissolved salts, the salts infuse in the concrete and mortar matrix. Upon evaporation of the water either unceasingly or sporadically, the salts crystallize in the pores

and the slow pressure buildup of the salts cause surface scaling. A significant damage on such concrete structures may be caused by the salt crystallization pressure (Thaulow and Sahu, 2004).

Salt crystallization on concrete surfaces depend on water and the evaporation rate. When water on concrete surface is supersaturated, the high evaporation rates cause crystallization just underneath the concrete surface. This may lead to severe deterioration (Liu *et al.,* 2012). This physical mode of concrete is mostly observed in marine areas where concrete is exposed to consistent sequences of wetting and drying (Liu *et al.,* 2012).

2.3.2 Chemical Attack

2.3.2.1 Efflorescence and Leaching

Efflorescence and leaching mode of chemical attack also referred to as lime bloom occurs when the dissolved salts are leached out of the concrete surface and the subsequent reaction with the atmospheric carbon dioxide. It is common in areas where water permeates through the concrete especially on the downstream or in circumstances where there is an alternate moistening and drying of concrete surface. Efflorescence principally comprises of $CaCO_3$ as a whitish deposit on the concrete surface (Sidney, 2019).

$$Ca(OH)_2 + CO_2 \rightarrow CaCO_3 + H_2O \qquad 2.10$$

Additionally, the gypsum added to regulate the workability and the setting of the cement may as well be precipitated on the surface of concrete after water evaporation. Whereas efflorescence is not a major threat on structural integrity, it signals a significant leaching within the concrete. In

extreme situations, it may facilitate the increase in concrete porosity and permeability. This results in formation of suitable pathways for ingress of harmful materials such as chlorides and sulphates into the concrete matrix (Ekström, 2001).

2.3.2.2 Sulphate Attack

Sulphate attack is regarded as the most comprehensive mode of chemical attack on concrete. This is due to availability of sulphate ions in most soils and mixing waters commonly used in mixing cement mortar/concrete (Sidney, 2019). Sulphate attack entails a chain of chemical reactions between sulphate ions and the principal constituents of cement paste (Tixier and Mobasher, 2003). Ingress of sulphate ions in concrete and /or mortar triggers structural degradation (Munyao *et al.*, 2019; Cheng *et al.*, 2015).

The mechanism of sulphate attack is initiated either through internal or external sources (Taylor, 1997). For instance, in external sulphate attack, the migration of sulphate ions into the concrete matrix goes along with imperceptible dissolution of CH and decomposition of C-S-H phases. Presence of sulphate ions in environments with pH below 7, results in formation of $C\bar{S}H_2$, which causes expansion, spalling and strength, decline. Due to the acidity of the environment, portlandite is, completely removed from the cement paste. The removal of portlandite promotes decomposition of C-S-H that causes loss of adhesion and stiffness (Irassar, 2009).

Internal sulphate attack results in decline of lime silica (C/S) ratio. The removal of the increased amount of Ca^{2+} from the cement-based structure causes strength loss of the hardened paste (Tixier and Mobasher, 2003). Further, the simultaneous formation of ettringite crystals and successive

volumetric strains in the hardened paste causes expansion and micro cracking of concrete. This phenomenon limits the long-term durability of such concrete based materials. (Cheng *et al.*, 2015; Clifton and Ponnersheim, 1994).

Generally, sulphate attack is more prone to portlandite and alumina phases of hydrated Portland cement (Kumar and Paulo, 2006). The alumina phase in form of C_3A serves as a point of attack by sulphate ions (Munyao, 2015). The hydration of Portland cements with more than 5% C_3A contains most of the alumina in the form of mono-sulphate hydrates, $C_3A.C\overline{S}.H_{18}$. When the C_3A content increases above 8 %, the hydration products will also contain $C_3A.CH.H_{18}$.

The availability of CH in the hydrated Portland cement paste facilitates the conversion of the two-alumina containing hydrates ($C_3A.C\overline{S}.H_{18}$ and $C_3A.CH.H_{18}$) into ettringite, $C_3A.3C\overline{S}.H_{32}$ in presence of sulphate ions. Ettringite is associated with expansion and spalling of concrete made structures. Equations 2.11 and 2.12 below describes the formation of ettringite (Kumar and Paulo, 2006).

$$C_3A.CH.H_{18} + 2CH + 3\overline{S} + 11H \rightarrow C_3A.3C\overline{S}.H_{32} \qquad 2.11$$

$$C_3A.C\overline{S}.H_{18} + 2CH + 2\overline{S} + 12H \rightarrow C_3A.3C\overline{S}.H_{32} \qquad 2.12$$

Subject to the cation type associated with the sulphate solution (Na^+, K^+, and or Mg^{2+}), both CH and C-S-H present in the hydrated Portland cement paste may be converted to $C\overline{S}H_2$ as shown in equations 2.13 – 2.15 (Taylor, 1997).

$$Na_2SO_4 + Ca(OH)_2 + 2H_2O \rightarrow CaSO_4.2H_2O + 2NaOH \quad (2.13)$$

$$MgSO_4 + Ca(OH)_2 + 2H_2O \rightarrow CaSO_4.2H_2O + Mg(OH)_2 \quad (2.14)$$

$$MgSO_4 + 2CaO.SiO_2.3H_2O + 8H_2O \rightarrow 3(CaSO_4.2H_2O) + 3Mg(OH)_2 + 2SiO_2.H_2O \quad (2.15)$$

In equation 2.13, the formation of NaOH as a by-product increases the alkalinity of the resultant solution. The high pH is critical in providing stability of the C-S-H. When sulphate ions are accompanied by Mg^{2+}, the conversion of portlandite to gypsum results in formation of insoluble magnesium hydroxide as a by-product. The formation of $Mg(OH)_2$ reduces the alkalinity of the system hence lowering the stability of C-S-H. The resultant calcium silicate hydrate is further attacked by the magnesium sulphate solution as shown in equation 2.15. This phenomenon makes magnesium sulphate attack more severe on concrete than any other form of sulphate attack (Taylor, 1997).

2.3.2.3 Chloride Attack

Chlorides are classified as among the most aggressive ions, which cause fast corrosion of reinforced concrete made materials (Wieslaw, 2014). A freshly placed concrete and/mortar is resistant to chloride attack (corrosion). This is because the composition of concrete is vastly basic with an approximate pH of 13 in the pore solution. The high pH is due to the presence of hydroxides of sodium and potassium hydroxides in the pore solution and the vast volume of portlandite (CH) ensuing from hydration reactions (Sidney, 2019).

The concentration of the chloride ion in contact with concrete and the accompanying cation influences the rate of chloride attack (Wieslaw, 2014). Chlorides may enter concrete through various sources among them mixing water rich in chloride ions, accelerating admixtures added to improve on the early strength of cement mortar/ concrete such as calcium chloride, de-icing salts used in pavement and bridge decks among other sources (Munyao, 2015). While chlorides induce corrosion of the rebar, in some instances where there is no reinforcement, chloride based salts are added as concrete admixtures to improve on the mechanical properties of cement (Nielsen and Geiker, 2003).

The ingress of chloride ions into the cement matrix is largely reliant on the type of the cement and the chloride binding ability (Marinescu and Brouwers, 2009). When chlorides ingress into the rebar, they destroy the passive iron oxide film. This leads to corrosion of the steel/ rebar. Corrosion results from the formation of the soluble iron-chloride complex that results in the deposition of loose porous rust on the surface of the rebar and releases chloride to continue the attack as illustrated in the mechanism below (Sidney, 2019).

$$Fe^{2+} + Cl^{-} \rightarrow [\ FeCl\ complex]^{+} \qquad 2.16$$

$$[FeCl]^{-} + 2OH^{-} \rightarrow Fe(OH)_2 + Cl^{-} \qquad 2.17$$

Chloride attack results in the corrosion of the reinforced concrete structure. Corrosion of concrete results in the creation of rust as a result of an expansive reaction, which eventually results in spalling of the concrete above the rusting rebar and cracking (Sidney, 2019). This process is,

followed by loss of the steel cross-section area due to corrosion, leading to a decline in the load bearing capacity of the section (Wieslaw, 2014). The formed cracks serve as a suitable channel for the entrance of other harmful materials, which influences further deterioration of the concrete. Corrosion of reinforced concrete is frequently, experienced in highway structures and bridges, in parking garages and in marine environments (Sidney, 2019).

2.3.3 Biodeterioration of Concrete and Mortar Structures

Microbial attack on concrete and mortar results in a degradation process known as microbially induced concrete corrosion (MICC) (Min *et al.,* 2020). MICC is a precise common degradation for concrete and mortar structures exposed to sewer environments (Sanchez –Silva and Rosowky, 2008; Robert *et al.,* 2002; Monteny *et al.,* 2000; O'Connel *et al.,* 2000). Concrete and mortar deterioration due to microbial attack has been one of the major challenges facing modern society subsurface infrastructure (Grengg *et al.,* 2017).

MICC results in increased cost of repair on the damaged structures as well as significantly contributing to health-related issues and the pollution of the environment through the emission of toxic gases such as hydrogen sulphide (Grengg *et al.,* 2017; Jiang *et al.,* 2017). Presence of high concentration of hydrogen sulphide gas, low pH and high moisture content in sewer systems offer a suitable environment for the growth of the deleterious microbes that reduce the concrete/mortar service life with time (Shipping *et al.,* 2013; Crispim and Gaylarde, 2005; Crispim *et al.,* 2003; Gaylarde *et al.,* 2003).

Hydrogen sulphide gas (H_2S) generated in the sewer systems facilitate the corrosion of concrete (Xuan *et al.,* 2019). The production of H_2S by sulphur reducing bacteria (SRB) and the subsequent oxidation of the formed H_2S gas by sulphur oxidizing bacteria (SOB) produces biogenic sulphuric acid (Li *et al.,* 2017). Sulphur oxidizing bacteria converts both organic and inorganic sulphur compounds in the sewer system to generate biogenic sulphuric acid (Wei *et al.,* 2010). Chemolithotrophic sulphur oxidizing bacteria of the genus *thiobacillus* are the most destructive biological agents that stimulate degradation of cementitious materials (Robert *et al.,* 2002).

The microbial generated sulphuric acid attacks the soluble constituents of the cement resulting to formation of expansive products that result in cracking (Negar and Nemkumar, 2019). The formation of cracks offer suitable conduits for faster diffusion of microorganisms and corrosive materials such as chlorides and carbon dioxide into the interior of the concrete. The entry of these materials into the concrete matrix lowers the concrete pH (Negar and Nemkumar, 2019). The low pH allows the passive film on the rebar to dissolve hence quickening the corrosion of the reinforcing bars. This action ultimately results in reduced service life of the exposed mortar and concrete structures (Munyao *et al.*, 2020; De Windt and Devillers, 2010).

Due to high alkalinity, fresh concrete is typically immune to microbial attack. The high alkalinity is due to the presence of sodium and potassium hydroxides as well as a high concentration of calcium hydroxide from the hydration process (Sidney, 2019; Sand, 1987). Roughness on the concrete surface is caused by the friction of structural elements with other materials and/or the erosive action of water. Along with the presence of moisture and nutrients, this environment favours the microbial colonization on the concrete surface. Colonization of concrete by sulphur-

reducing and sulphur-oxidizing bacteria has been linked to the environmental sulphur cycle (Yilmaz, 2010; Satoh *et al.,* 2009).

2.3.3.1 Process of Biodeterioration

Biodeterioration of concrete and mortar structures is a complex mechanism which involves biological, chemical and electrochemical processes (Song *et al.,* 2019; Grengg, 2018; Wu *et al.,* 2018; Li *et al.,* 2017; Sun *et al.,* 2016; Sun, 2015; House, 2013). The initiation and propagation of MICC process for the concrete and mortar follows a series of stages/ phases (Sun, 2015; House, 2013; Yuan, 2013; O'Connell *et al.,* 2010; Wells *et al.,* 2009).

Concrete deterioration is caused by the metabolic products resulting from microbial activities. This occurs when degrading bacteria colonize the exterior of the exposed concrete surface (Satoshi *et al.,* 2007). Sulphuric acid is formed from various types of sulphur in the environment depending on the bacteria that are present. Hydrogen sulphide, produced by sulphur reducing bacteria present in sewer systems is responsible for the production of biogenic sulphuric acid (Min *et al.*, 2020).

Formation of the aqueous hydrogen sulphide in the sewer systems is fundamental in inducing corrosion process on exposed metal and concrete or mortar material (US environmental protection agency, 2010). Equation 2.18 describes the postulated formation of the aqueous hydrogen sulfide in a typical sewer / wastewater system (House and Weiss, 2014).

$$SO_4 + 2C(\text{Organic Matter}) + 2H_2O \xrightarrow{SRB} 2HCO_3 + H_2S_{(aq)} \qquad 2.18$$

Sulphates and sulphur comprising materials like amino acids and proteins are present in most wastewater sewers (Sun, 2015). The concentration of the sulphate content (SO_4^{2-}) in domestic wastewater serving as the main source of sulphur ranges from 40-200 mg/L (Zhang *et al.,* 2008). In a typical sewer system, the sulphur reducing bacteria (SRB) reduces sulphate into sulphide as shown in equation 2.18. The reaction proceeds in sediments and biofilms through anaerobic environment (Min *et al.,* 2020; Kong *et al.,* 2018; Sun, 2015; House and Weiss, 2014; O'Connell *et al.,* 2010; Zhang *et al.,* 2008). Presence of organic substances available in wastewater systems serve as the food supply for the SRB (Sharma *et al.* 2008).

The radiation of the formed aqueous hydrogen sulphide ($H_2S_{(aq)}$) is affected by wastewater pH, the phase balance on gas and liquid status, discharge agitation and weather condition. Equations 2.19 and 2.20 describes the reaction equilibria of aqueous hydrogen sulphide in wastewater (House and Weiss, 2014; Zhang *et al.,* 2008, Yang *et al.,* 2005).

$$H_2S \leftrightarrow HS^- + H^+ \qquad 2.19$$

$$HS^- \leftrightarrow H^+ + S^{2-} \qquad 2.20$$

The formation of the hydrogen sulphide depends largely on the pH of the wastewater. Figure 2.1 gives the relationship of some strains of sulphur and the pH of the solution at equilibrium (Min *et al.,* 2020; House and Weiss, 2014).

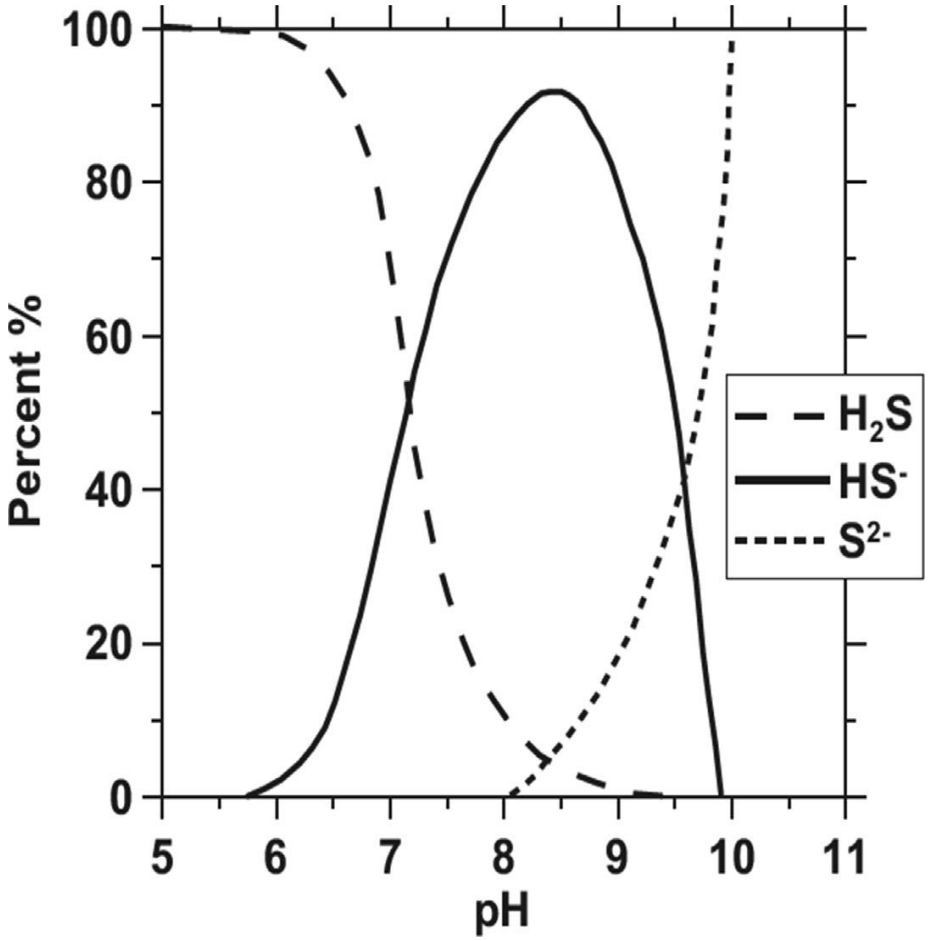

Figure 2.1 Relationship on pH of the solution and sulphur strains in equilibrium at 25° C (Min *et al.*, 2020; House and Weiss, 2014).

As illustrated in Figure 2.1, virtually, all the sulphur species occur as aqueous hydrogen sulphide ($H_2S_{(aq)}$) at pH below 6 with a notable shift of the sulphur species occurring as HS^- at pH 9 (Min *et al.*, 2020). According to the work done by Zhang *et al.* (2008), the authors reported that S^{2-} sulphur species are not considered owing to their irrelevance even at high pH. Based on the research findings by House and Weiss (2014) and Firer *et al.* (2008), the pH of the municipal water was found to range between 6-8 forming a suitable environment for the dominance of aqueous hydrogen sulphide species. At the headspace of the sewer system, the gaseous hydrogen sulphide

builds up depending on the ventilation conditions and the turbulence of the wastewater (House, 2013).

2.3.3.2 Production of Biogenic Sulphuric Acid

The generation of the biogenic sulphuric acid occurs through a series of abiotic and biotic reactions within the sewer system (Yang *et al.,* 2005). The formed acid induces corrosion of the exposed concrete and mortar. The entire corrosion process of the exposed concrete and mortar has been largely regarded as a three-step model with sulphur oxidizing bacteria playing a vital role in the entire process (Grengg *et al.,* 2018; Roberts *et al.,* 2002; Islander *et al.,* 1991). Growth and multiplication of sulphur oxidizing bacteria (SOB) on concrete and mortar structures is initiated when the pH falls to approximately 9 (Roberts *et al.,* 2002).

The first stage involves reduction of pH as a result of carbonation of the placed concrete /mortar and subsequent reactions of hydrogen sulphide in the sewer or wastewater system (Sun, 2015; Jana and Lewis, 2005; Roberts *et al.,* 2002; Davis *et al.,* 1998). Other than CO_2 and H_2S, production of other acids such as acetic, oxalic and glucuronic by some fungus present in fresh sewer system could lead to initial pH reduction of concrete and mortar (Gu *et al.,* 1998). The pH reduction provides suitable environment for the growth and colonization of SOB, which induces MICC (Joseph *et al.,* 2012).

In some circumstances, when the concentration of H_2S is above 600 ppm, SOB could directly oxidize hydrogen sulphide gas to form sulphuric acid through biotic reactions and actively reduce the concrete surface pH (Yamanaka *et al.,* 2002). This implies that there is a possibility of

introducing biotic reactions at the initial stages of concrete and mortar corrosion. Generally, stage 1 involves mostly abiotic reaction with minimal biological activities (Min *et al.,* 2020).

Collection of some sulphur oxidizing bacteria in presence of adequate moisture, nutrients and oxygen are capable of colonizing concrete surfaces and oxidize the available hydrogen sulphide gas (Xuan *et al.,* 2019). Colonization of SOB fundamentally relies on the concrete /mortar surface pH and the substrate appropriate for a particular microbe. A summary of sulphur oxidizing bacteria which have been identified and reported from corroded concrete and mortar layers along with their respective sulphur substrates as source of energy are tabulated in table 2.4 (Min *et al.*, 2020; Sun, 2015).

Table 2.4: Biological features of sulphur oxidizing bacteria established within rust coatings (Min *et al.,* 2020; Sun, 2015).

Sulphur Oxidizing Bacteria Species	Recommended pH to develop	Sulphur Substrate	Result
Thiobacillus thioparus	6 -10	H_2S, S^0, $S_2O_3^{2-}$	Polythionic acids, S^0
Halothiobacillus neapolitanus (previously, Thiobacillus neapolitanus)	6 -8	S^0, S_2O_32-	Polythionic acids, SO_4^{2-}
Starkeya novella (Previously, Thiobacillus novellus)	6 -8	$S_2O_3^{2-}$	S^0
Starkeya intermedius	5 -7	$S_2O_3^{2-}$	Polythionic acids, SO_4^{2-}
Thiobacillusplumbophilus	4 - 6.5	H_2S	-
Acidiphiliumspp. (previously, Thiobacillusacidophilis)	3 -10	H_2S, S^0	SO_4^{2-}
Thiomonasspp. (Previously, Thiobacillusintermedius)	3 - 9	H_2S, $S_2O_3^{2-}$	S^0, SO_4^{2-}
Acidithiobacillus ferrooxidans (Previously Thiobacillus ferrooxidans	~3	H_2S	S^0, SO_4^{2-}
Thiobacillus acidophilus	~3	H_2S	S^0,SO_4^{2-}
Acidithiobacillus thiooxidans	< 3	H_2S, S^0	S^0, $S_2O_3^{2-}$
Sulfobacillus spp.	1-3	H_2S, $S_2O_3^{2-}$	-
Thermothiobacillus	Poorly Characterized	H_2S, $S_2O_3^{2-}$ SnO_6^{2-}	SO_4^{2-}
Metallibacterium spp.	Identification not well done		
Burkholderiales spp.	Identification not well done		
Sphingobacteriales spp.	Identification not well done		
Xanthomonadalesspp.	Nonculturable		

Stage two involves colonization and oxidation of hydrogen sulphide by neutrophilic sulphur oxidizing bacteria (NSOB). *Thiobacillus thioparus*, one of the most common NSOB has the ability to colonize concrete surface and oxidize H_2S diffused into the condensed film at a pH of approximately 9. As described in table 2.4, oxidation of hydrogen sulphide gas results in formation of several sulphur states. The activity of *Thiobacillus thioparus* further lowers the surface pH of the concrete /mortar, making the environment more conducive for further colonization of the NSOB on the concrete surface (Yousefi *et al.,* 2014).

Facultative heterotrophs such as *Thiomonas intermedius*, *Starkeya novella* and *Halothiobacillus neapolitanus* colonize concrete surfaces at a much lower pH (George *et al.,* 2012; Herisson *et al.,* 2012). Lowering pH either because of microbial activity, carbonation or other activity creates a suitable environment for colonization of NSOB. However, as the pH decreases towards 4 ~5, the activity of NSOB is slowly subdued allowing the colonization of acidophilic sulphur oxidizing bacteria (ASOB) on the surfaces of the exposed cementitious materials (Grengg *et al.,* 2018).

Stage three of concrete corrosion due to MICC is the most damaging stage. According to Min *et al.* (2020), ASOB can directly oxidize hydrogen sulphide gas into sulphuric acid. Additionally, ASOB can oxidize thiosulphate ($S_2O_3^{2-}$) and elemental sulphur (S^0) accumulated on sewer walls following the direct oxidation of hydrogen sulphide gas by atmospheric oxygen. Activities related to acidophilic sulphur oxidizing bacteria reduces the pH further to approximately 1~2. *Acidithiobacillus thiooxidans, Acidithiobacillus ferrooxidans* and *Acidiphilium spp,* are among the most described prevailing acidophilic sulphur oxidizing bacteria (Li *et al.,* 2017; Cayford *et al.,* 2012; Nica *et al.,* 2000; Davis *et al.,* 1998; Islander *et al.,* 1991).

The resultant low pH values in the sewer system makes ASOB colonize and become the most dominant microbes on the surfaces of the cementitious materials. At this stage, the activities of ASOB results in generation of biogenic acid (Sun, 2015). The formed biogenic sulphuric acid reacts with calcium carbonate, calcium hydroxide and calcium silicate hydrate (C-S-H). These reactions result in formation of secondary gypsum as shown in equations 2.21 – 2.23 (Giradi and Maggio, 2011; Wells *et al.,* 2009; Ramsamy, 2006; Monteny *et al.*, 2000). Consequently, the formed gypsum reacts with the calcium aluminate phase to form ettringite as represented in equation 2.24 (Haifen, 2013).

$$H_2SO_4 + CaCO_3 \rightarrow CaSO_4 + H_2CO_3 \qquad 2.21$$

$$H_2SO_4 + Ca(OH)_2 \rightarrow CaSO_4.2H_2O \qquad 2.22$$

$$H_2SO_4 + CaO.SiO_2.2H_2O \rightarrow CaSO_4 + Si(OH)_4 + H_2O \qquad 2.23$$

$$3CaSO_4 + 3CaO.Al_2O_3.6H_2O + 26H_2O \rightarrow 3CaO.Al_2O_3.3CaSO_4.32H_2O \qquad 2.24$$

The above reactions are dependent on pH which varies with distance from the sewer depth. The products are thus formed as layers on concrete as illustrated in figure 2.2.

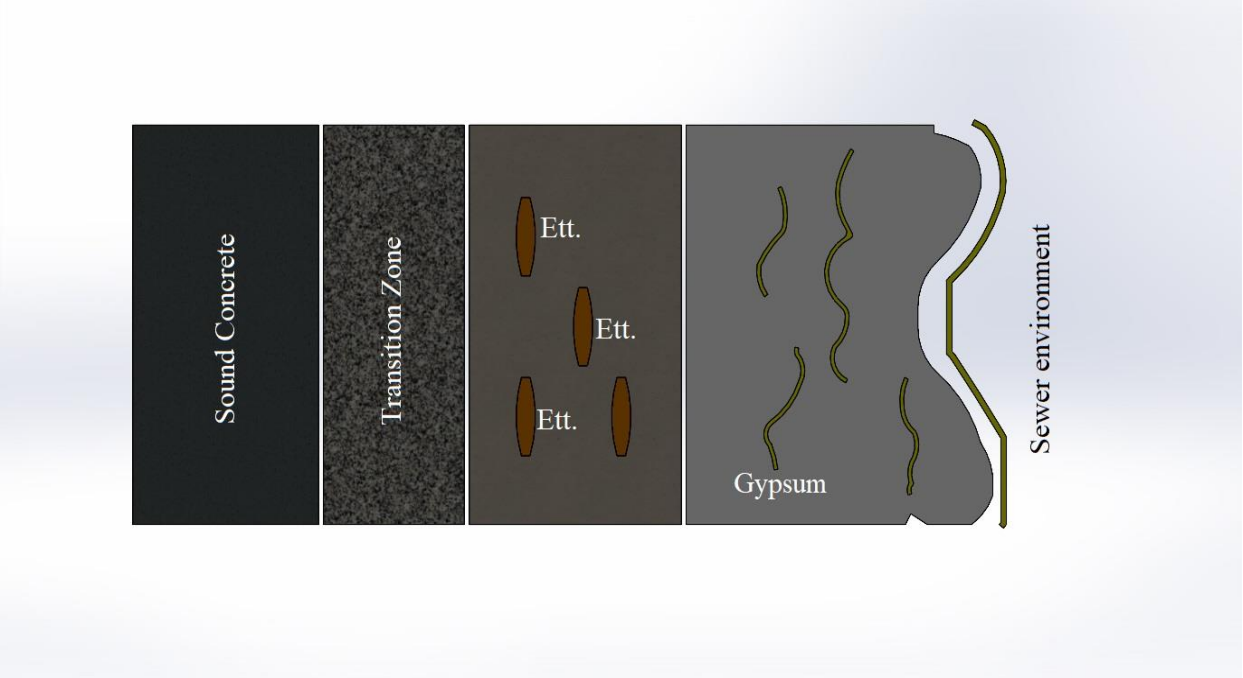

Figure 2.2: Simplified interpretation of various regions in the deteriorated concrete films (Min *et al.*, 2020)

The formation of secondary gypsum as described by equations 2.21 – 2.23 occurs at low pH of approximately 3, hence forms at the surface of the corrosion layer (Sun, 2015). Studies done by O'Connell, (2010), Okabe *et al.* (2007) and Davis *et al.* (1998), reported that, white and mush looking like material with no cohesive properties characterized the formed secondary gypsum at the surface of the corroded concrete and mortar material. According to Parande *et al.* (2006), the formed gypsum causes approximately 120 -220 % volume expansion of the attacked concrete material.

Ettringite crystals occur at high pH. This happens within the deeper sections of the concrete (O'Connell, 2010; Marchand *et al.*, 2003). The formation of ettringite through the reaction of gypsum and tricalcium aluminate as described in equation 2.24 causes more destruction to the

concrete and mortar (Monteny *et al.,* 2000). The formation of ettringite causes serious expansion of the exposed concrete and mortar. The approximated expansion due to ettringite formation ranges from 227-700% (Sun, 2015; Parande *et al.,* 2006). The expansion facilitates internal cracking and pitting of exposed concrete. The created cracks provide excellent paths for the entry of other harmful materials into the concrete structure such as carbon dioxide, sulphates and chloride ions (Wells *et al.,* 2009).

Whereas, gypsum and ettringite formation in the sewer environments are the main corrosion products, crack development at the corroding front of the reinforced concrete is mainly attributed to the dissolution of iron salts in the cement pores followed by rust precipitation (Sun, 2015). The formation of rust causes micro cracking at the corroding front (Jiang and Yuan 2014). The micro cracking due to iron precipitation is illustrated as the transition zone in figure 2.2.

2.4 Factors that influence Microbial induced concrete corrosion

Concrete and mortar disintegration due to microbial attack has primarily been associated with generation of biogenic sulphuric acid in sewer systems. The total service life or the durability of placed cement structures in sewer areas has been lowered due to microbial influence. Table 2.5 summarizes the effect of the influencing factors on determining the rate of MICC (Min *et al.,* 2020). As shown on table 2.5, there are factors that influence MICC rate positively (denoted as +), whereas those that have negative influence on MICC rate (denoted as -), and the factors which are obscure (denoted as NA).

Table2.5: Main factors affecting MICC rate in concrete sewers (Min *et al.,* 2020)

Factor	Description	Effect[1]	Reference
Waste -water characteristics			
Sulphate content	More sulphates provide more food to SRB for reduction, thus more sulphide formation	+	Sun, 2015; House, 2013
Dissolved Oxygen (D.O)	Immense D.O, limits the action of SRB hence subsequently lowering the transformation of sulphates into sulphides.	-	House, 2013
	High D.O increase the oxidation of aqueous H_2S hence lowering the volume of aqueous H_2S present in sewers	-	Wu *et al.,* 2018
Biochemical Oxygen Demand (B.O.D)	High B.O.D implies nutrients available for the bacteria to deplete DO, thus promoting sulphide generation	+	Wu *et al.,* 2018; House, 2013
pH	Elevated pH doesn't favour additional aqueous H_2S portion in the equilibria, hence preventing the H_2S gas build up	-	House and Weiss, 2014; Zhang *et al.,* 2008; Yang *et al.,* 2005
Temperature	Extreme temperatures increase the activity of the microbes in the slime layer. This promotes H_2S gas formation	+	Wu *et al.,* 2018; House, 2013
	Elevated temperatures promote the discharge of aqueous H_2S to the sewer gaseous phase	+	Wu *et al.,* 2018; House, 2013
Surrounding Factors			
Relative-humidity (R.H)	Generally, an elevated R.H favours condensation of the moisture on the walls of the sewer enabling development of biofilms. As a result, H_2SO_4 production is increased.	+	Wu *et al.,* 2018 ; Saucier and Herisson, 2015; Sun, 2015 ; Islander *et al.,* 1991
Temperature in the atmosphere	Elevated temperature accelerates the activity of the microbes within biofilms of sewer-walls hence speeding up the rates of corrosion	+	Sun, 2015; Joseph *et al.,* 2012; Saricimen and Maslehuddin, 1987
Properties of concrete			
Alkalinity	The alkaline nature of concrete allows reaction of the concrete constituent materials with the produced bio-acids.	-	House, 2013 ; Scrivener and De Belie, 2013; De Belie *et al.,* 2004
Calcium aluminate cement types (CAC)	Chemistry configuration of CAC types offer improved resistance to microbial induced corrosion in comparison to the conventional cements	-	Saucier *et al.,* 2015; Scrivener and De Belie, 2013
Geo-polymer	Generally, geo-polymers have shown improved performance in comparison to Portland cements under acid attack	-	Grengg *et al.,* 2018; Provis *et al.,* 2015; Shi *et al.,* 2000
Supplementary cementitious materials, porosity and ratio of water to cement	There has been no documented clarification on the performance of secondary cementitious materials when subjected to microbial	NA	Hewayde *et al.,* 2007; Monteny *et al.,* 2000

Microbes			
Sulphur Reducing Bacteria	Sulphur reducing bacteria hastens generation of aqueous H_2S. This process enhances microbial induced corrosion	-	House, 2013
Sulphur Oxidizing Bacteria	Generally, sulphur oxidizing bacteria encourages oxidation of gaseous H_2S. This results in generation of more volumes of sulphuric acid causing increased microbial induced corrosion	+	Wu *et al.*, 2018
Others	Some of the bacteria are identified as SRB or SOB, while the possible effects of other bacteria or microorganisms are not known	NA	Gu *et al.*, 1998
Hydraulics and design			
Turbulence (flow velocity)	Elevated turbulence increases liquid-gas surface area for H_2S to be released to the gas phase	+	Wu *et al.*, 2018; House, 2013
	High velocity encourages re-aeration which will lead to the growth of SOB and chemical oxidation, resulting in enhanced potential for the generation of rate of H_2SO_4	+	Wu *et al.*, 2018; House, 2013
	High velocity affects the thickness of the slime layer, which may impair sulphide generation and build up	NA	House, 2013
Time of Retention	An extended time of retention results in consumption of D.O in wastewater, hence increased discharge of H_2S to sewer-head zone	+	House, 2013
	An extended time of retention loosens the slime layer, this allows a pathway for penetration of sulphates and thus promoting activities of SRB.	+	Wu *et al.*, 2018; House, 2013
Condition of ventilators	(i) Sufficient ventilators promote discharge of aqueous H_2S to gaseous stage	+	House, 2013
	(ii) With sufficient ventilators, the gaseous phase concentration of H_2S is limited. This may result to lowered rates of microbial induced corrosion.	-	Grengg *et al.*, 2018

While much research has been conducted on various modes of concrete failures, it is important to acknowledge that biodeterioration remains a global threat on structures placed in sewer prone areas. The activities of bacteria in sewer and /or septic systems remain of significant importance in defining the durability and service life of cement - based structures. Some structural failures have suggested the possibility of the bacteria attack on cement material in sewer and water treatment plants. The extent in which different strains of bacteria colonize and ingress into the

concrete and mortar structures to cause deterioration is still a subject of debate. Concrete and mortar failures in aggressive environments may be due to physical, chemical or mechanical factors. The understanding on the interaction between the bacteria and the cement constituents is critical in defining the type of failure due to bacteria attack.

2.5 Fundamental Analytical Techniques

2.5.1 X-Ray Fluorescence (XRF)

XRF is a superior analytical technique used to determine the chemical composition of virtually all kinds of materials. It is a fast, accurate and non-destructive method with minimal sample preparation (Peter, 2003). The XRF technique applies the mutual fundamental principles, which encompasses interactions between beams and X-rays. The interaction of atoms with the radiation makes it possible for determination of main and minor elements in topographical materials by XRF.

Short wavelength radiation such as X-rays ionize the test materials. The inner shell electron is extricated and this makes the atom unstable. The outer shell electron replaces the missing inner electron. This results in release of energy since the inner shell electron is more strongly bound as compared with the outer electron shell (Skoog *et al.*, 2007). The primary incident X-ray referred to as fluorescent has higher energy than the emitted radiation. With known and fixed energy differences between electron shells, the emitted radiation always has characteristic energy and the resulting fluorescent X-rays can be used to detect the abundances of elements that are present in the sample (Steven, 2011).

2.5.2 X-Ray Diffraction (XRD)

XRD is a convenient analytical method commonly used in characterization of crystalline, fine-grained materials such as cement (Scrivener *et al.,* 2017). When compared to other classical quantitative analytical techniques such as Bogue calculation and optical spectroscopy, XRD offers a wide range of advantages such as ease in handling, accuracy and faster generation of results (Snellings *et al.,* 2014; Aranda *et al.,* 2012; Le Saoůt *et al.,* 2011). Just like the other kinds of electromagnetic radiation, the passage of X-radiation through a crystalline sample causes partial scattering of X-rays. This is due to the interaction between the electric vector of the radiation and the electrons in the atom of the crystalline sample (Skoog *et al.,* 2007). The scattering of the X-rays by the ordered environment in a crystal, results in constructive and destructive interferences among the scattered rays. Following the Bragg's law, construction interference happens when the distances between the scattering centers are of the same order of magnitude as the wavelength of radiation. This results in a diffraction peak (Skoog *et al.,* 2007).

The diffraction of X-rays by a crystalline material produces an XRD pattern consisting of peaks of varying intensities at characteristic angles (Scrivener *et al.,* 2017). The diffraction angle or position of the peaks is determined by the symmetry and the size of the unit cell through Braggs' law, while the intensities of the peaks relate to the nature and disposition of the atoms within the unit cell of the crystalline material. This way XRD produces patterns of peak positions and relative intensities that characterize different crystal structures and enable identifying their presence in unknown samples (Snellings *et al.,* 2014). XRD can be used to quantify the degree of hydration of the anhydrous cement and can provide information on the formation of individual hydrate phases (Scrivener *et al.,* 2017).

2.5.3 Fourier Transform Infra-Red (FT-IR)

Fourier transform infrared is the most preferred method of infrared spectroscopy (Thermo Nicolet Corporation, 2001). It is a non-destructive technique, precise and fast with ability to collect scans every second and it has greater optical through put. FTIR spectroscopic analysis technique has been very critical for years in both academia and industry. It has been widely used for structural and compositional analysis (Meisam *et al.,* 2020). An infrared spectrum characterizes a pattern of a sample with absorption peaks, which match with the frequencies of vibrations between the bonds of the atoms making up the material (Aastah, 2017). In IR spectroscopy, both absorption and transmission takes place.

FTIR operation follows an emission of a beam containing full spectrum of frequencies from the IR source. The beam enters an interferometer before it reaches the sample, where a beam splitter divides the original beam into two. The two split beams are interfered with each other by certain configuration of mirrors. The resultant beam from the interferometer is transmitted to the sample compartment and the light at particular wavelength absorbed by the test samples. The installed detector not only collects the light leaving the sample compartment, it also measures its intensity and produces the raw data ready for processing in the computer by Fourier transformation. FTIR can be used to characterize the composition of the hydrated cement materials (Scrivener *et al.,* 2015).

2.5.4 Scanning Electron Microscopy (SEM)

Scanning electron microscopy (SEM) is one of the most powerful technique used for studying the microstructure of cementitious materials (Scrivener *et al.,* 2017). The technique enables the visualization of morphology characteristics of the test sample (Shoukry *et al.,* 2016). The data

obtained in SEM tests is a function of interactions of the high-energy electron beam with the test material under investigation.

Many collisions occur before the electron's energy is completely dissipated due to the thick sample size. The interaction "volume" is the volume in which these collisions occur. The size of this interaction volume is a few microns for the cementitious materials, which are composed of elements with a faulty low atomic number. Secondary electrons (SEs), backscattered electrons (BSEs) and characteristic X-rays are the three most important signals produced. In all situations, images are created by scanning the electron beam across the surface in a raster pattern and determining the intensity of each point in the image using the signal detected at each location. The specimen is magnified simply by the scale difference between the incident beam and the picture rasters (Scrivener *et al.*, 2017).

CHAPTER THREE

MATERIALS AND METHODS

3.1 Introduction

This chapter describes the test samples, preparation procedures and the analytical techniques for the study. *Thiobacillus intermedius, Starkeya novella and Acidithiobacillus thiooxidans* bacteria spores were obtained from Leibniz-Institut DSMZ Deutsche Sammlung Von Mikroorganismen und Zellkulture GmbH in Germany. Analytical grade reagents were obtained from Kobian Kenya Limited and distilled water were used to prepare standard solutions. Culturing of bacteria solutions was conducted at the Microbiology Laboratory of University of Embu.

Test cements were sampled from Savannah Cement Limited at Athi River grinding plant in Machakos County, Kenya. Chemical analysis, XRF testing, physical and mechanical testing of the test cements were carried out at the laboratories in Savannah Cement Limited. Scanning Electron Microscopy (SEM) analysis on the hydrated mortars was carried out at the University of Pretoria-Hatfield campus, South Africa. FTIR analysis was carried out at the laboratories in United States International University (USIU)- Africa. XRD analysis was carried out at the government of Kenya laboratories in the Ministry of Transport and Infrastructure, Nairobi. The apparatus, both glass wares and plastic used to set up various tests were thoroughly washed using running water and a suitable detergent, rinsed with distilled water and dried appropriately in the oven set at 60 °C. All the tests were conducted in triplicates and average values obtained.

3.2 Materials

Commercial test cements of the type Ordinary Portland cement (OPC) type 42.5 and Portland pozzolana cement (PPC) type 32.5 were sampled from Savannah Cement Limited. Standard sand conforming to ISO 679:2009 and EN 196-1 was obtained from Xiamen ISO standard sand company limited in China and used to prepare all the test mortar prisms. Bacteria solutions from each of the bacteria strain were used as either mixing water, curing water or both. Distilled water was used to prepare the control mortar prisms.

3.3 Methods

3.3.1 Chemical Analysis of Test Cements

3.3.1.1 Loss on Ignition (LOI)

Loss on ignition in all the test cements was determined in accordance with KS EAS 148-2 (2017) standard. 1.000g of each test cement was weighed and placed in a crucible that had previously been ignited and tared. The covered crucible was placed in the electric furnace controlled at 975 °C ± 25 °C. After heating for 5 minutes, the lid of the crucible was slid slightly without removing it to allow for the escape of gases and moisture and to prevent the loss of particles adhering to the lid. The crucible was left in the furnace for a further 55 minutes. The crucible was cooled to room temperature in a desiccator and the constant mass determined. The observed LOI was expressed in percentage as calculated in the equation 3.1.

$$\text{Observed loss on ignition} = \left(\frac{(m_a - m_b)}{m_a} \right) \times 100 \qquad 3.1$$

Where m_a is the mass of the test portion and m_b is the mass of the ignited test portion

3.3.1.2 Gravimetric Determination of Sulphates

Sulphates, as SO_3 content in test cements was determined in accordance with KS EAS 148-2 (2017). 1.000g of each test cement was placed in a 250 ml beaker. In it, 90 mL of cold distilled water was added followed by 10 mL of concentrated hydrochloric acid. The mixture was stirred vigorously using a glass stirring rod. The solution was heated gently in an industrial hot plate and the sample crushed with a flattened end of a glass-stirring rod until decomposition of test cement was complete. The solution was allowed to digest for 15 minutes at a temperature just below boiling. The contents were filtered in a 400 mL beaker using Sartorius filter paper number 390.

The residue was washed thoroughly with hot water and the presence of free chlorides checked by using silver nitrate solution. The volume of the filtrate was adjusted to 250 mL. The resultant residue was kept in the original beaker for determination of insoluble residue (IR). The obtained filtrate was placed in hot plate and while stirring vigorously, 10 mL of 0.5M barium chloride was introduced drop wise. Heating was continued for a period of 15 minutes to properly form a stable precipitate. The solution was allowed to stand for a 24 hour duration in an oven with temperature kept at 60 °C.

Filtration was carried out using Sartorius filter paper number 392. The residue was carefully washed with hot distilled water until it was free from chlorides and the presence of chlorides tested using silver nitrate solution. The resultant residue was transferred into a silica crucible which was previously ignited and tared. SO_3 content was thereafter determined by igniting the residue for a period of 15 minutes at the furnace set at 975 °C ± 25 °C. The percentage SO_3 content was calculated as shown in equation 3.2.

$$SO_3 = \left(\frac{m_d}{m_c} \times 0.343 \right) \times 100 \qquad 3.2$$

Where m_c is the mass of the test portion and m_d is the mass of the precipitate.

3.3.1.3 Insoluble Residue (IR)

To the preserved residue obtained in section 3.3.1.2 above, 100 mL of 0.5M Na_2CO_3 solution was added and the contents boiled in hot plate for a period of 15 minutes until the solution turned brown in colour. The resultant mixture was filtered in a 400 mL beaker using Sartorius 390 filter paper and the residue washed using hot distilled water. The residue was further washed four times using hot solution of 0.5N HCl. The contents were rinsed with hot distilled water until the residue was free from chlorides. This was confirmed using a solution of silver nitrate. The residue was transferred into a silica crucible previously tared and ignited in a furnace set at 975 °C ± 25 °C. Cooling was done in a desiccator and the insoluble residue expressed in percentage as calculated in equation 3.3.

$$\text{Insoluble residue (IR)} = \left(\frac{m_f}{m_e} \right) \times 100 \qquad 3.3$$

Where m_e is the mass of the test portion and m_f is the mass of the ignited insoluble residue.

3.3.1.4 Chloride Content

KS EAS 148-2 (2017) standard was used to determine the chloride content in test cements. 5.000g of each test cement was placed in a 250 mL beaker. 50 milliliters of deionized water was carefully measured with measuring cylinder and introduced into the sample. While stirring using glass rod, 50 mL of 0.5N HNO_3 was gently added. The mixture was boiled on a hot plate and 5 mL of 0.05M

$AgNO_3$ was added to the boiling solution. The contents were further boiled for one minute. The resultant mixture was filtered into a 500 mL conical flask using sartorius filter paper number 390 which had previously been washed with 0.01N HNO_3 solution.

The residue was washed using 0.01N HNO_3 until the volume of the filtrate reached 200 mL. 5 mL of ammonium ferrous sulphate indicator solution was added to the filtrate and the solution titrated against 0.05M ammonium thiocyanate solution while shaking vigorously. The end point was characterized by a faint reddish colour change. The volume of the NH_4SCN used was recorded as V_1. The same procedure was repeated without the test cement sample and the volume of NH_4SCN recorded as V_2 for the blank titration. The chloride (Cl^-) content in test cements was expressed in percentage as calculated in equation 3.4.

$$Cl^- = 0.1773 \times \frac{(V_2 - V_1)}{m_1} \qquad 3.4$$

Where m_1 is the mass of the test cement portion, V_1 is the volume of the ammonium thiocyanate solution used for the titration of the test solution and V_2 is the volume of the ammonium thiocyanate used for the titration of the blank solution.

3.3.2 X-Ray Fluorescence (XRF) Analysis

The XRF instrument employed in determination of the cement oxides was of the model Epsilon 3^{XLE}. The oxides of Calcium, Magnesium, Alumina, Iron, Silica and Sodium and Potassium expressed as alkalis from each test cement were determined. The test samples were first pulverized in Herzog pulverizer machine and sieved through a 45μ sieve. This was done to achieve a uniform particle size distribution. 0.900g of each of the pulverized test cement was precisely placed in a

platinum crucible and in it, 9.000g of lithium tetraborate added to serve as flux was added. The contents were mixed carefully and resultant mixture fused in a M4 gas fusion. The temperature was set at 1200 °C unit and the fusion was carried out for a period of 17 minutes to form a cement bead. The formed cement beads were kept in desiccator for a period of 24 hours to stabilize before transferred into the XRF unit for measurement. This procedure was repeated three times for each test cement and the average oxide values tabulated.

3.3.3 Growth of Microbial Cultures

Pure spores of *Thiobacillus intermedius, Starkeya novella and Acidithiobacillus thiooxidans* obtained from DSMZ- German collection of microorganisms and cell cultures GmbH were cultured in accordance with BS EN 12322: 1999 at the Microbiology Laboratory of University of Embu. For each bacteria strain, 1000mL broth medium was prepared using the specified nutrients to achieve a microbial solution with optical density of 1.0 at 600 nm determined using UV/VIS spectrometer. The prepared bacterial solutions were kept separately for a period of 5 days. This was done to facilitate attainment of stable pH state.

3.3.3.1 Culturing of *Thiobacillus intermedius*

The medium for the actively growing culture of *Thiobacillus intermedius* was prepared as per the DSM- 18155 supplier's manual as shown in table 3.1. 0.10 g of NH_4Cl, 3.00 g of KH_2PO_4 and 20.00 g of Agar dissolved in 900 mL distilled water. The pH of the resultant contents was adjusted to 6.0 using NaOH to achieve the desired optimal growth of the bacterium (Munyao *et al.*, 2020c). The prepared solution was labelled as solution A. 0.01 g of $MgCl_2.6H_2O$, 0.14 g of $CaCl_2.2H_2O$ were dissolved in 100.00 mL distilled water. This formed the stock solution that was sealed and

labeled as solution B. Both solutions A and B were autoclaved at a temperature of 127°C separately and allowed to cool.

Table 3.1: Composition of the *Thiobacillus intermedius medium*

Culture Medium	**Quantity**
NH_4Cl	0.10 g
KH_2PO_4	3.00 g
Agar	20.00 g
$MgCl_2.6H_2O$	0.10 g
$CaCl_2.2H_2O$	0.14 g
$Na_2S_2O_3.5H_2O$	5.00 g
Yeast Extract	1.00 g

After cooling, solutions A and B were mixed together to form the medium for the bacterial growth. The spores of *Thiobacillus intermedius* was introduced into the cooled solution medium. In it, prepared solution of $Na_2S_2O_3.5H_2O$ and yeast were further added to serve as the nutrients for the bacteria. Incubation of the bacteria was monitored in a shaker maintained at 30 °C for a period of 7 days. The concentration of the bacteria was maintained at 1.0 X 10^7cells/mL as measured using a spectrophotometer. The obtained bacterial solution was packaged and transferred to laboratories at Savannah Cement Limited. The obtained solution was used as both mixing and curing media for the test cements.

3.3.3.2 Culturing of *Starkeya novella*

Preparation and growth of *Starkeya novella* was conducted in accordance with DSM 506 requirement. Table 3.2 shows the composition of the culture medium.

Table 3.2: Composition of *Starkeya novella* medium

Culture Medium	**Quantity**
$Na_2HPO_4.12H_2O$	10.60 g
KH_2PO_4	1.50 g
NH_4Cl	0.30 g
Yeast Extract	0.30 g
Phenol red solution(0.1% w/v)	2.00 ml
Batco Agar	15.00 g
$MgSO_4.7H_2O$	0.10 g
$Na_2S_2O_3.\ 5H_2O$	5.00 g

10.60 g of $Na_2HPO_4.12H_2O$ was accurately weighed into a sterilized glass container. In it, 1.50 g of KH_2PO_4 was added followed by 0.30 g of NH_4Cl and 0.3 g of yeast extract. 2.00 ml of phenol red solution was then added followed by 15.00 g of the bacto agar. 0.10 g $MgSO_4.7H_2O$ was then added and the resultant contents dissolved into 1000 ml distilled water. The prepared solution was autoclaved at temperature of 125 °C. It was then allowed to cool.

Spores of *Starkeya novella* was introduced into the cooled solution. $Na_2S_2O_3.\ 5H_2O$ prepared from dissolving 5.00 g of $Na_2S_2O_3.\ 5H_2O$ into 50.00 ml of distilled water was then added to the mixture. The incubation of the bacteria was carried out for a period of 5 days. The bacteria concentration

maintained at 1.0 X 10^7 cell/ml was monitored using spectrophotometer. The resultant bacteria solution was packaged and transferred to laboratories at Savannah Cement Limited. The solution was used as both mix and curing media for the test cements.

3.3.3.3 Culturing of *Acidithiobacillus thiooxidans.*

Table 3.3 gives the summary of medium composition for the *Acidithiobacillus thiooxidans.*

Table 3.3: Composition of *Acidithiobacillus thiooxidans* medium

Culture Medium	**Quantity**
KH_2PO_4	3.00 g
$MgSO_4.7H_2O$	0.50 g
$(NH_4)_2SO_4$	3.00 g
$CaCl_2.2H_2O$	0.25 g
$Na_2S_2O_3.\ 5H_2O$	5.00 g

DSM 14887-preparation method was adopted to prepare the medium for the *Acidithiobacillus thiooxidans* bacteria. Definite amounts of KH_2PO_4, $MgSO_4.7H_2O$, $(NH_4)_2SO_4$ and $CaCl_2.2H_2O$ as provided in table 3.3 were dissolved in 1000 mL of distilled water. The pH of the resultant mixture was adjusted to 4.4 using sulphuric acid. Autoclaving was then done at a temperature maintained at 121° C for 15 minutes. The prepared $Na_2S_2O_3.\ 5H_2O$ was sterilized through filtration and added to the autoclaved mixture. Spores of the *Acidithiobacillus thiooxidans* was added to the cooled mixture and incubated statically without shaking for a period of 30 days. The obtained bacteria solution of concentration 1.0 X 10^7 cells/ml was packaged and transferred to laboratories at

Savannah Cement Limited. The solution was used as both mixing and curing media for the test cements.

3.3.4 Determination of Optical Densities for the Microbial Solutions

Hitachi UV-1900 UV- visible wavelength spectrophotometer instrument was used to determine the optical density for each of the bacterial solution. 1 mL of each of the cultured bacterial solution was placed in a 1.6 mL optical polystyrene cuvette. The cuvette holding the sample solution was then placed in the spectrophotometer instrument set at a wavelength of 600 nm. OD-600 measurements were employed to determine the bacterial growth as well determine the cell numbers at the beginning of the experiment and to construct the growth curves of the bacteria. The obtained bacterial concentration was maintained during the casting and the curing of the test cements.

3.3.5 Physical Analysis

Physical analysis of the test cements was carried out to determine the standard consistency setting time and soundness of the test cements. Preparation of the cement paste for setting time and soundness was done using each bacteria solution and labelled according to the bacteria and cement type. For OPC test cement, the prepared cement paste using the bacteria solution were labelled as OPC (SK), OPC (TI) and OPC (AT) while in PPC it was labelled as PPC(SK), PPC(TI) and PPC (AT) respectively. The control cement paste prepared using distilled water were labelled as OPC (H_2O) and PPC (H_2O) respectively. Each test was carried out in triplicates and the average values obtained.

3.3.5.1 Determination of Setting Time

3.3.5.1.1 Standard Consistence Test

Prepared microbial solutions for each test bacteria were used as mixing water in determination of setting time for each test cement. Distilled water was used as a control in both OPC and PPC test cements. In order to determine the setting time of the test cements, standard consistency was first carried out in accordance with KS EAS 148-3 (2017) to evaluate the water demand requirement. Vicat apparatus with the plunger were used to perform the test. 125 g of water / bacterial solution was weighed and carefully put into the paste mixer bowl already mounted on the mixer unit of the model NJ-160. In it, 500 g of the test cement was carefully added. The mixer was switched on and automatically ran at a slow speed for the first 30 seconds to ensure uniform mixing of cement and water and thereafter at high speed for a period of 210 seconds. After mixing, th**e** paste was transferred immediately to the mould, which had been previously placed on a lightly greased plane glass base-plate and filled in excess without undue compaction or vibration. The excess was removed by a gently sawing motion with a straight-edged implement in such a way as to leave the paste filling the mould and having a smooth upper surface.

The Vicat apparatus was calibrated with the plunger by lowering the plunger to rest on the baseplate to be used and adjusting the pointer to read zero on the scale. The plunger was raised to the stand-by position. Immediately after levelling the paste, the mould and baseplate were transferred to the Vicat apparatus and positioned centrally under the plunger. The plunger was lowered gently until it was in contact with the paste. Pausing was done for two seconds to evade the original momentum and compelled velocity of the parts in motion. Subsequently, the parts in motion were released promptly and the plunger allowed to vertically go through the paste at the

central point. Releasing of the plunger was done four minutes from zero time and the scale read when penetration stopped.

Scale-reading was recorded, and it indicated the length from the bottom-part of the plunger and the baseplate whereas the amount of the water used was determined in percentage form by cement mass. After each penetration test, the used plunger was cleaned immediately. Repeatability tests were carried out with cement pastes comprising of various amounts of water till a distance of 6 mm between the baseplate and the plunger was achieved. The water content of that paste was recorded to the nearest 0.5 % as the water for standard consistency.

3.3.5.1.2 Determination of initial setting time

The Vicat apparatus was calibrated by lowering the needle to rest on the baseplate and adjusting the pointer to read zero on the scale. The needle was raised to the stand-by position. A Vicat mould was filled with paste of standard consistence and levelled. The filled mould and the baseplate were placed in the humidity cabinet, after a suitable time, it was transferred to the Vicat apparatus and placed under the needle. The needle was lowered gently until it was in contact with the paste. Pausing was done to avoid initial velocity or forced acceleration of the moving parts. The moving Part was the released quickly and the needle allowed to penetrate vertically into the paste. The scale was read when the penetration ceased.

The scale reading was recorded which indicated the distance between the end of the needle and the baseplate, together with the time from zero. The penetration was repeated on the same specimen at conveniently spaced positions, not less than 10 mm from the rim of the mould or from each other at conveniently placed intervals. Between the penetration tests the specimen was kept

in the humidity cabinet. The Vicat needle was cleaned immediately after each penetration. The time measure from zero was recorded at which the distance between the needle and the baseplate was 4 mm as the initial setting time of the cement to the nearest 5 minutes. The required accurateness was ensured by decreasing the duration gap between penetration tests close to the endpoint and observing the successive results not to fluctuate.

3. 3.5.1.3 Determination of final setting time

The filled mould was inverted on its base-plate so that the tests for final set were made on the face of the specimen original in contact with the base-plate. The needle was fitted with a ring attachment which aided in observing very minute penetrations correctly. The time measured from zero at which the needle first penetrated only 0.5 mm into the specimen was recorded as the final setting time of the cement.

3.3.5.2 Determination of Soundness

Soundness test was done in accordance with KS EAS 148-3 (2017). Le Chatelier apparatus was used where the mould was of spring brass with indicator needles. A pair of plane glass base and cover were provided for each mould. Each test cement paste prepared using either distilled water or bacterial solution was subjected to soundness test.

The test was carried out simultaneously on three specimens of the same batch of cement paste. The paste was prepared from a known normal consistency as defined in section 3.3.5.1.1. A lightly oiled Le Chatelier mould was placed on the lightly oiled baseplate and filled instantly without undue compaction or vibration using only the hands and a straight-edged implement to the level

of the top surface. During filling, split of the mould was prevented from accidental opening. The mould was covered with the lightly oiled cover plate, and the complete apparatus immediately placed in the humidity cabinet. It was maintained for 24 h at 25 ^{0}C.

At the end of the 24 h period, the distance between the indicator points was measured to the nearest 0.5 mm. The water was gradually brought to boiling, with the moulds kept submerged, during 30 min and the water bath maintained at a boiling temperature for 3 h. The mould was allowed to cool to 25 ^{0}C. The distance between the indicator points was measured to the nearest 0.5 mm. For each specimen the measurements were recorded and the difference calculated. The mean of the three values was then calculated to the nearest 0.5 mm.

3.3.6 Mechanical Analysis

The mechanical performance of the test cements at different regimes were monitored using the compressive strength development. The prepared bacteria solutions were used as either mixing water or both as mixing and curing media for the prepared test cements. Mortar prisms prepared using bacterial solution as mixing water and cured in water for the OPC test cement were labelled as OPC SK-H, OPC TI-H and OPC AT-H whereas mortar prisms prepared and cured in bacterial solutions were labelled as OPC SK-SK, OPC TI - TI and OPC AT-AT. Similar labeling method was adopted for PPC test cements as well. The prepared mortar prisms using distilled water and cured in 1.5% sulphuric acid were labelled as OPC- H^+ and PPC- H^+ while the control mortar prisms prepared and cured in distilled water were labelled as OPC H-H and PPC H- H respectively.

3.3.6.1 Mortar Preparation and Curing

KS EAS 148-1 (2017) standard was adopted in preparation of the test cement mortar prisms. The automated mortar mixer of the model JJ-5 was used in mortar preparation. Mortar prisms from each of the test cements of the size 40 mm x 40 mm x 160 mm were prepared from a batch of a plastic mortar. 450 g of each of the test cement was carefully weighed and placed into a mixing bowl. In it, 225 g of water was added. The mixer was allowed to run slowly for 30 seconds. 1350 g of standard sand already placed in an automated pour trough was steadily added for the next 30 seconds. The mixer was switched to a higher speed and the mixing continued for an additional 30 seconds. The mixer was stopped for 90 seconds and during the first 15 seconds all the mortar adhering to the wall and bottom of the bowl was removed with a rubber scraper and placed in the middle of the bowl. The mixing was finally continued at a higher speed for further 60 seconds.

The moulding of the specimen was done immediately after the preparation of the mortar. With the mould and hopper firmly clamped to the jolting table and using a suitable scoop, in one or more increments, the first of two layers of mortar (each about 300 g) was put into each of the mould compartments directly from the mixing bowl. The layer was spread uniformly using the larger spreader held vertically with its shoulders in contact with the top of the hopper and drawn forward. The first mortar layer was compacted using 60 jolts. The second layer of mortar was put in and leveled with the smaller spreader and compacted with a further 60 jolts. The mould was lifted gently from the jolting table and the hopper removed. The excess mortar was immediately struck off with the metal straight edge held almost vertically and moved slowly with a transverse sawing motion once in each direction. The surface of the specimens was smoothened using the same straight edge held almost flat. The moulds were labeled to identify the specimens and their position

relative to the jolting table. The moulds with the mortar were placed into a temperature-controlled cabinet at a temperature of 22 ± 1 °C for 24 hours duration. Demoulding of the mortar prisms was done after 24 hours. The prisms were properly labelled as described in section 3.3.6. Curing was done by submerging the marked prisms vertically in curing containers filled with distilled water or bacteria solution at 25 ± 2 °C in a curing room. All the test cements were subjected to a maximum curing period of 90 days.

3.3.6.2 Determination of Compressive Strength

Compressive strength was determined in accordance with KS EAS 18-1 (2017). Compressive strength performance for each test regime was monitored after 2^{nd}, 7^{th}, 28^{th} 56^{th} and 90^{th} day of curing. The equipment used to determine the compressive strength was of the model YAW-300. Each mortar prism to be tested was first split into two using flexural strength machine model DKZ-5000. The mortar prism was then centered to the platens of the compressive equipment within ± 0.5 mm and longitudinally such that the end face of the prism overhangs the platens or the auxiliary plates by about 10 mm. Increasing of the load was done smoothly at the rate of 2400 ± 200 N/s over the entire load application until fracture. Triplicate results were obtained for all the test regimes. Compressive strength was calculated and expressed in MPa.

3.3.7 Mineralogical and Microscopic Analysis of Hydrated Cement

3.3.7.1 Fourier Transform Infra-Red Spectroscopy (FTIR) Analysis

FT-IR analysis was carried out on hydrated cement mortars after 28^{th} day of curing. The equipment model was Jasco FTIR -4700 with ATR pro head and TGS detector. Both control and microbial test samples for PPC and OPC were first pulverized using Herzog pulverizing equipment. The

resultant powder for each of the test sample was carefully sieved through a 45µ sieve and kept in airtight sample bag. Each sample was loaded into the FTIR equipment set at 10 scans per second with resolution set at 4.0 cm^{-1}. The scan range of the FTIR was set at 600 – 4000cm^{-1}.

3.3.7.2 X-ray Diffraction (XRD) Analysis

The XRD analysis was carried out on the hydrated mortars of control and microbial PPC and OPC test cements after 28th day of curing. Bruker AXS XRD equipment model D2 Phaser SSD 160. Samples were finely ground using Herzog-pulverizing machine and sieved through 45µ sieve. The obtained powder for each test sample was kept in airtight sample containers. During the analysis, each sample was loaded into a sample holder and the surface carefully levelled. The sample surface area and thickness was maintained large enough to avoid beam overflow and sample transparency deviation.

3.3.7.3 Scanning Electron Microscopy (SEM) Analysis

The scanning electron microscopy study was determined after 28th day of curing using Zeiss Ultra Plug FEG- SEM instrument. Sample preparation was done in accordance with ASTM C1723-16. A slice of each hydrated mortar sample of 3 mm size was separately immersed in a cylindrical container filled with isopropanol for a period of 7 days. The isopropanol solvent was changed at an interval of every 24 hours for a period of 3 days. This was done to stop the hydration and ensure optimal removal of water from the hydrated mortars. After stopping the hydration, the samples were transferred into a vacuum drying in a desiccator for a period of 48 hours.

The samples were then impregnated using a low viscosity epoxy resin of the type EPO-TEK-301. After impregnation, the resin was left to harden for a period of 24 hours. The samples were then subjected to polishing using the SiC paper at 150 rpm with isopropanol as a lubricant. The samples were then further rinsed with isopropanol and then polished with sprays of diamond powder. The fully polished samples were kept in air-tight desiccators for a period of 2 days. This was done to allow evaporation of all the chemicals, which could contaminate the SEM chamber. Samples were then loaded in SEM equipment for analysis.

3.3.8 Sorptivity Coefficient Analysis

Both control and microbial test samples were subjected to sorptivity testing after 28^{th} day of curing in accordance with ASTM C 1585-04. The hydrated mortars from each of the test regime (control and bacterial treated mortar prims) were dried in an oven set at 100 °C and their masses recorded in grams (M_i grams) prior to the application of the water proofing resin. A water proofing resin was used to make a coat of two layers on all sides of the dried test mortar prism excluding the top and bottom as the exposure parts. This was done in order to ensure unidirectional absorption/ flow through the untreated side only. Water was put into a 400ml beaker to a height of 50 mm and in it, test prism already applied with water proofing resin was immersed with the untreated coated side facing downwards at 2 mm above the base of the mortar as shown in figure 3.1.

Figure 3.1: Experimental set up for Sorptivity Test

After the lapse of the first time interval (0.25 hours) the test prism was carefully removed from the water and wiped using a clean face towel. Its mass was recorded and immediately immersed in water to monitor the subsequent time intervals. At every time interval, the mass was weighed and recorded. This sequence was repeated for all the test samples until the 168th hour when the saturated mass of infiltration was obtained. The sorptivity coefficient (k) for all the test motors was obtained using equation 3.5

$$\frac{Q}{A} = kt^{1/2} \qquad 3.5$$

Where Q represented the amount of water absorbed while A was the cross-section area of the test sample in contact with water and t was time in hours. The values of k (sorptivity coefficients) were determined graphically by plotting Q/A against the square root of time.

After every defined time interval (0.25 hours – 168 hours), the percent water absorptivity for all the test mortar regimes was determined using equation 3.6 below

$$\%W_{Abg} = \left(\frac{M_{An} - M_i}{M_i}\right) * 100 \qquad 3.6$$

Where W_{Abg} is the percent increase/gain of water absorption by the test mortar after immersion in water for a given period expressed in hours, M_{An} is the mass increase of mortar after the n^{th} time of exposure in water. In this study, the time of immersion varied from 0.25 hours up to 168 hours. M_i is the initial mass of test mortar before immersion in water.

3.3.9 Ion Diffusion Analysis

Both control and microbial mortar prisms made using OPC and PPC were subjected to diffusivity test after the 28^{th} day of curing. ASTM C1556 (2016) test standard method was adopted in determination of diffusivity test. The test mortar prisms measuring 40 mm X 40 mm X 160 mm were reduced to a size of 40mm X 40 mm X 100 mm using diamond-cutting disc. According to ASTM C1556 (2016), an electrochemical cell was set up and the test mortar prism was placed between two cells and properly covered with a fabric material.

500 mL of water was filled in the anodic chamber and an equivalent volume of 3.5% NaCl or Na_2SO4 was put in the cathodic chamber. Stainless steel was placed on both sides of the test prism to serve as an electrode. The electrodes were connected to a 12 ± 0.1 V D.C power source. The container was covered at the top using a polythene paper. Monitoring of the current between the electrodes through the mortar was recorded after every 30 minutes using a milli-ampere. The

container was covered at the top using a polythene paper. The entire experimental set up was maintained at a temperature of 22 ± 1 °C for a period of 36 hours. During this period, the solutions were stirred using a glass rod periodically. After the 36 hours, the test mortar prism was carefully removed from the set up and allowed do drain for 30 minutes.

The test mortar prisms were polished using a sand paper on the 40 mm X 40 mm surfaces. Drilling of the test samples was done at an interval of 10 mm using a drill bit with a radius of 15 mm along the 100 mm length surface of the test prism up to 80 mm. The collected sample from each interval (10mm, 20 mm, 30 mm, 40 mm, 50 mm, 60 mm, 70 mm and 80 mm) were dried in a laboratory oven set at 105 °C for a period of 1 hour. The obtained samples were further pulverized using Herzog pulverizing machine and sieved through 45μ sieve. The samples were then kept in airtight sample containers for chloride or sulphate analysis as defined in KS EAS 148-2 (2017).

3.3.9.1 Chloride and Sulphate Profiling Analysis

As defined in KS EAS 148- 2:2017, the chloride and sulphate ions were determined at each depth of penetration. According to Crank (1975), the approximation of apparent ion diffusion (chloride/ sulphate) coefficient was achieved under non-steady state condition assuming boundaries $C_{(x,\,t)} = 0$ at $t = 0$, $0 < x < \infty$, $C_{(x,\,t)} = C_s$ at $x = 0$, $0 < t < \infty$, constant effects of coexisting ions, linear chloride binding and one-dimension diffusion into semi-infinite solid. Equation 3.7 gives the Crank's solution to Fick's second law of diffusion.

$$C_{(x,t)} = C_s\left\{1 - \text{erf}\left(\frac{x}{(4D_{mig}\,t)^{1/2}}\right)\right\} \qquad 3.7$$

Where $C_{(x, t)}$ is the concentration of chloride/ sulphate ions at any depth *x* in the mortar bulk at time t, C_s is the surface concentration and D_{app} is the apparent diffusion coefficient. The error correction function, erf, is the Gaussian error function gotten from computer spreadsheets. The chloride / sulphate profiles were obtained from fitting equation 3.7 for each ion separately to experimentally determined chloride and sulphate profile concentration thus determining the values of D_{app} and C_s mathematically for chlorides and sulphates. Apparent diffusion coefficient (D_{app}) calculated from chloride / sulphate profiles is a common practice since D_{app} shows the capability of the mortar/concrete to resist chloride or sulphate penetration in a natural setting. D_{app} was determined using equation 3.8

$$D_{app} = \frac{RT}{Z_i F} D_{mig} \frac{Int^2}{\Delta\Phi} \qquad 3.8$$

Where R is the Gas constant, F is the faraday constant, T is the temperature of the electrolyte in K, Zi is the valency of the ion I, ΔØ is the effective applied voltage in V, t is the duration of the test/ exposure in seconds

3.4 Data Analysis

Test results were carried out in triplicates and the average values calculated. The significance difference in the means of normal consistency, setting times and soundness tests for control pastes prepared using OPC and PPC were determined using t-test. Similar analysis tool was adopted to determine the mean differences between the means of OPC and PPC pastes prepared using the selected bacteria solutions. One way Anova was used to determine the performance of the three selected bacteria on test cements. Graphical representation of results was used where applicable.

CHAPTER FOUR

RESULTS AND DISCUSSION

4.1 Introduction

This chapter presents the results and the discussion of the experimental study carried out on commercial OPC and PPC when exposed to different strains of deteriorating bacteria. The results include chemical composition of the commercial OPC and PPC, setting time and soundness for the cement pastes, compressive strength at different curing periods, sorptivity, Fourier transform infrared, X-Ray Diffractometer and Scanning Electron Microscopy for cured mortars.

4.2 Chemical Composition of the Test Cements

Table 4.1 gives the average chemical composition of the test cements. Except LOI and IR, the other parameters are expressed in terms of oxides. Both test cements met the chemical composition requirements as defined in KS EAS 18-1 (2017). From the test results, it is evident that CaO, SiO_2, Al_2O_3 and Fe_2O_3 form the main oxide composition of the test cement. These oxides provide the main hydration products in cement. Upon hydration, the resultant CH forms a suitable binding point with silica and alumina to form the C-S-H and C-A-H as the main hydration products. The formed hydration products improve physical, mechanical and microstructural properties of cement (Neville, 2011).

Table 4.1: Average Chemical Composition of Test Cements

% Oxide Composition	Cement Type	
	OPC	PPC
CaO	63.58 ± 0.05	44.20 ± 0.12
SiO_2	21.50 ± 0.02	32.80 ± 0.04
Al_2O_3	5.10 ± 0.01	10.80 ± 0.02
Fe_2O_3	3.55 ± 0.01	5.85 ± 0.01
MgO	2.20 ± 0.01	0.96 ± 0.03
SO_3	2.20 ± 0.03	2.10 ± 0.01
Na_2O	0.15 ± 0.01	0.06 ± 0.02
K_2O	0.62 ± 0.01	0.15 ± 0.01
IR	0.50 ± 0.01	27.92 ± 0.02
LOI	1.20 ± 0.03	2.30 ± 0.02

OPC exhibited significantly higher CaO content as compared to PPC. This was as expected since OPC is made up of 95% clinker and 5% gypsum (KS EAS 18-1:2017). Clinker is comprised of limestone as the main raw material, which upon calcination results in formation of CaO. The main phases of OPC (C_3S and C_2S) upon hydration results in increased calcium hydroxide (CH) in the pore solution. Equations 4.1 and 4.2 gives the hydration mechanism of C_3S and C_2S.

$$2C_3S + 6H \rightarrow C_3S_2H_3 + 3CH \quad 4.1$$

$$2C_2S + 4H \rightarrow C_3S_2H_3 + CH \quad 4.2$$

With high CH content in the pore solution of OPC, it makes it more vulnerable to attack by aggressive ions such as chlorides and sulphates (Munyao, 2015; Mutitu, 2013). The decreased CaO in PPC was attributed to clinker substitution with pozzolana. Generally, natural pozzolans have less than 2% CaO (KS EAS 18-1:2017).

The silica (SiO_2) content on the other hand was higher on PPC than OPC. This was attributed to the pozzolana addition in PPC. Natural pozzolans contain 55-60 % silica content. Whereas Portland clinker has silica in form of C_2S and C_3S, the additional amorphous silica from pozzolana helps improve the late strength development for pozzolanic cements (Munyao, 2015; Mutitu, 2013; Muthengia, 2009). The excess silica from PPC reacts with the resultant CH upon hydration to form secondary C-S-H, which offers long-term strength and durability of concrete structures. Incorporation of pozzolana in OPC increases the SiO_2 content that ultimately result in improved mechanical properties of cement (Mohamed *et al.,* 2016). Equation 4.3 shows the reaction between the resultant CH and SiO_2 in pozzolana.

$$3CH + 2S + 3H \rightarrow C_3S_2H_3 \qquad 4.3$$

PPC exhibited higher alumina (Al_2O_3) content than OPC. This was due to higher alumina composition in pozzolanic materials. The alumina content in OPC exists as C_3A phase. This phase is known to generate high heat of hydration that makes OPC have higher early days (1, 2 and 7 days) strength as compared to PPC. The alumina content in natural pozzolana only reacts with excess CH in the hydrated pore solution to form CAH as shown by equation 4.4.

$$A + H + CH \rightarrow CAH_2 \qquad 4.4$$

The formed secondary cementitious materials (C-A-H and C-S-H) through pozzolana addition in PPC results in a denser concrete or mortar material with reduced risk of attack by aggressive materials. This improves the durability of the placed pozzolanic cement structures.

The iron (Fe_2O_3) content was higher on PPC than OPC. This was attributed to pozzolana addition. Most of natural pozzolans contain iron content ranging from 10- 15% (KS EAS 18-1:2017). Ferrite when expressed as tetracalcium aluminoferrite (C_4AF) in Portland cement clinker has no cementing value in terms of mechanical and physical properties. This phase helps in giving cement the grey colour. During the calcination process, the ferrite acts as a flux to lower the calcination temperature (Neville, 2011).

The magnesium (MgO) content in Portland cements should be maintained below 5% (KS EAS 18-1:2017). From the test results, both OPC and PPC test cements conformed to the MgO requirement. When MgO in cement is above 5%, it causes expansion of the cement paste, mortar and /or concrete. The expansion may result to formation of micro-cracks within the concrete that forms suitable pathways for ingress of harmful materials such as carbon dioxide, sulphates and /or chloride ions, which are deleterious to concrete or mortar (Neville, 2011). Further, excess MgO slows down the initial hydration of cement. This affects the initial setting time (Munyao, 2015). The reaction between MgO and water results in formation of insoluble $Mg(OH)_2$. The formed $Mg(OH)_2$ precipitates on the cement grains forming a protective layer, which retards further hydration of cement. The reaction may lower the cement pore water pH (Liu *et al.*, 1992).

The sulphate (SO_3) content in both test cements met the KS EAS 18-1 (2017) requirement (≤ 3.5%). SO_3 mainly as $CaSO_4.2H_2O$, reduces the risk of flash setting (Ahmed *et al.,* 2021; Franco *et al.,* 2018; Silen and Mohammed, 2018). The SO_3 content plays a vital role in mitigating the heat generated by C_3A phase during the hydration. The hydrated sulphate, mainly as ettringite precipitates over the C_3A forming an impermeable layer that prevents early and fast hydration of C_3A. With time, the crystal cracks slowly allowing for C_3A hydration. The alternate crystallization and cracking slows the hydration process at early hours of cement hydration allowing for workability and placement of concrete or mortar (Ahmed *et al.,* 2021; Shupeng *et al.,* 2018; Kosmatka *et al.,* 2002)

The alkali content (Na_2O and K_2O) commonly expressed as total alkali or sodium equivalent met the desired KS EAS 18-1 (2017) requirement (≤ 0.6%) in the test cements. Presence of alkalis in cement provides the alkalinity in the hydrated cementitious material (Neville, 2011). The alkalinity content in cement protects the rebar in reinforced concrete from corrosion (Muthengia, 2009). Further, Na_2O and K_2O plays a vital role in providing a medium through which the cement phases react (Theodore and Karen, 2012).

The insoluble residue (IR) content in OPC test cement conformed to the desired KS EAS 18-1 (2017) requirement. While the standard limits insoluble residue for OPC at 5% maximum, there is no requirement for insoluble residue in PPC. OPC is expected to have nearly all the material dissolve when digested in hydrochloric acid. This is attributed to high reactivity of silica and alumina contained in clinker. Previous studies by Kraiwood *et al.,* (2000) showed that higher insoluble residue content in OPC reduces its mechanical properties. PPC on the other hand

incorporates natural pozzolana (25 - 40%) which has approximately 75% - 90 % insoluble materials (KS EAS 18-1:2017). The unreactive silica and alumina content in natural pozzolans make PPC based cements exhibit higher insoluble residue content (Munyao, 2015).

Loss on ignition, commonly expressed as LOI gives an indication of the amount of organic and volatile matter within the cement. According to KS EAS 18-1 (2017) and BS EN 197-1 (2011), LOI for both OPC and PPC should be below 5%. From the test results, OPC and PPC conformed to the standard requirements for LOI.

Based on the chemical analysis results, the test cements met all the desired chemical requirements as described in the Kenya and East African cement standard. This implied that the cements were suitable to be subjected to other physical and mechanical tests such as setting time, soundness and compressive strength.

4.3 Phase Composition of Test Cements

The phase composition of the test cements as given in table 4.2 was calculated using Bogue formula (Bogue, 1929).

Table 4.2: Phase Composition of Test Cements

% Phase Composition	**Cement Type**	
	OPC	**PPC**
C_3S	51.62 ± 0.02	36.13 ± 0.03
C_2S	22.7 ± 0.01	15.9 ± 0. 01
C_3A	7.52 ± 0.01	5.26 ± 0.02
C_4AF	10.8 ± 0.01	7.56 ± 0.01

The cement phases, which are estimated from Portland clinker, influence the performance of the placed concrete or mortar after hydration (Scrivener *et al.,* 2015). As expected, OPC exhibited higher percentage content in all the main cement phases. This was attributed to higher clinker proportion in OPC as compared to blended PPC (KS EAS 18-1: 2017). Cristelo *et al.* (2016), Munyao (2015) and Kurokawa *et al.* (2014), made similar observations.

C_3S and C_3A phases are responsible for early strength development. This explains why OPC exhibit very high strength at early days (KS EAS 18-1:2017; BS EN 197-1: 2011). The C_2S phase influences the strength development beyond 28 days after the placement of concrete and /or mortar while C_4AF provides the grey colour of the Portland cement (Neville, 2011). The reduced phase composition in PPC was attributed to the clinker substitution with pozzolana. Both test cements met the desired phase composition as defined in BS EN 197-1 (2011).

4.4 Physical Analysis

4.4.1 Standard Consistency Results

Figure 4.1 show the standard (normal) consistency of control OPC paste (OPC-H_2O) and the pastes of OPC subjected in varied bacteria solutions (OPC-AT, OPC -TI and OPC-SK).

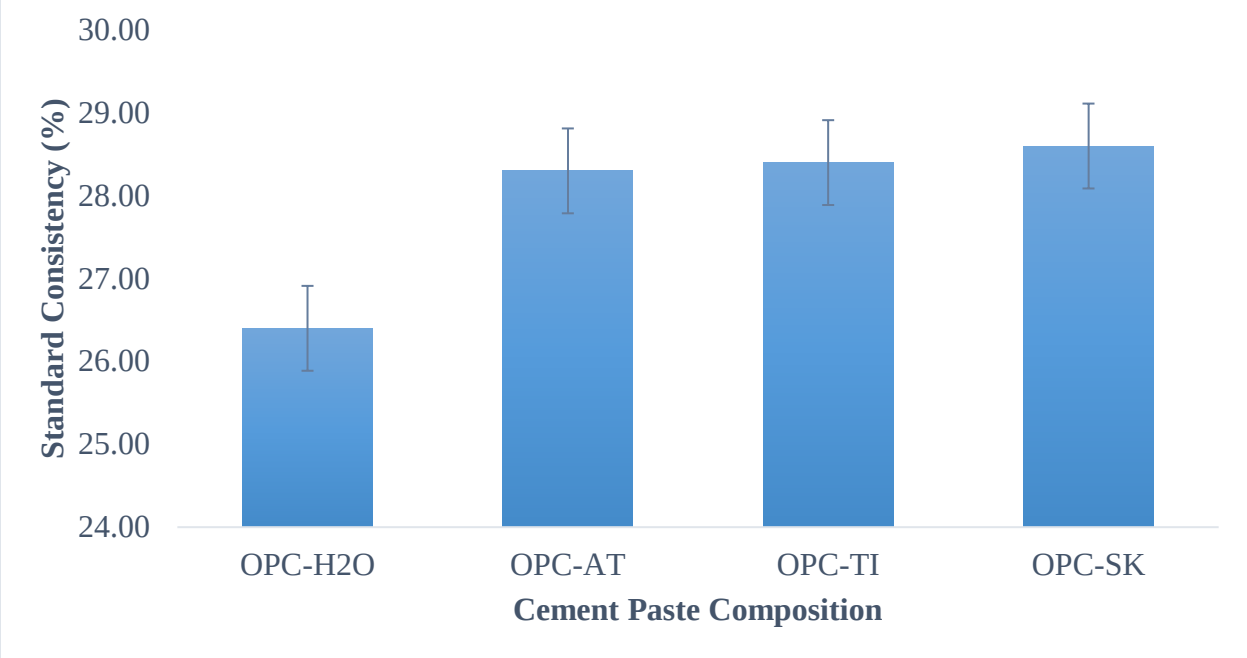

Figure 4.1: Standard consistency of control OPC Paste and Pastes of OPC Prepared in varied bacteria solutions as the Mixing water

The water demand (standard /normal consistency) for the control OPC (OPC-H_2O) varied significantly when compared with OPC- TI, OPC - AT and OPC - SK (T-test analysis carried out at 95% confidence level gave the t_{cal} value of 7.55, 6.93 and 3.67 for OPC -TI, OPC - AT and OPC- SK against the t_{crit} of 2.78). The OPC pastes prepared with bacteria solutions as the mix water required higher amounts of water to achieve workable paste. This was attributed to the different nutrients used to prepare the bacteria feed.

Figure 4.2 show the standard (normal) consistency of control PPC paste (PPC-H_2O) and the pastes of PPC subjected in varied bacteria solutions (PPC-AT, PPC -TI and PPC-SK).

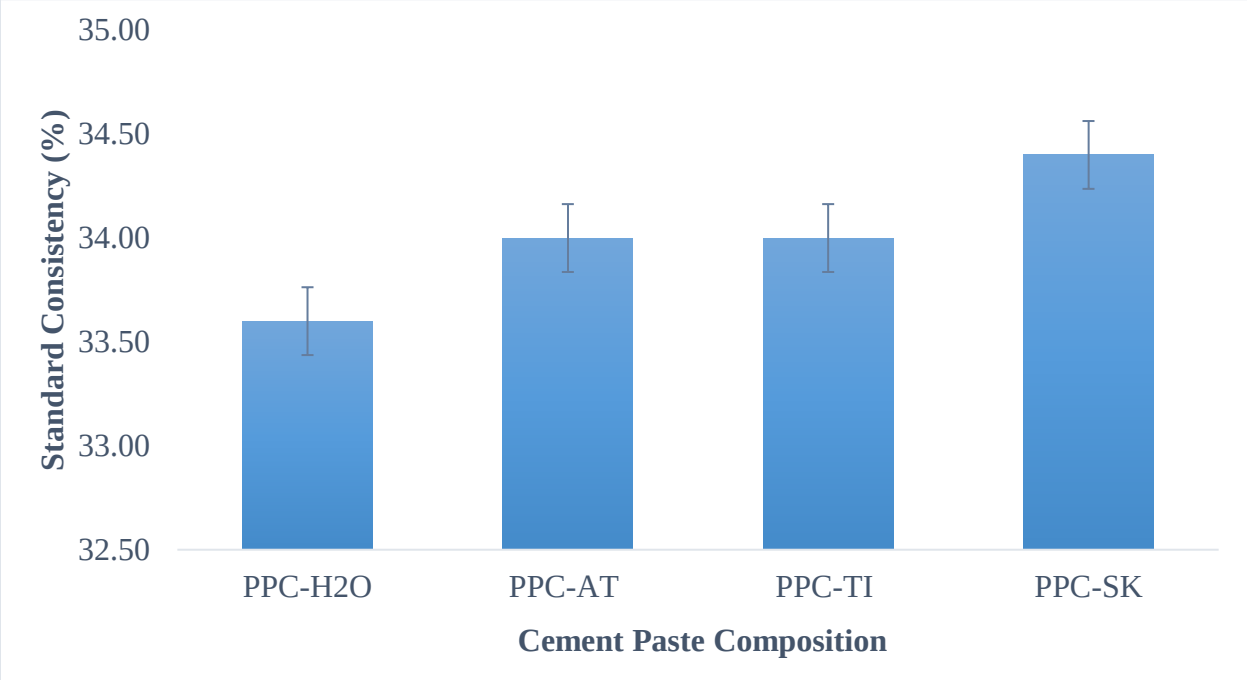

Figure 4.2: Standard consistency of control PPC Paste and Pastes of PPC Prepared in varied bacteria solutions as the Mixing water

The water demand of the PPC pastes prepared with the varied bacteria solutions (PPC- AT, PPC –TI and PPC-SK) varied significantly with the water demand of the control PPC (T-test analysis results carried out at 95% confidence level, showed the t_{cal} values of 4.43, 3.46 and 4.90 for PPC-AT, PPC-TI and PPC-SK respectively). PPC pastes prepared with bacteria solutions as mixing water required higher amounts of water to achieve the desired workability. This was attributed to sulphates, phosphates and chloride salts used to prepare the bacteria feeds (Dongxing *et al.*, 2021). Similar observations were made by (Shiyu *et al.*, 2021; Yingjie *et al.*, 2021).

The water demand of control OPC varied significantly with that of control PPC (T-test analysis gave the t_{cal} of 12.12 against the t_{crit} of 2.78). The high-water requirement in PPC was due to the pozzolana effect. Addition of pozzolana increases the fineness of the resultant product and hence high amount of water is required to achieve sufficient workability (Sihem *et al.,* 2021). Replacement of OPC with some pozzolanic materials such as fly ash and silica fume was found to increase the water requirement of the replaced OPC. This was attributed to the pozzolanic pore fineness (Dave *et al.,* 2017). Similar observations were made by Patrick *et al.* (2012).

The standard consistency test results met the desired requirements for all the test scenarios. BS EN-197 (2011) defines water demand for OPC and PPC to be maintained at ≤ 30% and ≤ 35% respectively. The observed differences in normal consistency of the control pastes and pastes prepared with microbial solutions for both PPC and OPC test cements was attributed to the composition of the different bacterial nutrients. Mutitu (2020), while studying on the effect of microbial biocementation on physico-chemical and mechanical properties of mortars made from Portland cement observed that bacterial nutrients influence the water uptake by the cement. This affects the normal consistency of the resultant cement paste. Hamdy *et al.* (1999), made similar observations.

4.4.2 Setting Time Results

Figures 4.3 and 4.4 show the initial setting time (IST) and final setting time (FST) for the controls of OPC and PPC and their respective pastes prepared using selected bacteria solutions as mixing water.

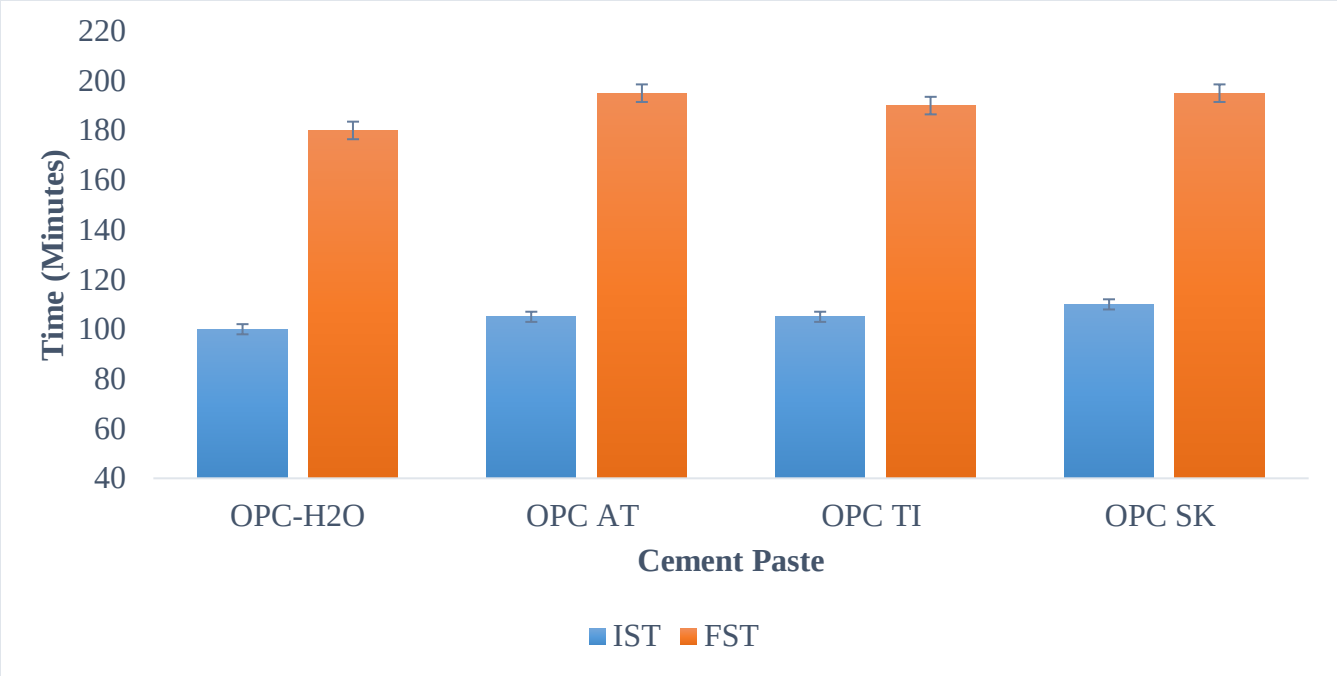

Figure 4.3: Initial and Final Setting Times for Control OPC and OPC Paste prepared using selected bacteria solution as the mixing water.

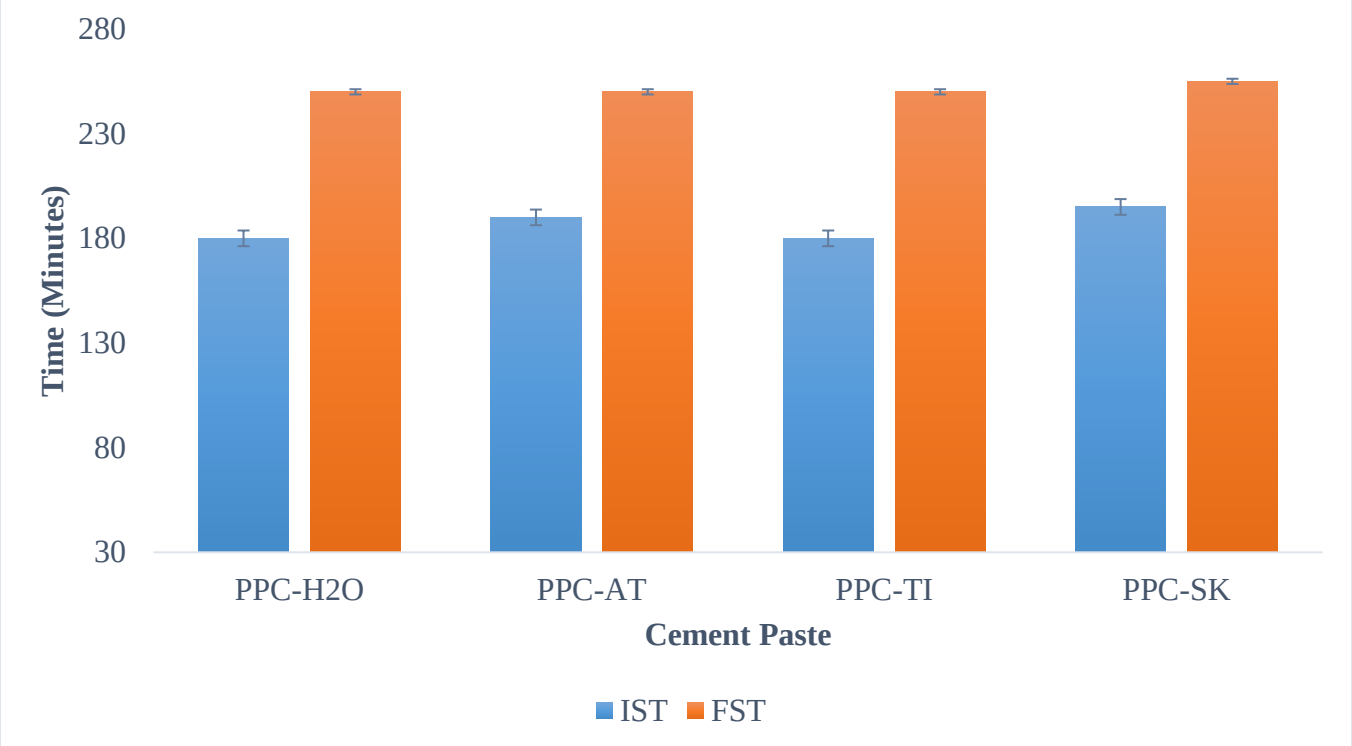

Figure 4.4: Initial and Final Setting Times for Control PPC and PPC Paste prepared using selected bacteria solution as the mixing water.

The T-test analysis results showed that there was no observed significant difference between the initial setting times of the control OPC and OPC-TI, OPC- AT and OPC - SK (The t_{cal} value for the initial setting times of OPC -TI, OPC-AT and OPC-SK was 0.77, 0.87 and 1.73 respectively against t_{crit} of 2.78). Equally, there was no observed significant difference between the final setting times of the control OPC and the OPC-TI, OPC- AT and OPC - SK (T_{cal} values for the final setting times of OPC-TI, OPC- AT and OPC was 2.32, 1.73 and 2.60 respectively against t_{crit} of 2.78). The same was observed in PPC where the control PPC and the pastes made from the selected bacteria did not show any significance difference in both initial and final setting times. The t_{cal} values were all lower than the t_{crit} with p- values above 0.05.

The similarity between the setting times (IST and FST) of controls and bacteria prepared OPC and PPC pastes was attributed to the short time required for the Portland cement to set. It perhaps required much more time of exposure for the bacteria to influence the setting pattern of the test cement. Further, some reagents used as source of nutrients for the bacteria such as dihydrogen phosphate (KH_2PO_4) supports in setting of Portland cement (Zilgma and Dagnija, 2021).

Based on the setting time test results, both control and bacterial treated pastes of OPC and PPC met the desired initial and final setting times as described in Kenya cement standard. Both cements set within the required range as provided in the Kenya cement standard hence the bacteria did not influence the setting patterns of the test cements. This was attributed to the slow activity of the bacteria and shorter duration of exposure. The recommended initial setting time for OPC is greater than 60 minutes whereas the one for PPC is greater than 75 minutes. The final setting times for either OPC or PPC should not exceed 600 minutes (KS EAS 18-1:2017).

4.4.3 Soundness Test Results

Table 4.3 shows the soundness test results for control and bacterial treated pastes of OPC and PPC respectively.

Table 4.3: Soundness Test Results for Control and Bacterial Prepared Pastes of OPC and PPC

Cement Paste Type	**Soundness (mm)**	**KS EAS 18-1 REQUIREMENT**
OPC (H_2O)	1.2 ± 0.01	≤ 10 mm
OPC AT	1.35 ± 0.01	
OPC TI	1.4 ± 0.02	
OPC SK	1.4 ± 0.01	
PPC (H_2O)	0.5 ± 0.02	
PPC AT	0.7 ±0.03	
PPC TI	0.51 ± 0.01	
PPC SK	0.9 ± 0.02	

Based on the soundness test results, there was no significance difference in soundness of PPC-H_2O with PPC - AT and PP-TI (The t_{cal} values for PPC-AT and PPC-TI were 2.45 and 0.16 against the t_{crit} of 2.78). It was however, noted that PPC-H_2O differed significantly with PPC-SK (The t_{cal} for PPC-SK was 6.93 way above the t_{crit} of 2.78). The soundness of OPC- H_2O differed significantly with the soundness of OPC - AT, OPC- TI and OPC- SK. The calculated t-values for the OPC-AT, OPC-TI and OPC-SK were 5.20, 17.32 and 8.66 against the t_{crit} of 2.78. Nonetheless, the test cements met the desired soundness requirement as described in KS EAS 18-1 (2017).

The observed difference between the soundness of test cements prepared with bacteria solutions and the control pastes was due to the bacteria feed which could have relatively influenced the marginal growth in cement unsoundness for the pastes prepared with bacteria solutions. The composition of bacterial feed comprised of salts of magnesium. Presence of magnesium content in cement paste causes unsoundness of cement paste and or mortar (Konstantinos *et al.,* 2021).

The soundness of the control PPC and OPC was significantly different (T-test analysis gave the t_{val} of 12.12 against the t_{crit} of 2.78 at 95% confidence level). OPC exhibited high soundness values when compared to PPC. This was attributed to the chemical composition of the cements as described in table 4.1. According to KS EAS 18-1 (2017), the oxides of calcium and magnesium contribute largely to the unsoundness of cement. OPC exhibits both high CaO and MgO contents. Studies by Ali and Mullick (1998) revealed that high content of MgO in cement results in expansion due to formation of insoluble magnesium hydroxide (Ali and Mullick, 1998). The hydration of CaO and MgO results in formation of secondary hydration products as shown in equations 4.5 and 4.6. The resultant products are expansive and may result to cement unsoundness (Odler, 2007; Macphee and Lachowski, 1998).

$$CaO + H_2O \rightarrow Ca(OH)_2 \qquad 4.5$$

$$MgO + H_2O \rightarrow Mg(OH)_2 \qquad 4.6$$

All the physical characteristics (standard consistency, setting times and soundness) of the test cement prepared with distilled water and selected microbial solutions conformed with the KS EAS

18-1 (2017). This implied that the activity of the test bacteria did not affect the above physical characteristics of the test cements significantly. This was attributed to the shorter exposure period and hence too early to detect the effect of the bacteria. There was thus need to expose the bacteria prepared mortars to further tests which required more exposure duration.

4.5 Microstructural Analysis

4.5.1 Scanning Electron Microscopy (SEM)

Plates 4.1 and 4.2 represent the SEM micrographs for the control OPC and PPC mortars after 28th day of curing.

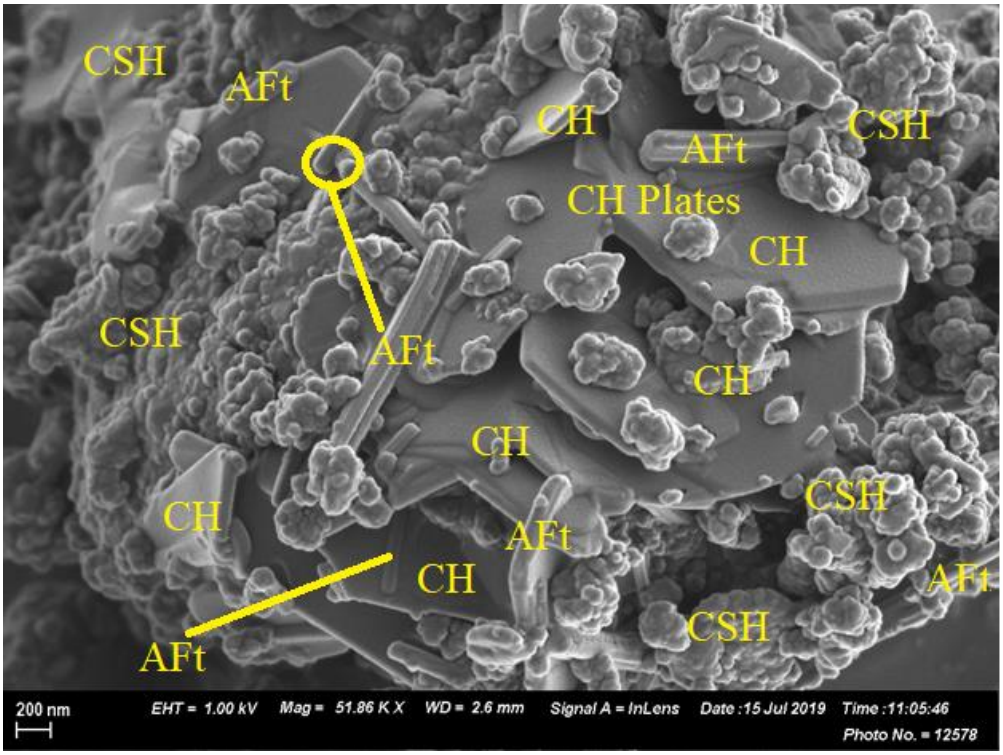

Plate 4.1: SEM Morphology for OPC H-H after 28th of curing

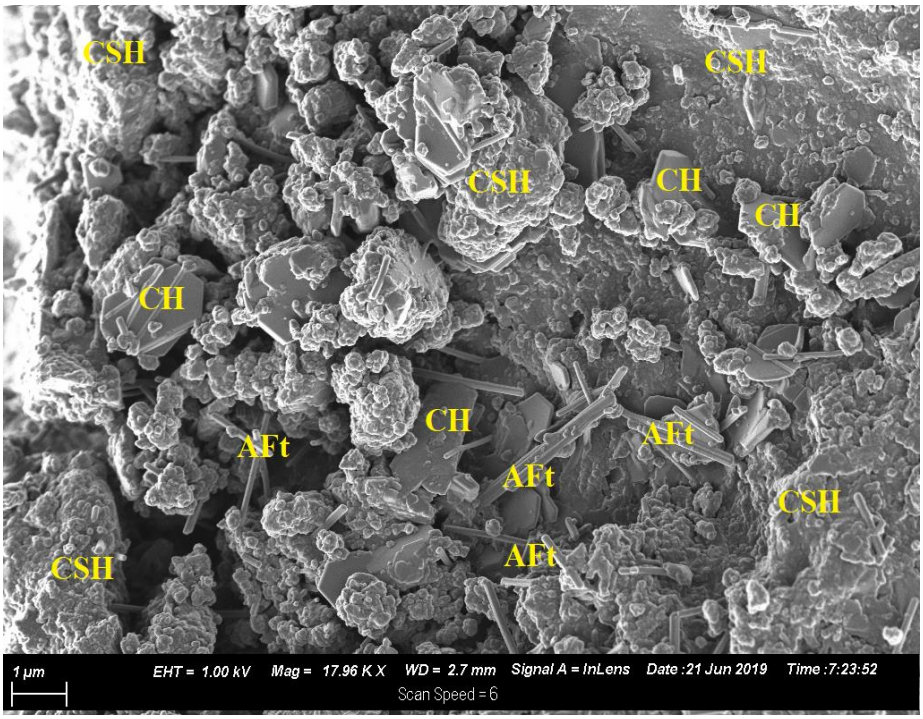

Plate 4.2: SEM Morphology for PPC H-H after 28th day of curing

The SEM micrographs for the control mortars show that OPC H-H was dominated by high quantities of hexagonal calcium hydroxide (CH) plates and calcium silicate hydrates (C-S-H) paste as the main hydration products. This was attributed to high C_3S and C_2S phases in OPC as described in table 4.2 (Scrivener *et al.,* 2015). The hydration phases filled the pore spaces initially occupied with water and unhydrated cement grains (Xu and Xiao, 2021). Presence of ettringite (AFt) was because of the initial gypsum added to improve on cement workability during placement and control setting time (Suhua *et al.*, 2021). There was no signs of crack formation due to the compact and well filled packing of hydration products in the hydrated cement mortar (Xu and Xiao, 2021; Munyao *et al.*, 2020b).

The control PPC exhibited reduced CH plates in the pore matrix and extensive formation of C-S-H paste. This was attributed to pozzolanic activity (Walid *et al.,* 2017). The silica content in pozzolana combines with CH through pozzolanicity reaction to generate secondary cementitious C-S-H material. The resultant mortar of PPC based cement is more dense making it more resistant to damage by aggressive media (Ali *et al.*, 2021; Meddah *et al.,* 2020; Meysam *et al.,* 2018). Equation 4.7 show the reaction involved during pozzolanic activity (Taylor, 1999).

$$2SiO_2 + 3Ca(OH)_2 + 5H_2O \rightarrow 3CaO.SiO_2.8H_2O \qquad 4.7$$

The SEM micrographs for the mortars of OPC and PPC prepared with *Acidithiobacillus thiooxidans, Thiobacillus intermedius* and *Starkeya novella* are presented in plates 4.3- 4.8 as OPC AT-AT, OPC TI-TI, OPC SK-SK, PPC AT-AT, PPC TI-TI and PPC SK-SK respectively.

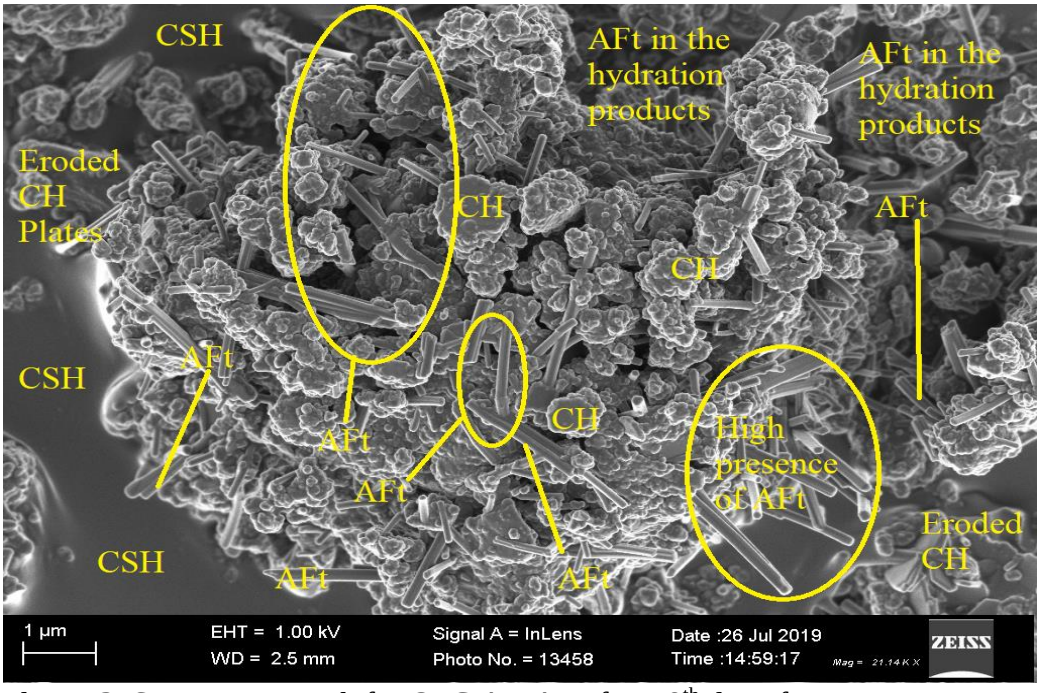

Plate 4.3: SEM Micrograph for OPC AT-AT after 28th day of curing

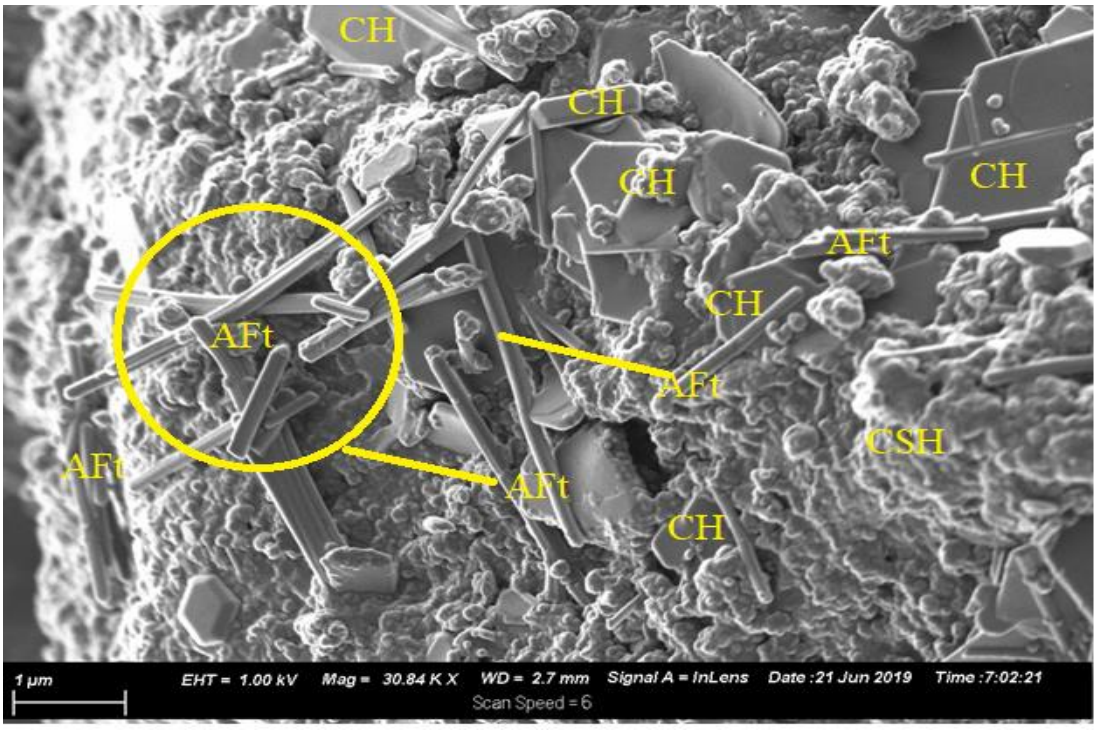

Plate 4.4: SEM Micrograph for OPC TI-TI after 28th day of curing

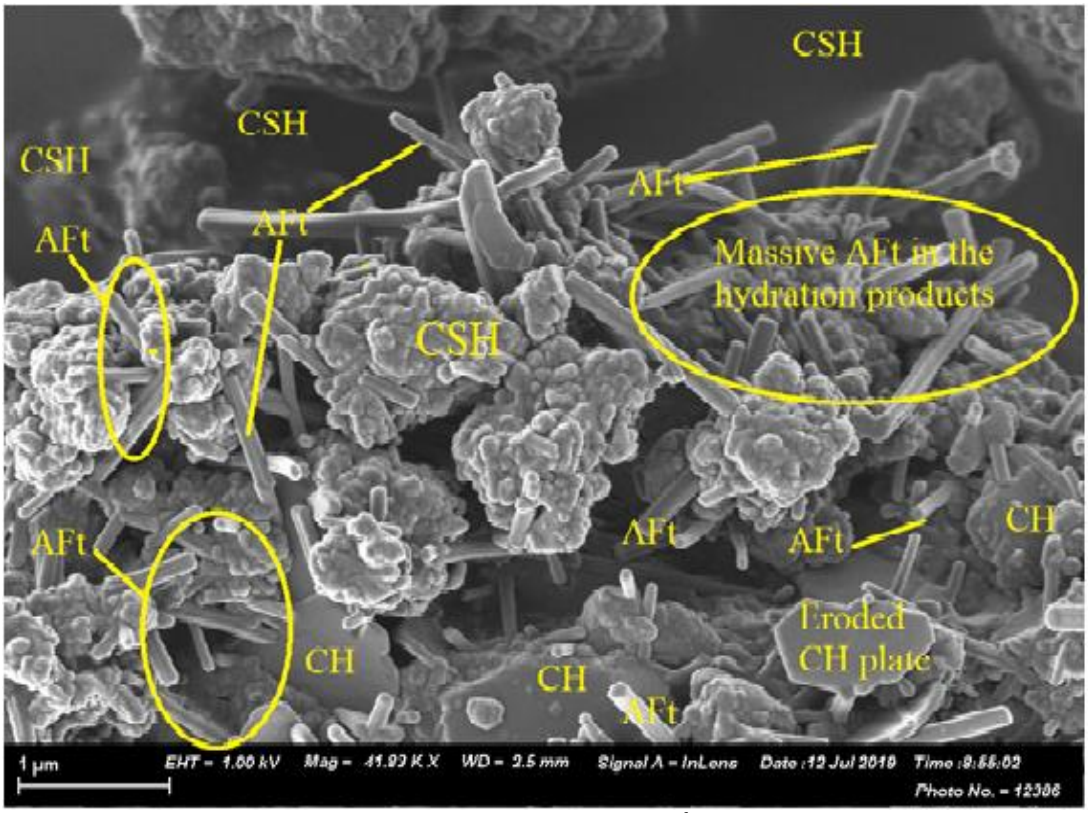

Plate 4.5: SEM Micrograph for OPC SK-SK after 28th day of curing

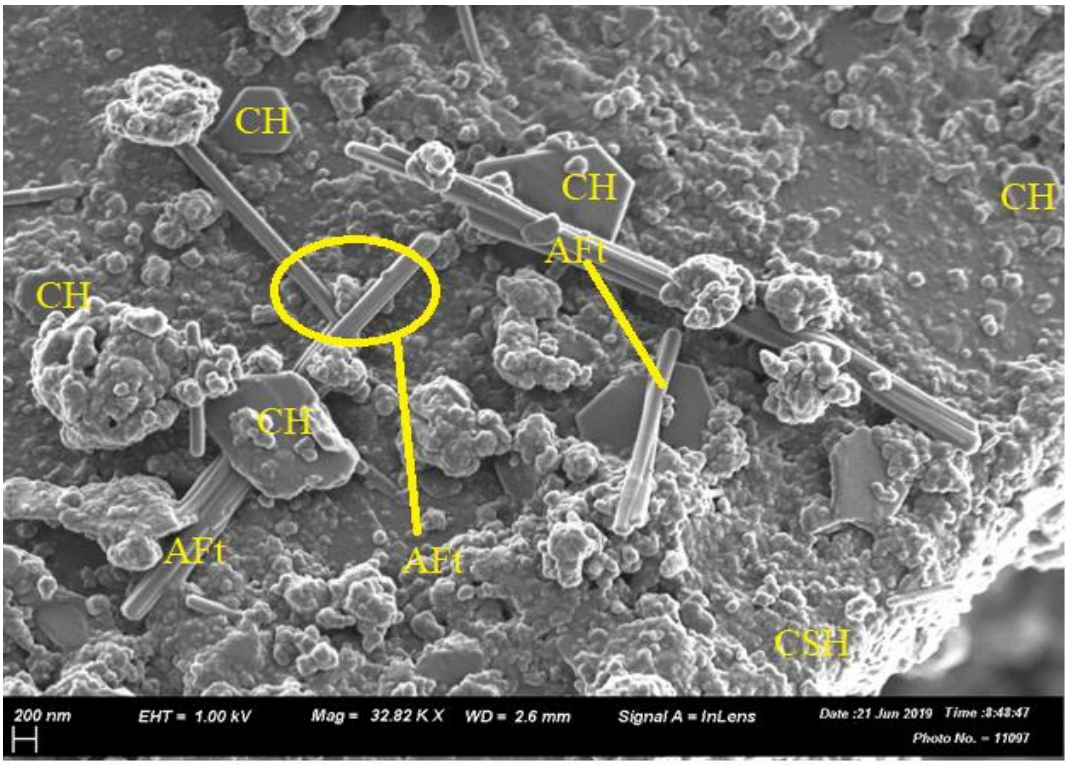

Plate 4.6: SEM Micrographs for PPC AT- AT after 28th day of curing

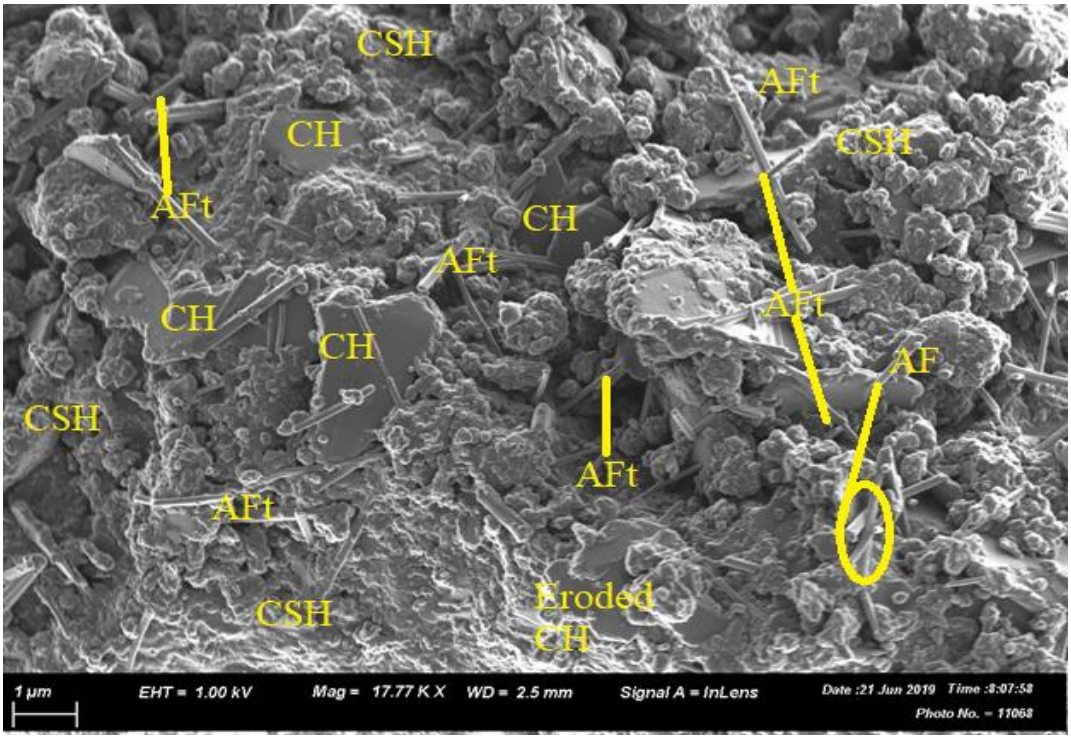

Plate 4.7: SEM Micrographs for PPC TI – TI after 28th day of curing

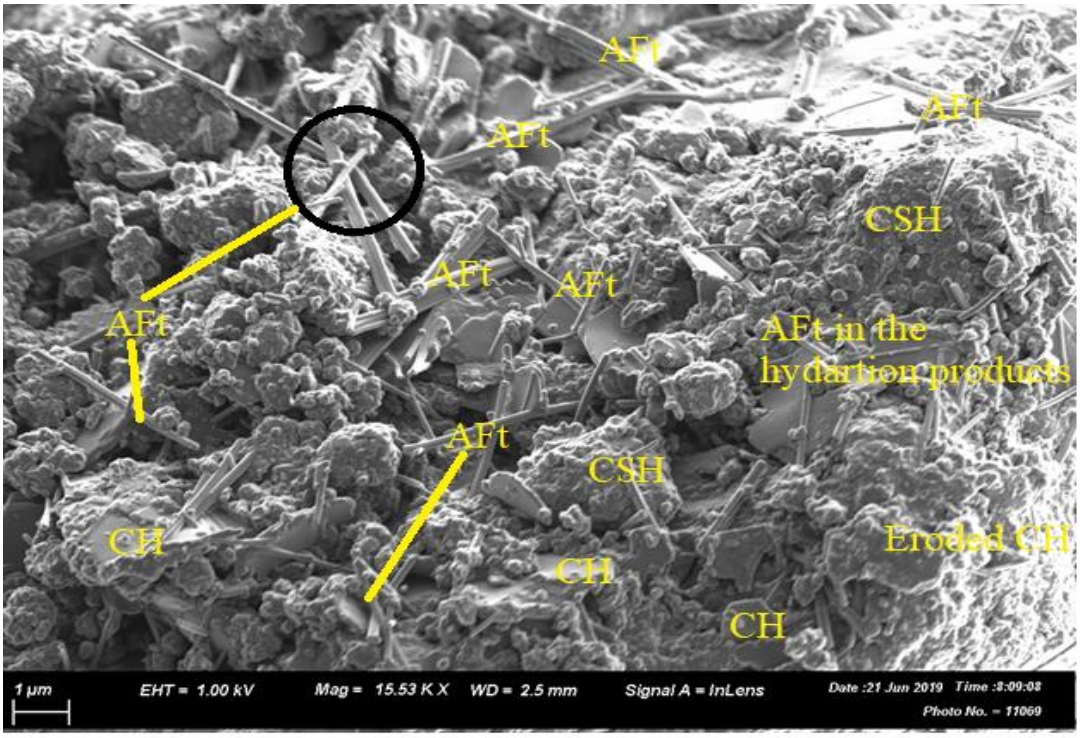

Plate 4.8: SEM Micrographs for PPC SK-SK after 28th day of curing

The OPC and PPC microbial prepared mortars exhibited pronounced ettringite (AFt) formation on the pore matrix characterized by needle-like shaped materials. This was attributed to the biogenic sulphuric acid generated by the bacteria activity. The formed biogenic acid facilitated the formation of delayed ettringite within the pore matrix. Similar observation was made by Sravanthi *et al.* (2015). Presence of external sulphate source favours the formation of delayed ettringite on the pore matrix of the exposed mortar and concrete (Yushan *et al.*, 2019). Ettringite crystals result in volume expansion of concrete and mortar causing spalling and degeneration of exposed structure. Equation 4.8 shows the formation of ettringite crystals in the pore matrix of the mortar or concrete (Yushan *et al.*, 2019; Sun, 2015).

$$3CaSO_4 + 3CaO.Al_2O_3.6H_2O + 26H_2O \rightarrow 3CaO.Al_2O_3.3CaSO_4.32H_2O \quad 4.8$$

The observed erosion of the calcium hydroxide (CH) plates on the microbial prepared mortars of OPC and PPC was because of biogenic sulphuric acid attack on the residual calcium hydroxide in the pore matrix. This would weaken the hydration products, reducing the life span of the exposed structure. Additionally, the acid attack would cause the pore matrix more porous, allowing the harmful external materials to enter the mortar or concrete and cause further damage to the placed structure (Joshi *et al.*, 2019; Sun, 2015).

Results from the SEM micrographs showed that the selected bacteria had a negative influence on the microstructure of the commercial OPC and PPC. Amongst the test bacteria, *Starkeya novella* exhibited adverse effects on the microstructure of the test cements. The formation of the observed deleterious material (ettringite) within the pore structure of the exposed mortars in the selected test bacteria would significantly influence the mechanical performance of the placed concrete and/ or the mortar structure.

4.5.2 FTIR Characterization of Hydrated Test Cement Mortars Exposed to Bacteria

Figures 4.5 and 4.6 represent the FTIR spectrums for the control and bacteria prepared mortar prisms.

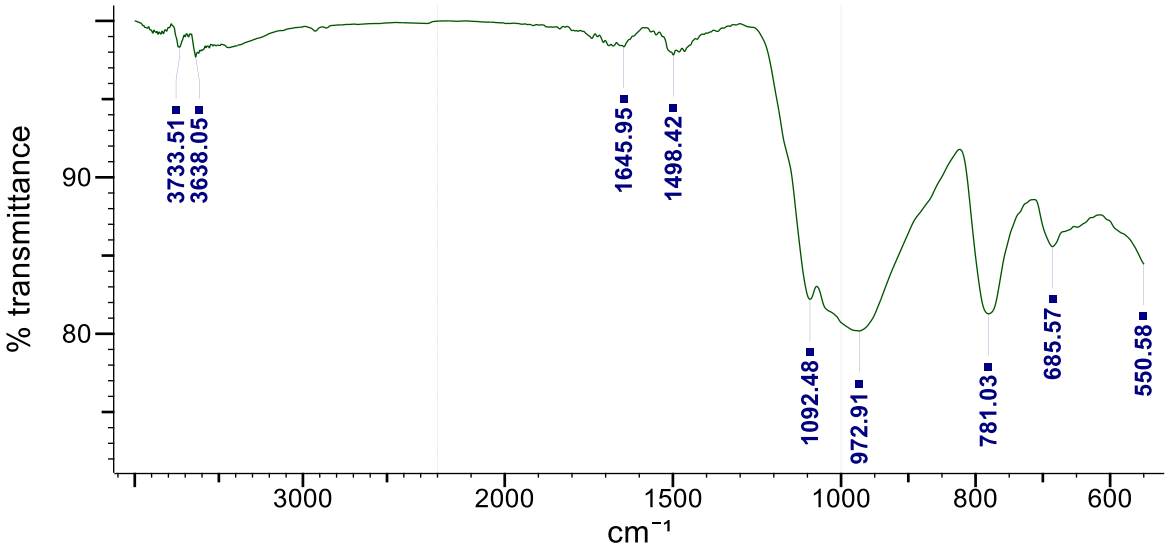

Figure 4.5: FTIR Spectra for control test mortar after 28th day of Curing

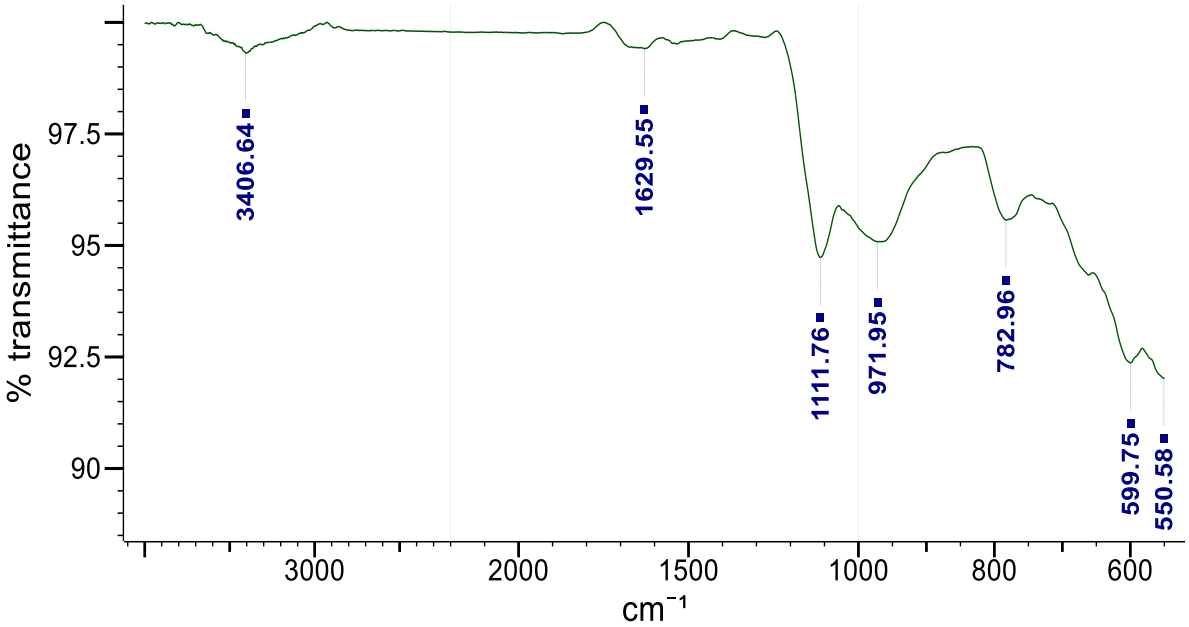

Figure 4.6: FTIR Spectra for bacteria test mortar after 28th day of Curing

The characteristic wave numbers for the control mortar tests as tested using FTIR are shown in Figure 4.5. The major bands were shown at 550.58 cm^{-1}, 685.57 cm^{-1}, 781.03 cm^{-1}, 972.91 cm^{-1}, 1092.48 cm^{-1}, 1498.42 cm^{-1}, 1645.95 cm^{-1}, 3638.05 cm^{-1} and 3733.51 cm^{-1}. Si-O stretching was

observed at 781.03 for the control mortar cement. This observation was in line with the work done by Ariffin *et al.* (2013). The workers (Ariffin *et al.,* 2013) attributed the wavelength band between 780- 800 cm^{-1} to the stretching of O-Si-O bonds within the quartz crystalline phase of the hydrated cement. Yudong *et al.* (2019) and Fernandez- Jimenez *et al.* (2005) made similar observations.

The bands observed at 972.91 cm^{-1} and 1092.48 cm^{-1} were associated with polymerization of silica to form calcium silicate hydrate (C-S-H) as the main hydration products. The C-S-H gel was clearly identified from the SEM results as reported in section 4.5.1 in this work. The asymmetric stretching vibration of Si-O-Si associated with C-S-H phase formation occurs between 960 -1100 cm^{-1} (Yilmaz and Suna, 2014; Shi *et al.,* 2011; Stepkowska *et al.,* 2005; Mollah *et al.,* 2003). The bands observed at 550.58 cm^{-1}, 685.57 cm^{-1} and 781.03 cm^{-1} represents Al-O bonds. These bands are associated with the reaction of aluminate and silicates in the hydrated cements to form the aluminosilicates (Yudong *et al.,* 2019; Renaudin *et al.,* 2007). The band at 1498.42 cm^{-1} was associated with C-O bond. This was due to the carbonation of the hydrated mortar. Reaction of the atmospheric carbon (IV) oxide with the cement would result in secondary formation calcium carbonate in the hydrated mortar (Anu *et al.*, 2020; Run-sheng *et al.*, 2019).

The band associated with chemically bound water was identified at 1645.95 cm^{-1}. This peak was due to the bending vibration of water in sulphates (Rikard *et al.,* 2009). The bound water was attributed to gypsum ($CaSO_4.2H_2O$) added at the initial production of cement to regulate setting time and workability of the mortar. Borhan *et al.* (2010) made similar observation. The bands at 3638.05 cm^{-1} and 3733.51 cm^{-1} were associated with the calcium hydroxide (Zhu *et al.,* 2018; Mollah *et al.,* 2000). As observed from the SEM results, the calcium hydroxide plates were very

visible in the control mortars. The hydration of Portland cement results in formation of calcium hydroxide as one of the main hydration products. This observation agreed with the work done by Anu *et al.* (2020); Zhu *et al.* (2018) and Santa *et al.* (2013).

The FTIR main bands identified in mortars prepared with bacteria solutions were as shown in figure 4.6. The main bands were identified at 550.58 cm^{-1}, 599.75 cm^{-1}, 782.96 cm^{-1}, 971.95 cm^{-1}, 1629.55 cm^{-1} and 3406.64 cm^{-1}. After the exposure of the test cement into the bacteria solution, a peak at 1111.76 cm^{-1} that was missing in control mortars was observed. This peak was attributed to the sulphate ions responsible for delayed ettringite formation. The typical sulphate absorption bands occur between 1100 – 1200 cm^{-1} (Rikard *et al.,* 2009). The observed sulphate band in bacteria prepared mortars was perhaps responsible for the massive ettringite formation in bacteria prepared mortars (Lee *et al.,* 2016). As reported in SEM results, ettringite formation was pronounced in bacteria prepared mortars. This was attributed to biogenic sulphuric acid generated by the selected test bacteria (Anu *et al.,* 2020; Yudong *et al.,*2019*).*

The presence of C-S-H in bacteria prepared mortars was only identified at 971.95 cm^{-1}. This was attributed to the C_3S phase contained in clinker. This observation was in line with work done by (Bjőrnstrőm *et al.,* 2004). There was no observed formation of C-O bond at 1498.42 cm^{-1} in bacteria prepared mortars. This perhaps contributed to low C-S-H gels in bacteria mortars. Absence of calcium carbonate in the bacteria prepared mortars implied that the formed biogenic acid consumed the resultant calcium hydroxide from the hydration and hence there was no residual calcium hydroxide to react with the atmospheric carbon (IV) dioxide (Yudong *et al.,* 2019).

The band associated with bound water (O-H bending) in bacteria prepared mortars was observed at 1629.55 cm^{-1}. This was in line with the observation made in the case of the control mortar. However, it was noted that O-H stretching associated with calcium hydroxide in the hydrated mortar of bacteria prepared cement appeared at 3406.64 cm^{-1}. The peak was not as pronounced as observed in control mortars. This peak was in line with the SEM analysis where the bacteria prepared mortars exhibited erosion of calcium hydroxide plates (Qian et *al.*, 2008).

The bands associated with Al-O resulting in formation of aluminosilicates compounds occurred at 550.58 cm^{-1}, 599.75 cm^{-1} and 782.96 cm^{-1}. The additional band at 599.75 cm^{-1} was evidence of bacteria attack on the aluminate phase of cement. Puertas *et al.* (2000) and Kledyński *et al.* (2017) made comparable observations. FTIR analysis was in agreement with the SEM test results reported in this work. Bacteria prepared mortars showed peaks that agreed with deleterious products such as ettringite as observed in SEM morphology.

4.5.3 XRD Characterization of Hydrated Control and Microbial Cement Mortars

Figure 4.7 and 4.8 show the XRD analysis for the control and microbial OPC mortars after 28th day of curing.

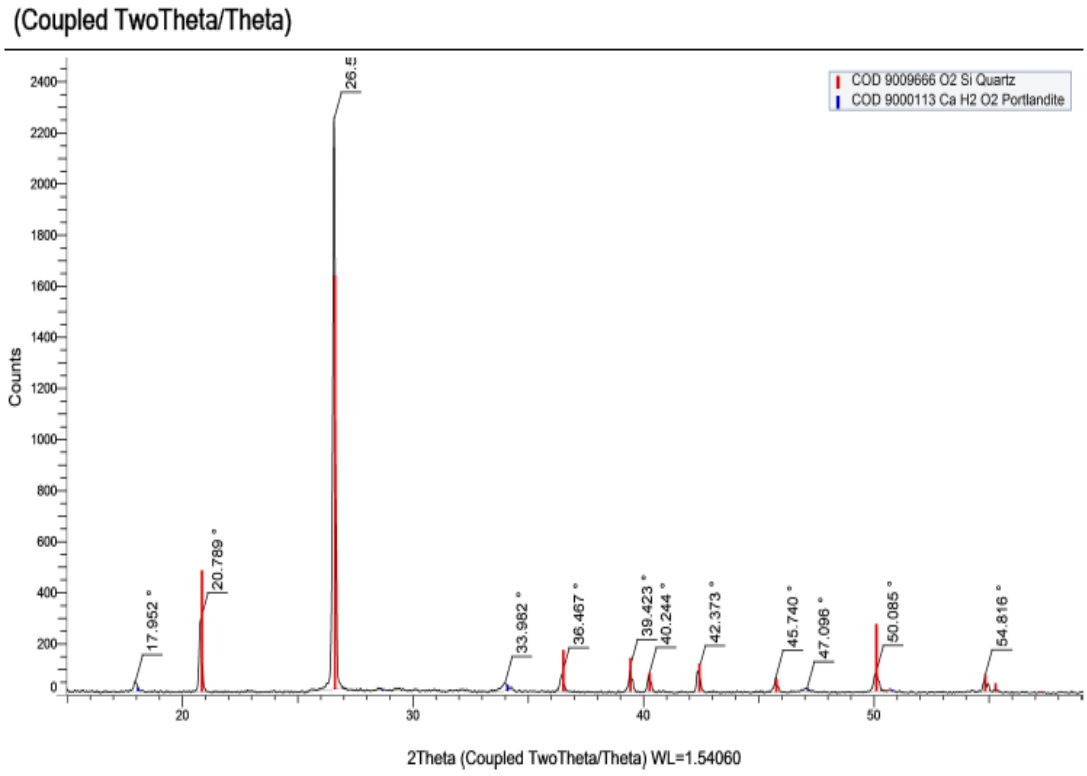

Figure 4.7: XRD diffractogram for OPC H-H after 28th day of curing

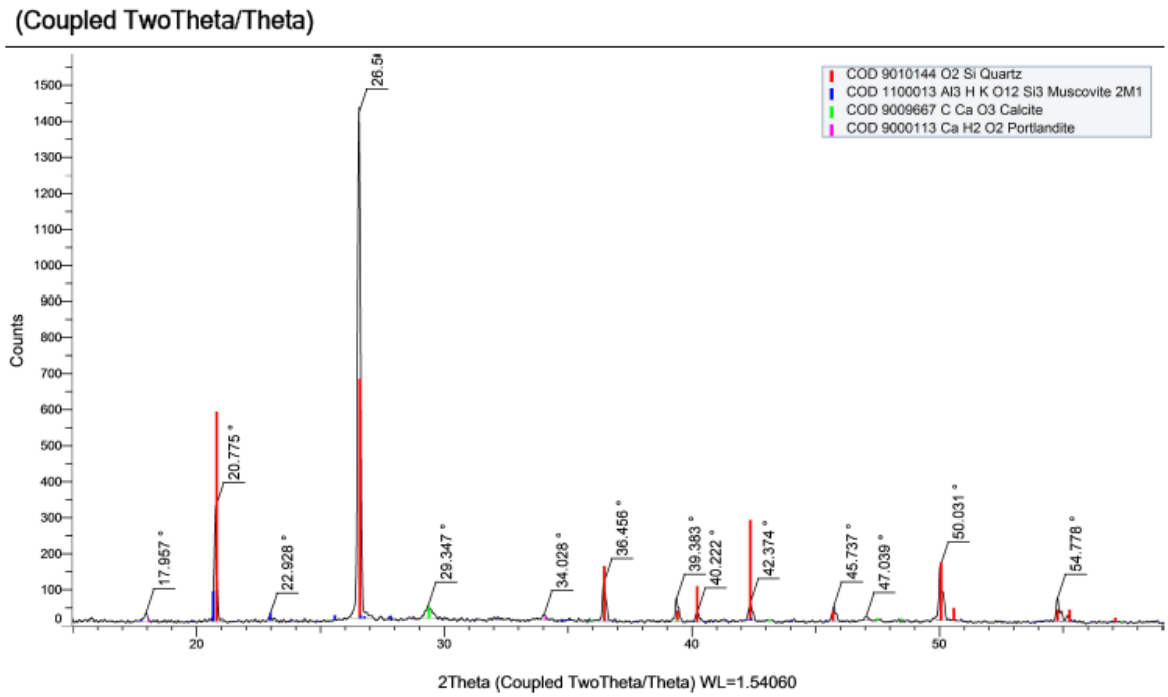

Figure 4.8: XRD diffractogram for microbial OPC SK-SK after 28th day of curing

The XRD analysis for OPC H-H showed the formation of Portlandite even at 28 days of curing. This was as observed in SEM morphology for OPC H-H. Portlandite (CH), is the main hydration product that forms when cement react with water. Presence of portlandite after 28 days of curing was attributed to the unreacted CaO from cement clinker. This phase forms the attack point by the destructive agents such as sulphates and chlorides for the OPC (Snelling *et al.*, 2014). In presence of external ingress of sulphates, CH is attacked and the resultant product is ettringite which is expansive and deleterious (Yongcheng *et al.,* 2021).

The OPC mortars prepared with *Starkeya novella* bacteria medium showed formation of calcite and muscovite as the new products. The calcite formation ($CaCO_3$) was attributed to the reaction of the excess Portlandite in the hydrated OPC with atmospheric carbon dioxide (Vineet *et al.,* 2018). The process of carbonation was perhaps activated by the *Starkeya novella* activity (Yudong *et al.,* 2019). There was no evidence of formation calcite in control OPC H-H.

OPC SK-SK showed 10% formation of muscovite ($Al_3HKO_{12}Si_3$) as a new product. The formation of muscovite in cement mortar and concrete lowers the compressive strength of the placed material. Muscovite formation in concrete appreciably influences the reduction of compressive strength (Maregesi, 2021). The inclusion of 2% muscovite in cement lowers the resultant compressive strength by 20% (Maragesi, 2021).

The formation of muscovite further reduces the slump of the concrete by half (Leeman and Holzer, 2001). Reduction of concrete slump increases water demand of the batched concrete. As observed and previously reported in this work, there was appreciable increase in water demand for the OPC

SK-SK mortar prisms. The XRD results for the bacteria prepared OPC mortars agree with the physical characteristics of the bacteria prepared pastes previously reported in this work.

Figures 4.9 and 4.10 represent the XRD diffractogram for the control and microbial PPC mortars

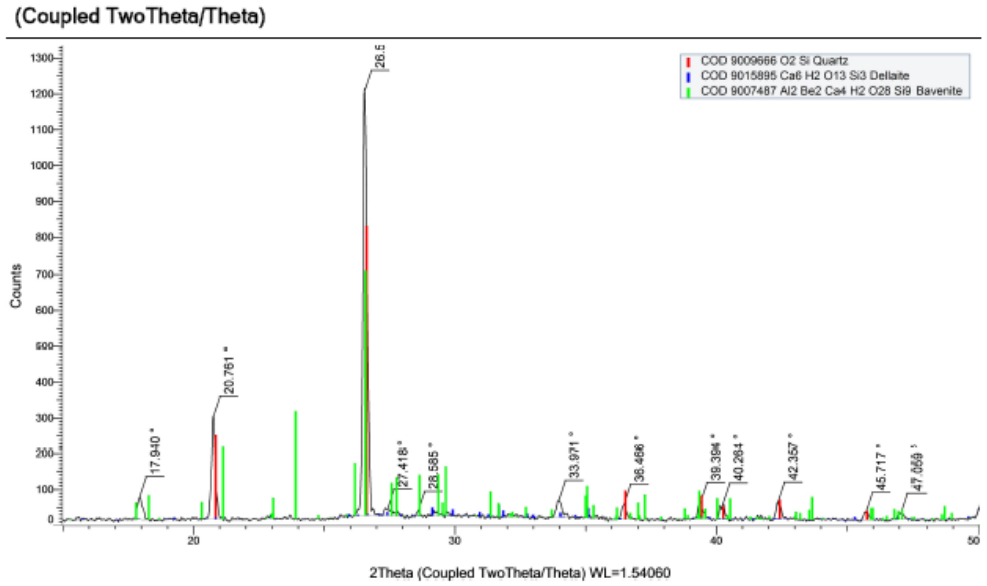

Figure 4.9: XRD diffractogram for PPC H-H after 28th day of curing

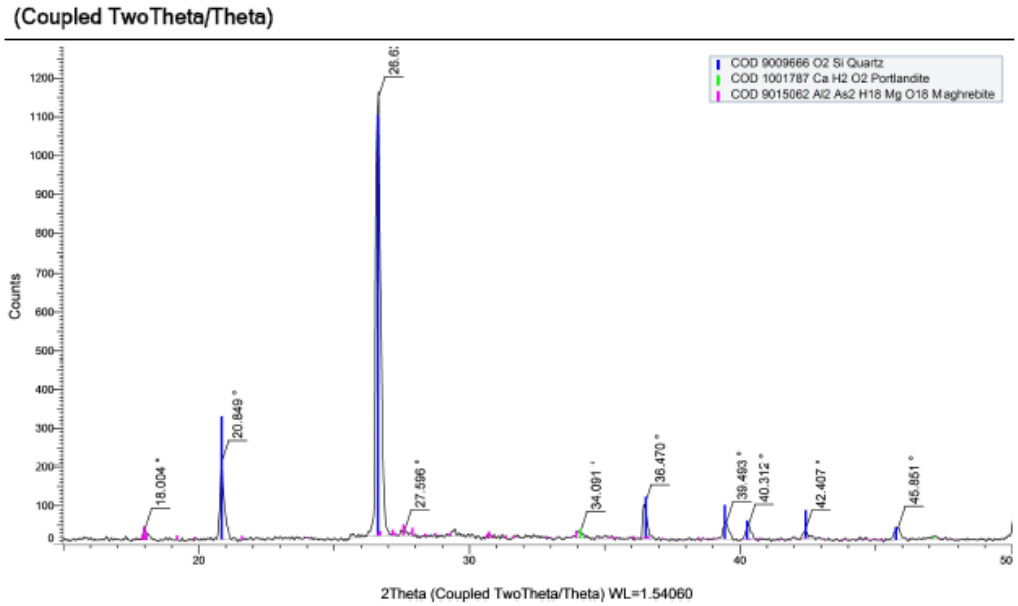

Figure 4.10: XRD diffractogram for microbial PPC SK-SK after 28th day of curing

The XRD diffractogram for control PPC show the formation of dellaite and bavenite as new hydration products. Dellaite, ($C_6SiO_3O_{11}(OH)_2$ commonly known as C-S-H is an important hydration product that makes the resultant cement mortar dense and impermeable (Vineet *et al.,* 2018). The formation of dellaite in control PPC was attributed to the pozzolanic activity. The products of pozzolanic activity follows the reaction between the reactive silica from the pozzolans with the calcium from cement clinker and water to form additional calcium silicate hydrate product (Diandian *et al.,* 2021; Hadigheh *et al.,* 2017).

The PPC mortars prepared with microbial solutions exhibited formation of maghrebite ($Al_2As_2H_{18}MgO_{18}$) as a new compound in the pore matrix. This compound has the potential of causing expansion of mortars and concrete due to the presence of magnesium content (Yan *et al.,* 2021). Maghrebite formation in either concrete and/or mortar causes unsoundness in placed concrete or mortar (Mshali *et al.,* 2012). As reported in the physical analysis results in this work, the bacteria prepared pastes exhibited increased unsoundness. This was perhaps due to the formation of the maghrebite from the bacteria activities.

The characteristic products from the XRD diffractogram for all the mortars prepared with microbial solutions in either PPC and /or OPC agreed with the other test results such as setting time, soundness and SEM previously reported in this work. The microstructural analysis showed formation of new products for the test cements exposed the bacteria solution. The formed products (Ettringite, Muscovite, Dellaite and Maghrebite) could later affect the mechanical properties of the placed concrete and mortar and hence cause subsequent structural failures.

4.6 Mechanical Analysis

4.6.1 Compressive Strength Test Results for Control Mortars

Figure 4.11 represent the compressive strength performance for the control PPC and OPC mortar prisms. PPC H-H and OPC H-H refers to the mortars of PPC and OPC prepared using distilled water as the mixing water and cured in distilled water as the curing media respectively.

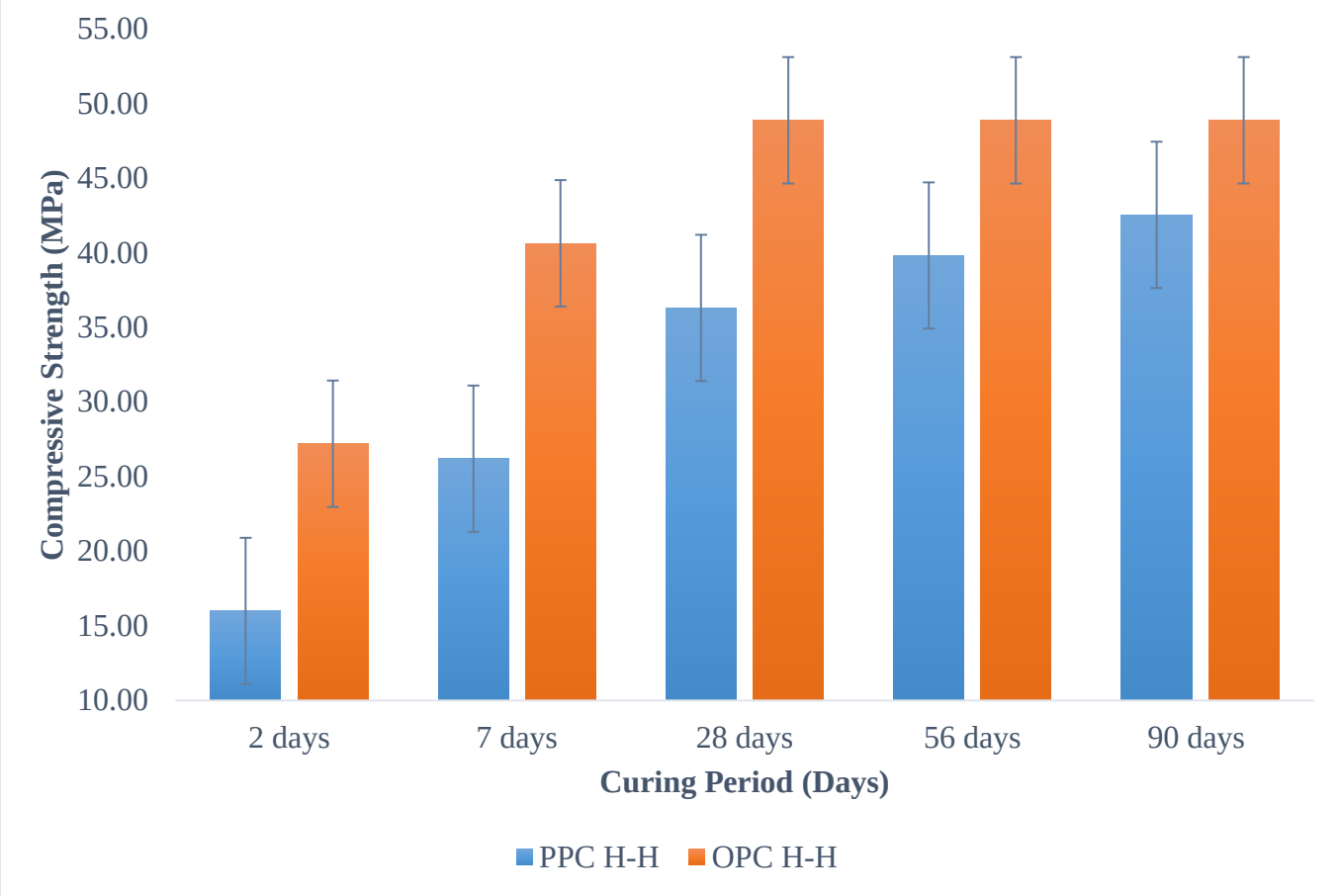

Figure 4.11: Compressive Strength Performance of control mortars of PPC and OPC

Compressive strength development increased with increase in the curing period for both PPC and OPC mortars. Cement gains strength through hydration process. Curing facilitates formation of the hydration products responsible for the strength development. The formation of C-S-H gel

through the hydration of C_3S and C_2S enhances the strength development of cement mortar and/ or concrete (Diandian and Rahil, 2021). As described in equations 4.1 and 4.2, C-S-H is the main hydration product responsible for the strength development of cement mortar and /or concrete.

The strength development of OPC varied significantly with that of PPC across all the curing periods. Table 4.4 gives the summary T-values of t-test analysis of OPC and PPC compressive strength at different curing ages. The T-test analysis was carried out at 95% confidence level. The T-values were compared against the T-critical at each curing period. T_{calc} was higher than T_{crit} across all the curing duration. This implied that the strengths of OPC significantly varied with those of PPC at all curing ages.

Table 4.4: Summary of T-test values for the compressive strength between OPC and PPC at different curing ages. (T_{crit} = 2.78 at 4 degrees of freedom)

	2 days	**7 days**	**28 days**	**56 days**	**90 days**
T_{cal}	5.85	7.46	11.65	9.16	7.31
P_{val}	0.00	0.00	0.00	0.00	0.00

The higher compressive strength of OPC over PPC was attributed to the phase composition of the test cements as described in table 4.2. C_3S and C_2S contributes to the strength development of cement. The reaction of C_3S and C_2S with water results in formation of C-S-H phase, which is responsible for the strength development. OPC neat contains higher percentage of these phases

(C_3S and C_2S) than PPC hence enhanced strength performance. This was evident from the SEM morphology where OPC exhibited high formation of CH plates.

The low compressive strength development of PPC was attributed to the pozzolana addition. The pozzolana- lime reaction proceeds very slowly resulting in reduced heat of hydration. This lowers the early strength development in PPC. Further, the substitution of clinker with pozzolana results in reduced C_3A, which is responsible for early strength development. The compressive strength of PPC continued to develop even after 28 days of curing. This was attributed to pozzolanic activity. As described in equations 4.1 and 4.2, the resultant CH from hydration of Portland cement reacts with silica and alumina from pozzolana to form C-S-H and C-A-H as secondary cementitious materials. The formed secondary C-S-H improves the mechanical properties of the pozzolanic cement. As illustrated in equation 4.3 and 4.4, the formation of secondary C-S-H and C-A-H describes the pozzolanic activity reaction. This was further confirmed from the SEM morphology given in plate 4.2 where control PPC showed advance formation of secondary C-S-H gels.

Both test cements met the minimum desired compressive strength of 32.5 MPa for PPC and 42.5 MPa for OPC after 28 days of curing as described KS EAS 18-1 (2017) and BS EN 197-1 (2011). This implied that the compressive strength change observed in either of the test cements when mixed with varied bacteria solutions as either mixing water or curing media, was due to the bacteria influence.

4.6.2 Compressive strength for Bacteria Prepared Mortars of OPC and PPC

Figures 4.12 and 4.13 show the compressive strength results of mortars of PPC and OPC when prepared using bacteria solutions as either mixing water and/ or curing media. The T-test analysis

for the compressive strength performance between the control PPC and the mortars of PPC prepared with varied bacteria solutions is summarized in table 4.5 whereas the T-test analysis for the compressive strength performance between the control OPC and the mortars of OPC prepared with selected bacteria solutions is summarized in table 4.6 respectively.

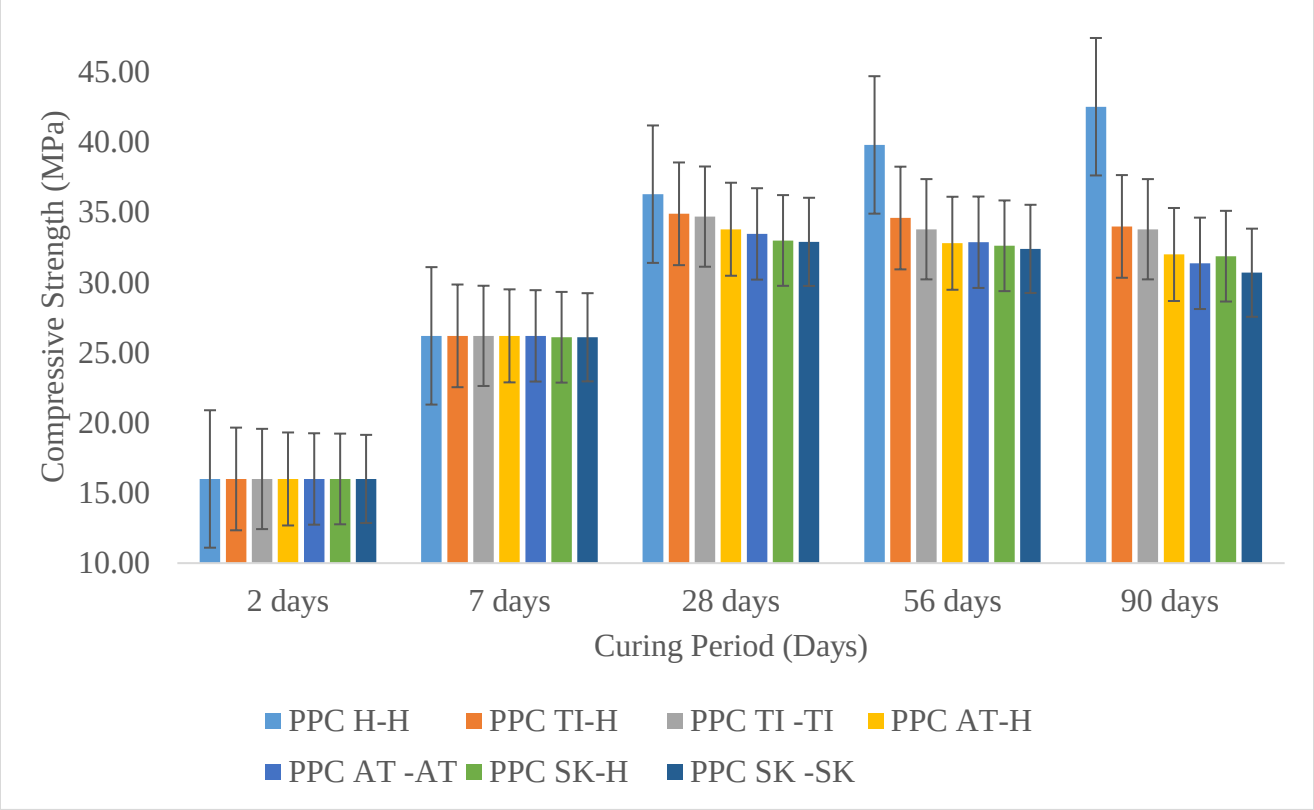

Figure 4.12: Compressive Strength of PPC Mortars prepared with selected bacteria solutions as either mixing water and/or curing media

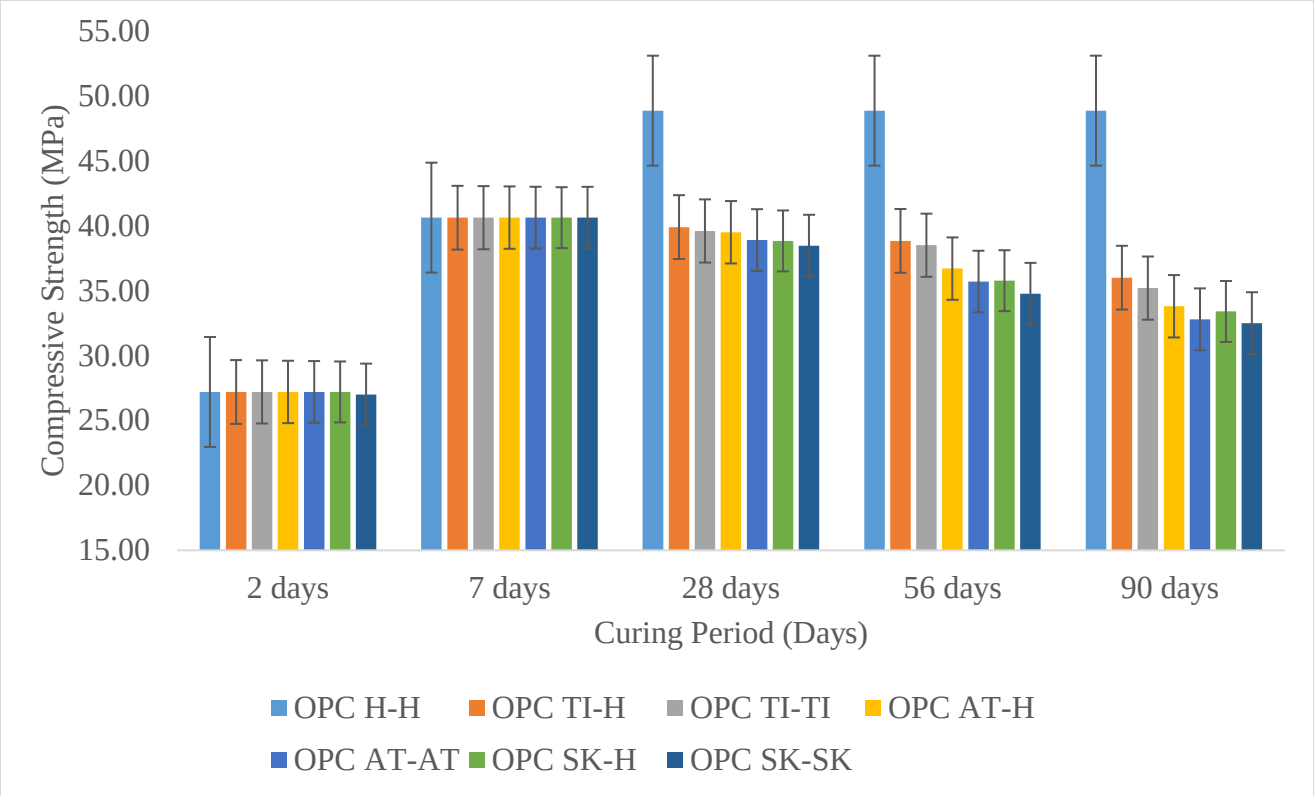

Figure 4.13: Compressive Strength of OPC Mortars prepared with selected bacteria solutions as either mixing water and/or curing media

Table 4.5: T_{cal} values for the control PPC and PPC Mortars prepared with varied bacteria solutions at different curing ages (T_{crit} = 2.78 at 4 degrees of freedom)

		Cement Mix Composition					
Control Mortar	Age of Testing	PPC AT-H	PPC AT-AT	PPC TI-H	PPC TI-TI	PPC SK-H	PPC SK-SK
PPC H-H	2 days	0	0	0	0	0	0
	7 days	0	0	0	0	1.73	1.73
	28 days	4.43	5.46	8.08	9.24	15.85	18.62
	56 days	11.65	12.62	11.92	14.71	15.58	19.53
	90 days	6.76	7.83	10.98	12.11	13.32	19.44

Table 4.6: T_{cal} values for the control OPC and OPC Mortars prepared with varied bacteria solutions at different curing ages (T_{crit} = 2.78 at 4 degrees of freedom)

		Cement Mix Composition					
Control Mortar	Age of Testing	OPC AT-H	OPC AT-AT	OPC TI-H	OPC TI-TI	OPC SK-H	OPC SK-SK
OPC H-H	2 days	0	0	0	0	0	0.23
	7 days	0.5	0	2	0.15	0	0.63
	28 days	6.21	13.01	11.67	15.07	17.31	9.77
	56 days	13.74	12.94	12.57	19.17	9.14	9.09
	90 days	17.07	17.63	18.22	17.08	9.16	14.2

The test results show that there was no significant difference ($T_{cal} < T_{crit}$) between the controls and their respective bacteria prepared mortars at 2 and 7 days of testing. Table 4.5 and 4.6 show that the t_{cal} values at 2 and 7 days were all less than the t_{crit} value of 2.78. This implied that the bacteria did not affect the strength of either PPC or OPC at the early days of curing. This perhaps was due to the alkalinity of the fresh placed mortar that would hinder the activity of bacteria at the early days of curing.

It was however observed that at 28th, 56th and 90th day of curing, there was observable significance difference in strength performance between the mortars prepared with selected bacteria solutions and the respective control mortars. T_{cal} values as shown in table 4.5 and 4.6 were higher than the T_{crit} value. The mortars prepared with the bacteria solutions gave significantly low compressive strengths compared with the controls. The bacteria's degrading effect was responsible for the decrease in compressive strength observed in microbial mortars.

In order to evaluate the effect of bacteria on compressive strength development, the percentage decrease in compressive strength of PPC and OPC mortars when subjected to the bacteria solution either as mixing media or both as mixing and curing media was calculated using equation 4.9 (Yudong *et al.*, 2019).

$$\%\ CS_{decrease} = \left(\frac{C_sB_m - C_sC_m}{C_sC_m}\right)X100 \qquad 4.9$$

Where CS is the compressive strength, C_sB_m is the compressive strength of the mortar prepared with bacteria solution and C_sC_m is the compressive strength of the control mortar. Figures 4.14 and 4.15 give the percentage decrease in compressive strength for PPC and OPC respectively.

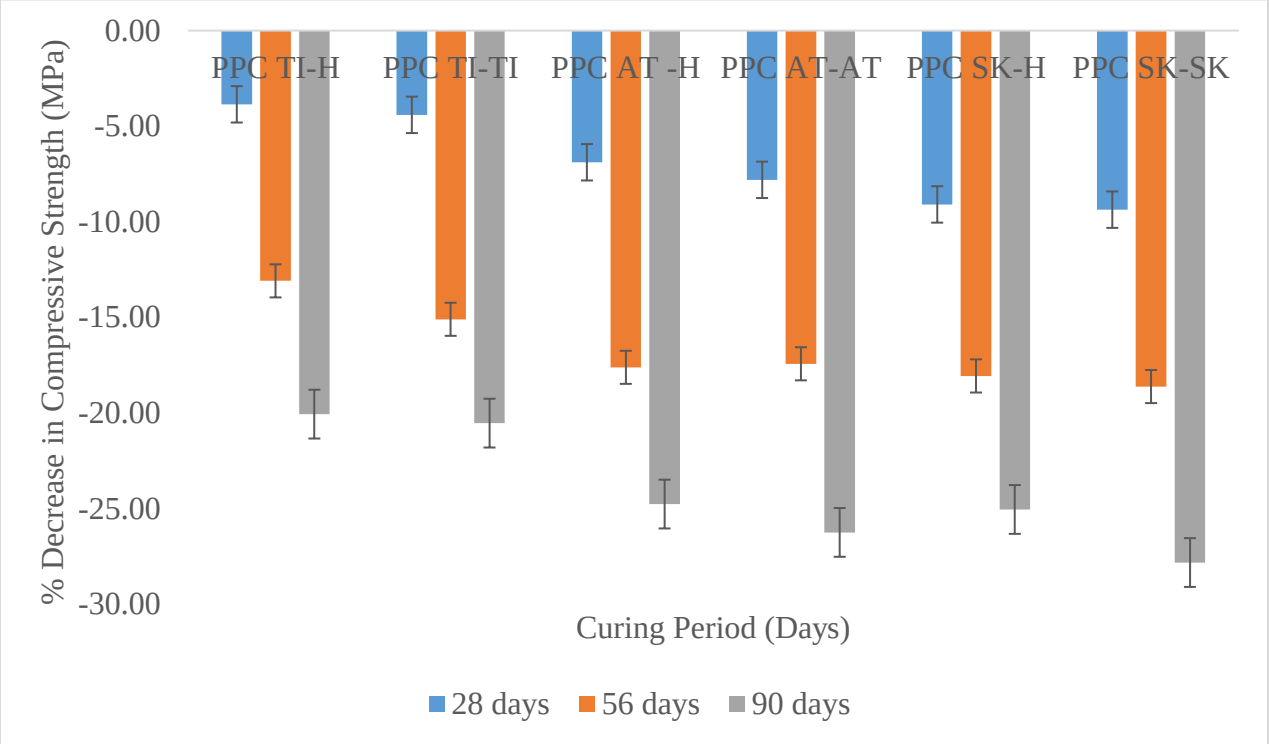

Figure 4.14: Percentage Decrease in Compressive Strength of PPC Mortars

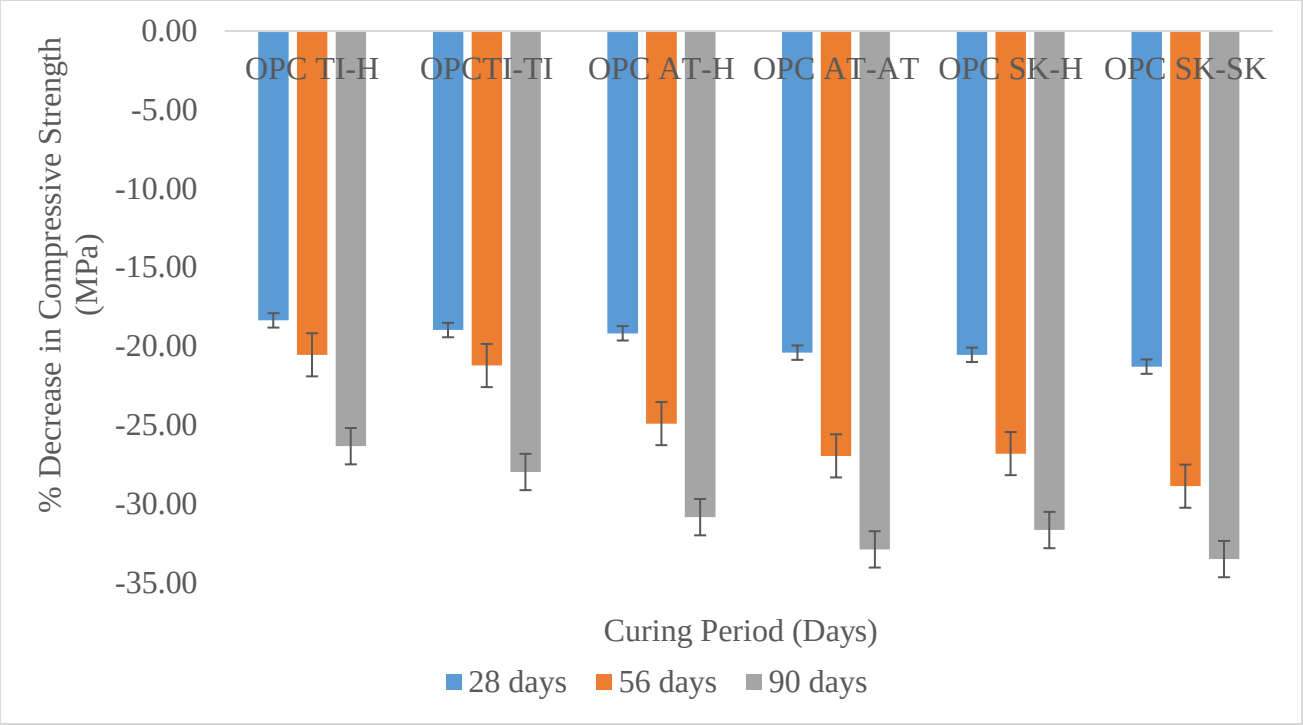

Figure 4.15: Percentage Decrease in Compressive Strength of OPC Mortars

Compressive strength of test cements (PPC and OPC) decreased significantly from 28th day of curing when mixed either with bacteria solution as mixing media and/or both as mixing and curing media. Like the t-test comparison between the controls and the specific bacteria, the analysis of variance showed that the bacteria species used significantly affected the compressive strength performance of both PPC and OPC after 28th day of curing. Tables 4.7 and 4.8 show the single factor analysis of variance for PPC and OPC mortars in varied bacteria solutions after curing for 28 days. From the analysis, each specific bacteria when used as either mixing media or both mixing and curing media significantly affected the performance of either OPC and/or PPC. The Fcal was greater than the F crit with P-values below 0.05.

Table 4.7: Analysis of variance for PPC mortars in varied bacteria solutions at 28 days of curing

Groups	Count	Sum	Average	Variance		
PPC AT-H	3	101.40	33.80	0.00		
PPC AT -AT	3	100.40	33.47	0.09		
PPC TI -H	3	104.70	34.90	0.00		
PPC TI-TI	3	104.10	34.70	0.00		
PPC SK-H	3	99.00	33.00	0.04		
PPC SK-SK	3	98.70	32.90	0.01		
Source of Variation	SS	df	MS	F calc	P-value	F crit
Between Groups	10.74	5	2.15	89.94	0.00	3.11
Within Groups	0.29	12	0.02			
Total	11.03	17				

Table 4.8: Analysis of variance for OPC mortars in varied bacteria solutions at 28 days of curing

Groups	Count	Sum	Average	Variance		
OPC AT-H	3	118.5	39.50	0.00		
OPC AT-AT	3	116.7	38.90	0.00		
OPC TI-H	3	119.7	39.90	0.00		
OPC TI-TI	3	118.8	39.60	0.00		
OPC SK-H	3	116.5	38.83	0.04		
OPC SK-SK	3	115.4	38.47	0.04		
Source of Variation	SS	df	MS	F Cal	P-value	F crit
Between Groups	4.51	5	0.90	62.4	0.00	3.11
Within Groups	0.17	12	0.01			
Total	4.68	17				

While each test bacteria (*Thiobacillus intermedius, Acidithiobacillus thiooxidans* and *Starkeya novella*) revealed a negative effect on the strength of either PPC or OPC mortars, *Starkeya novella* exhibited higher compressive strength decline of 27.82% and 33.50% for PPC and OPC mortars at 90th day of curing respectively. The observed compressive strength decline was due to the sulphuric acid produced by the test bacteria activity. The generated acid would cause erosion on the hydration products, lowering the mechanical properties of the test mortars.

The generated biogenic sulphuric acid reacts with portlandite (CH) as the main hydration product to yield gypsum. The formation of secondary gypsum causes volume expansion of exposed concrete and/or mortar to approximately 120 -220 % (Parande *et al.*, 2006). The resultant gypsum further reacts with aluminate phase of the cement to form ettringite. Ettringite causes volume expansion more than gypsum. It is estimated to cause volume expansion of approximately 227-700% (Sun, 2015). Equations 4.10 and 4.11 show the reaction between the biogenic acid and the subsequent reaction between gypsum and aluminate phase of cement resulting to formation of ettringite (Sun, 2015).

$$H_2SO_4 + Ca(OH)_2 \rightarrow CaSO_4.2H_2O \qquad 4.10$$

$$3CaSO_4 + 3CaO.Al_2O_3.6H_2O + 26H_2O \rightarrow 3CaO.Al_2O_3.3CaSO_4.32H_2O \qquad 4.11$$

Biogenic sulphuric acid generation through the microbial activities of acidophilic sulphur oxidising bacteria contribute to lining degradation and corrosion of concrete and mortar in sewer pipes (Valix and Shanmugarajah, 2015). The colonization of the microbes on the surface of the

concrete and mortar material and subsequent formation of the biogenic acid lowers the surface pH. This results in reduction of the mechanical properties of the exposed concrete and mortar surface (Jean *et al.,* 2013). Among the test bacteria, *Starkeya novella* was found to be more deleterious. This particular strain of the bacteria has the ability to oxidize thiosulphate into sulphuric acid (Munyao *et al.,* 2020b; Sun *et al.,* 2015).

PPC mortars (figure 4.12) exhibited some resistivity to bacterial attack when compared to OPC microbial mortars (figure 4.13). This was attributed to pozzolanic activity (Muthengia, 2009). Pozzolans consist of reactive silica and alumina, which reacts with the CH as the main hydration product to form additional secondary cementitious material (C-S-H and C-A-H). This reaction lowers the concentration of CH in pore solution hence inhibiting the pozzolanic cements from attack by external materials such as biogenic acid, sulphates and chlorides (Walid *et al.,* 2017).

The mechanical properties of the test cements were in agreement with the microstructural analysis previously reported. The reported erosion of CH plates and the advance formation of ettringite crystals within the pore matrixes of the exposed mortars in bacteria solution as observed in SEM justified the observed decline in mechanical properties of bacteria prepared mortars. The selected bacteria showed a potential to degrade and lower the mechanical properties of the commercial made OPC and PPC mortars.

4.6.3 Effect of chemical sulphuric acid on compressive strength of PPC and OPC Mortars

Figure 4.16 show the percentage decrease in compressive strength for PPC and OPC (as calculated using equation 4.9) when cured in 1.5% chemical sulphuric acid.

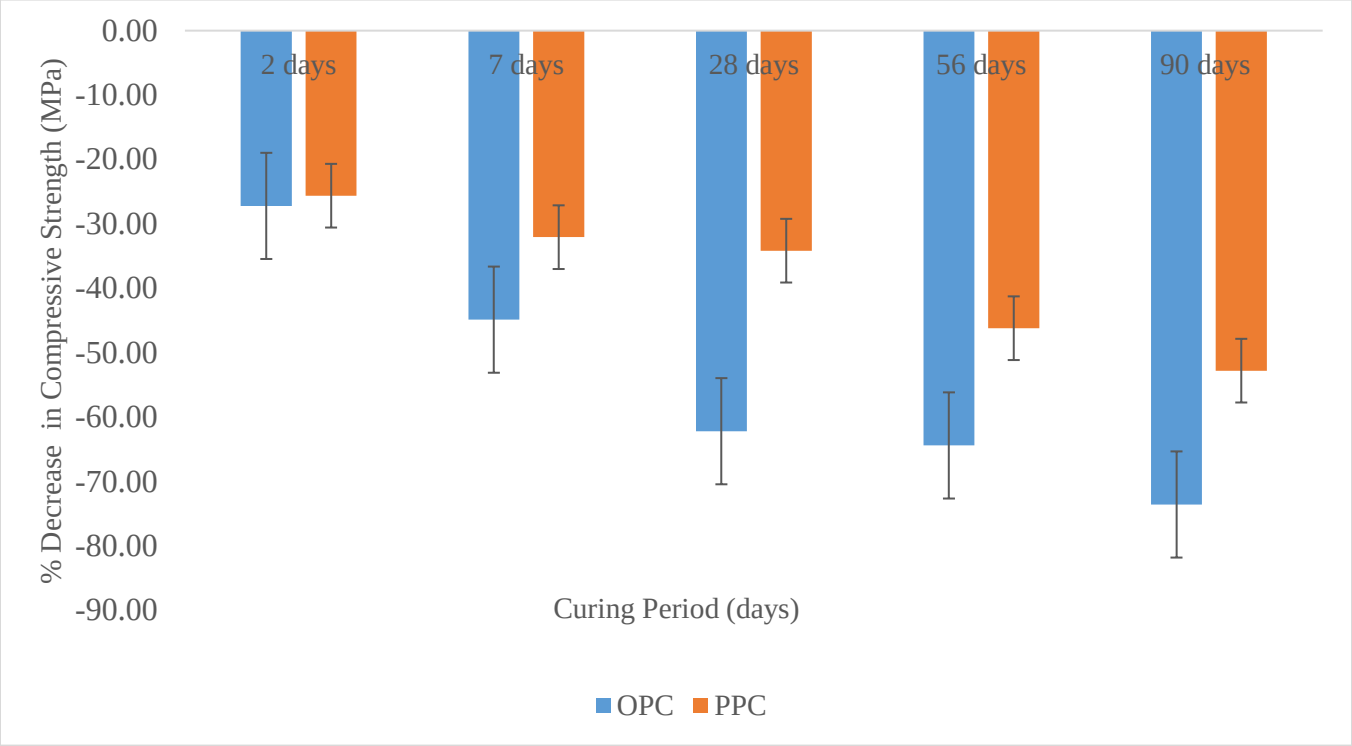

Figure 4.16: Compressive Strength Decrease of OPC and PPC Mortars when cured in 1.5% chemical sulphuric acid

The deterioration process observed in test mortars exposed to sulphuric acid mirrored the mortar performances in bacteria solutions. However, the chemical sulphuric acid exhibited extreme deterioration of cement strengths as early as at 2 days of exposure. Presence of chemical sulphuric acid as a curing media subjected the test cements to very low pH. The dissociation of sulphuric acid into H^+ and SO_4^{2-} lowered the pH of the pore solution. This allowed immediate attack of the CH and CSH by the H^+ resulting in formation of secondary gypsum (Fulin *et al.,* 2021). The formed $C\bar{S}H_2$ triggered formation of ettringite. This is as described in equations 4.10 and 4.11.

OPC mortars showed extreme decline in compressive strength. The sharp decline in compressive strength for OPC mortars was attributed to high CH and C-S-H phases in the pore solution (Lei *et al.,* 2019). These are the main hydration phases, which are prone to attack by either acids, chlorides

or sulphate ions (Zheng *et al.*, 2020). The extent of degradation increased with increase in curing period. Similar trend was observed in mortars prepared with microbial solutions. This was attributed to higher pore formation as the acid reacted with the soluble constituents of the cement (Yongchung *et al.*, 2021). The sharp continued decline in strength was further attributed to the micro cracks because of continued formation of ettringite (Hadigheh *et al.*, 2017; Yuan *et al.*, 2013). There was observed whitish formation at the top of the mortar prisms with rust-like stain on the surfaces of the exposed mortars as shown in plate 4.9. This was attributed to the acid attack on the soluble constituents of the cement. The whitish material was attributed to the formation of secondary gypsum as shown in equation 4.10 (Javad and Mahdi, 2019; Bakharev, 2005).

Plate 4.9: Mortar Prisms Exposed in sulphuric acid as a curing media

4.7 Water Absorptivity

The percentage water absorptivity for PPC and OPC mortars prepared with distilled water as controls and selected microbial solutions was calculated as defined in equation 3.6. Figure 4.17 show percentage gain in absorptivity for the control test cements of PPC and OPC.

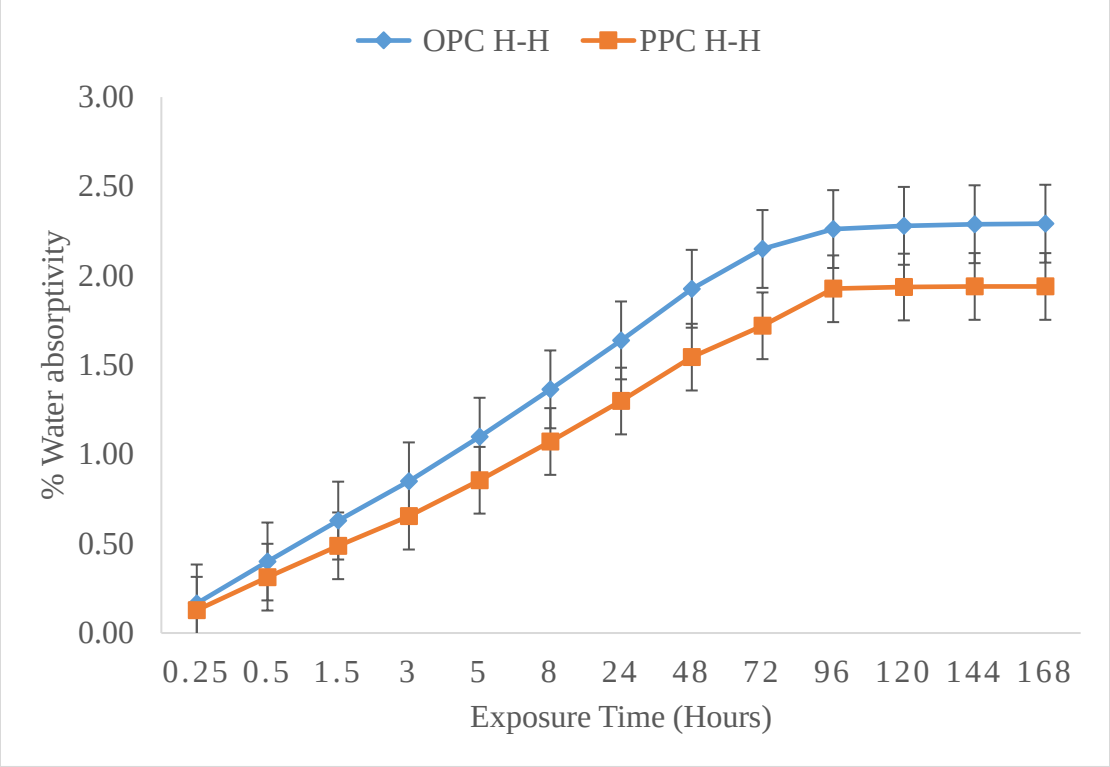

Figure 4.17: Percent water absorptivity for control PPC and OPC after 28th day of curing.

The percent water absorptivity in both test cements increased with increase in exposure duration. This was attributed to the hygroscopic nature of cement (Fangzhou *et al.*, 2021). Due to the heat generated during the hydration, cement mortar form pores that allow water ingress into the mortar matrix (Aiman *et al.*, 2019). It was however noted that after the 120th hour, there was no appreciable water absorption in either OPC or PPC. This was perhaps due to water saturation into

the mortar matrix. Table 4.9, gives the summary of T-test analysis for the percentage water absorption between OPC H-H and PPC H-H.

Table 4.9: T_{cal} values for the water absorptivity between the controls of OPC and PPC at varied exposure duration (T_{crit} = 2.78 at 95% confidence level).

	Exposure Duration (Hours)												
	0.25	0.5	1.5	3	5	8	24	48	72	96	120	144	168
Tcal	3.02	8.87	10.86	11.94	13.96	15.00	18.41	19.43	22.67	21.37	21.37	22.71	24.13
P-value	0.04	0.00	0.00	0.00	0.00	0.00	0.00	0.00	0.00	0.00	0.00	0.00	0.00

There was observed significant difference in percent water absorptivity between control OPC and PPC as shown in table 4.9 ($T_{cal} > T_{crit}$ and p-value below 0.05 across all the exposure duration). OPC exhibited higher percentage gain in water absorptivity than PPC in all the exposure duration. This was attributed to pore structure of the OPC mortar matrix. The neat OPC has higher CaO content, C_3S and C_3A phases, which upon hydration releases a high amount of heat (Hailong and Le, 2020). The generated heat makes the surface more porous hence increasing its permeability (Zhang and Zong, 2014).

The control PPC mortars exhibited reduced water absorptivity because of the pozzolana reaction between the CH and the reactive silica and alumina from pozzolana. The resultant products (C-S-H and C-AH) are denser and hence lowers the permeability of the PPC based cements (Diandian *et al.,* 2021). In addition, the pozzolana grains pack well within the matrix of the mortar /concrete making it compact with minimal pores. This improves the reduction of water absorption by 45% for pozzolana-based cements (Walid *et al.,* 2017).

Figures 4.18 and 4.19 represent the water absorptivity results for the mortars of OPC and PPC prepared with solutions of *Thiobacillus intermedius, Acidithiobacillus thiooxidans and Starkeya novella* bacteria at different treatment scenarios respectively.

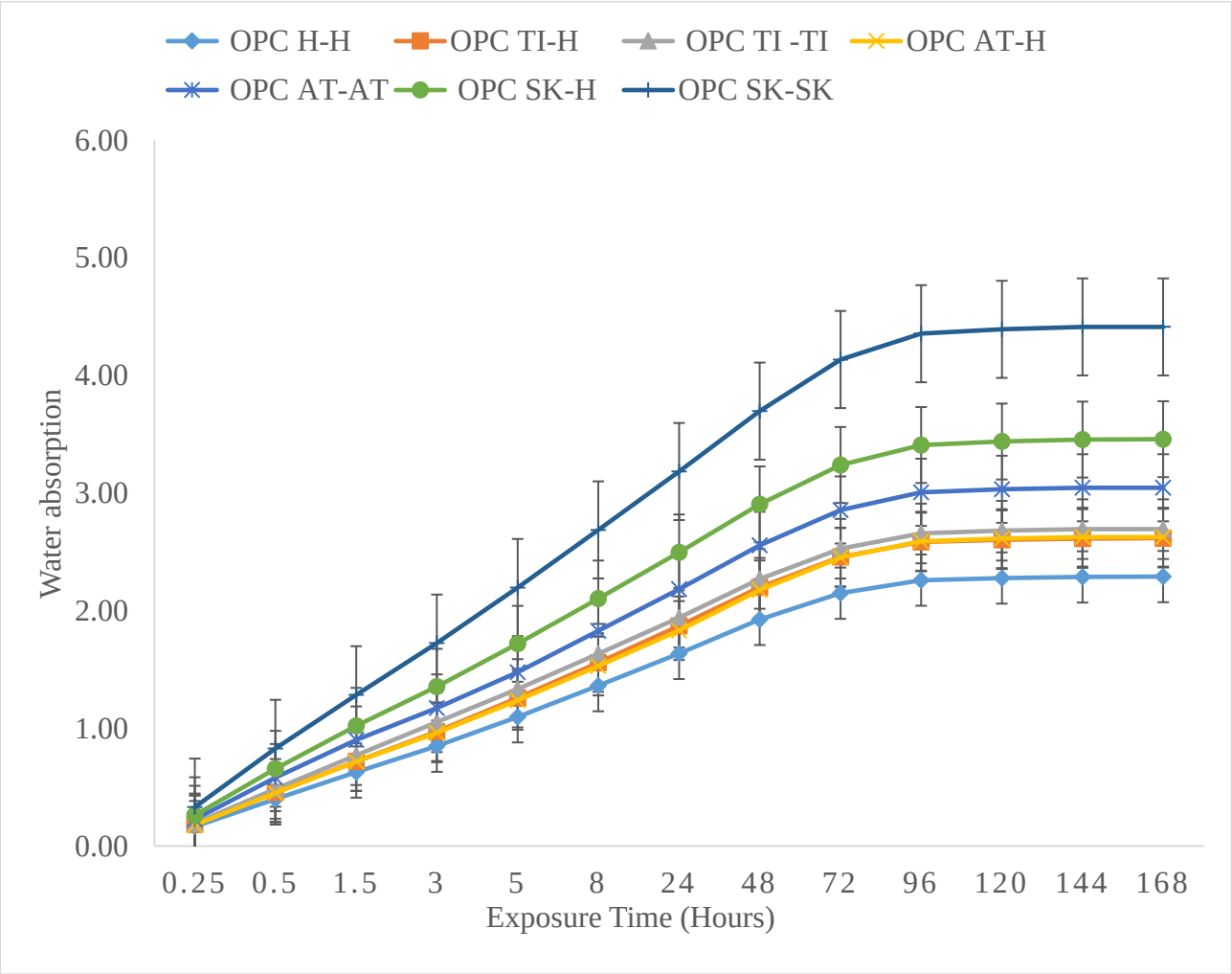

Figure 4.18: Water absorptivity for OPC mortars in varied bacteria solutions after 28th day of curing

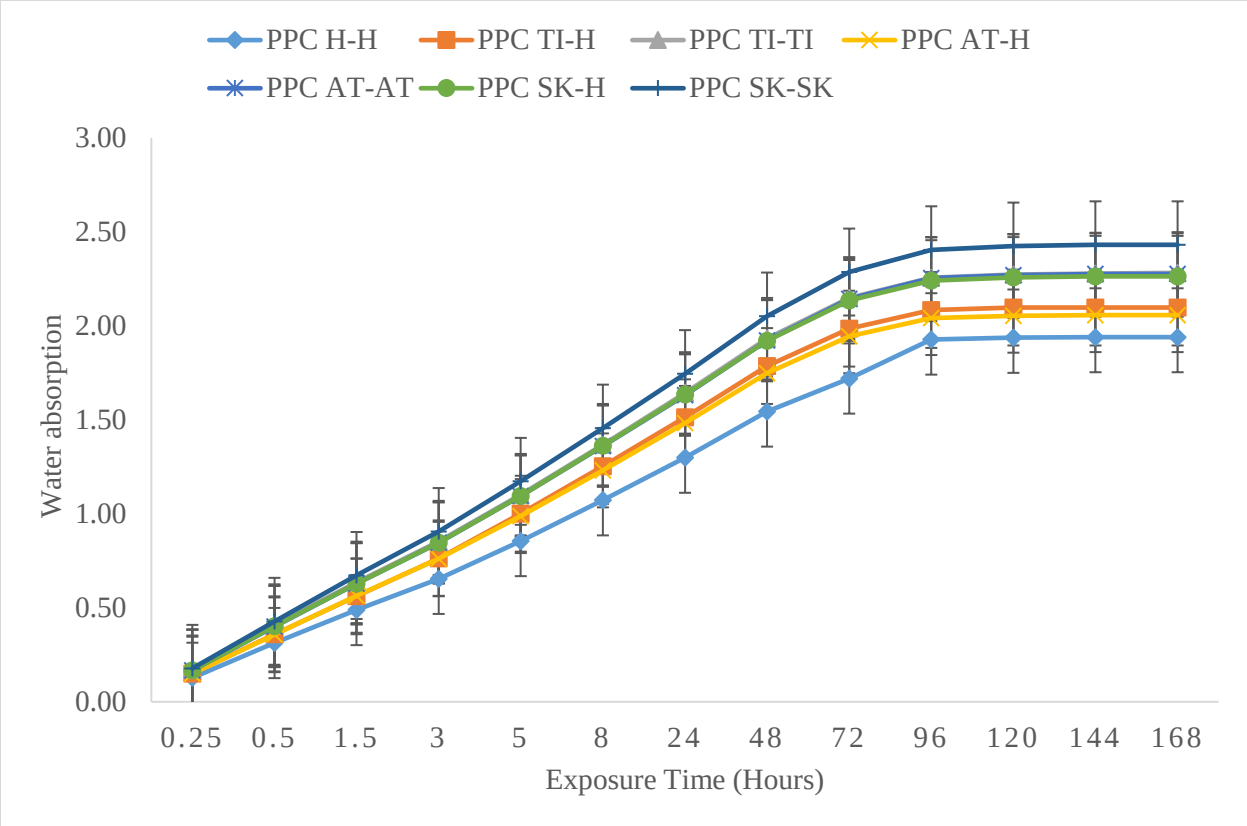

Figure 4.19: Water absorptivity for PPC mortars in varied bacteria solutions after 28th day of curing

The water absorptivity gain increased with increase in exposure duration for both OPC and PPC microbial treated mortars. This was as observed in control mortars. Tables 4.10 and 4.11 show the summary of statistical T-test analysis capturing the T_{cal} values at different exposure duration for control OPC and PPC mortars prepared with respective selected bacteria solutions respectively. The comparison for t-test was made for either OPC or PPC control mortars with a specific bacteria solution as either mixing or curing media at a given time. The statistical analysis shows that there was significance difference between the control OPC and the mortars of OPC prepared and cured in varied bacteria solutions. This was observed across the different exposure durations. A similar trend was observed in PPC mortars.

Table 4.10: T_{cal} values between OPC control and OPC Mortars prepared with varied bacteria solutions at different exposure durations (T_{crit} = 2.78 at 95% confidence level)

Control Mortar	Exposure Duration (Hours)	Cement Mix Composition					
		OPC TI-H	OPC TI-TI	OPC AT-H	OPC AT-AT	OPC SK-H	OPC SK-SK
OPC H-H	0.25	3.52	3.69	3.34	7.25	11.07	19.49
	0.5	4.12	3.73	6.16	12.01	11.53	22.64
	1.5	5.51	3.90	6.95	10.95	13.22	20.86
	3	7.75	5.54	8.51	18.75	12.36	25.96
	5	9.49	8.77	7.15	16.39	15.91	24.35
	8	9.03	12.92	10.41	16.66	17.73	20.10
	24	8.12	16.68	13.25	12.22	16.27	18.01
	48	10.95	18.82	10.31	19.00	16.86	24.54
	72	12.61	16.30	16.44	18.84	13.49	24.77
	96	11.40	18.29	10.20	19.70	13.43	26.00
	120	9.43	18.99	12.06	19.97	14.02	25.71
	144	11.68	18.33	11.07	19.87	14.30	25.10
	168	10.11	18.23	16.09	19.80	19.52	26.10

Table 4.11: T_{cal} values between PPC control and PPC Mortars prepared with varied bacteria solutions at different exposure durations (T_{crit} = 2.78 at 95% confidence level)

Control Mortar	Exposure Duration (Hours)	Cement Mix Composition					
		PPC TI-H	PPC TI-TI	PPC AT-H	PPC AT-AT	PPC SK-H	PPC SK-SK
PPC H-H	0.25	3.13	3.61	3.26	3.44	3.09	3.87
	0.5	3.65	4.74	5.00	8.88	8.89	11.63
	1.5	4.66	5.45	8.67	9.04	7.07	9.07
	3	3.14	3.98	6.14	10.11	5.08	3.67
	5	4.03	4.17	5.68	4.13	4.14	7.31
	8	5.77	6.06	9.47	5.32	5.27	6.75
	24	5.60	7.38	11.98	11.38	4.60	5.18
	48	4.12	5.70	5.61	6.45	6.53	6.28
	72	3.24	5.59	6.63	5.18	3.15	8.84
	96	4.24	4.59	8.60	8.80	7.84	9.41
	120	5.34	5.57	8.63	9.15	3.53	7.62
	144	5.38	6.53	4.48	4.81	3.96	6.00
	168	5.91	7.87	5.71	5.86	4.22	6.29

Single factor Anova analysis further showed that the absorptivity of the test cements varied significantly when subjected in the selected test bacteria as either mixing or curing media. Table 4.12 gives the analysis of variance for OPC mortars when subjected to the selected bacteria after 28 days of curing.

Table 4.12: Analysis of variance for absorptivity test of OPC mortars in bacteria solutions

Groups	Count	Sum	Average	Variance		
OPC AT-H	39	210.39	5.39	7.84		
OPC AT-AT	39	243.09	6.23	9.79		
OPC TI-H	39	201.84	5.18	7.08		
OPC TI-TI	39	206.67	5.30	7.14		
OPC SK-H	39	266.79	6.84	11.63		
OPC SK-SK	39	334.53	8.58	18.40		
Source of Variation	SS	df	MS	F cal	P-value	F crit
Between Groups	333.75	5	66.75	6.47	0.00	2.25
Within Groups	2351.64	228	10.31			
Total	2685.40	233				

The prepared mortars of OPC and PPC, cast and cured using bacteria solution as both mixing and curing media exhibited higher absorptivity gain as compared to those mortars prepared using bacteria solutions and cured in water. Table 4.13 indicates the summary of the percentage gain in water absorptivity for the microbial prepared mortars of OPC and PPC.

Table 4.13: Percentage gain in water absorptivity for OPC and PPC microbially prepared mortars at 28 days of curing.

	Cement Type			
Test Bacteria	OPC		PPC	
	Mortar Test Regime	% Water Gain	Mortar Test Regime	% Water Gain
Thiobacillus Intermedius	OPC TI-H	11.19	PPC TI-H	5.11
	OPC TI-TI	17.66	PPC TI-TI	10.46
Acidithiobacillus thiooxidans	OPC AT-H	14.70	PPC AT-H	6.04
	OPC AT -AT	33.03	PPC AT -AT	17.30
Starkeya novella	OPC SK-H	50.93	PPC SK-H	16.67
	OPC SK-SK	72.75	PPC SK-SK	25.32

The percent water absorptivity gain was higher in OPC mortars prepared with microbial solutions than in PPC mortars. This was observed across all the treatment regimes. The increase in absorptivity for the OPC mortars prepared with microbial solutions was attributed to the phase composition of OPC (Hailong and Le, 2020). OPC has high affinity for attack by aggressive material such as sulphates and chlorides due to high content of C_3A phase (Bakharev, 2005). This is as described in table 4.2. The activity of the bacteria facilitated the formation of aggressive media (generation of biogenic sulphuric acid) which attacked the surface of the OPC matrix (Yu *et al.*, 2018).

Starkeya novella exhibited the highest gain in water absorptivity across the test cements. This was due to the ability of the *Starkeya novella* bacteria to generate high amounts of sulphuric acid as compared to other test bacteria. The absorptivity results of the microbial treated mortars agreed with the compressive strength data, SEM, XRD and FTIR data for the microbial treated mortars. The secondary products observed in SEM, XRD and FTIR could have contributed to increase in porosity of the exposed mortars to the bacteria solutions. This enhanced the observed higher uptake of water by the microbial prepared mortars.

The absorptivity results show that the bacteria activity made the PPC and OPC mortar surfaces more porous and hence allowed the ingress of external water. Absorptivity is a critical property in evaluating the durability of cement-based materials (Vimal, 2009). The more porous the concrete is, the higher the uptake of water and the lower the mechanical properties (Veera, 2021). Compressive strength development of concrete and mortar is dependent on the volume of C-S-H, which is indirectly proportional to the pores in the placed mortar and concrete (Mindess *et al.*, 2003). Further, this explains why the compressive strength of the microbial prepared mortars was low. The activity of these deleterious bacteria in most of sewer areas would perhaps influence the ingress of other injurious materials into the placed concrete and mortar and cause more damage.

4.7.1 Sorptivity Coefficients

Sorptivity coefficients for control OPC and PPC and varied mortars of OPC and PPC prepared with selected microbial solutions as either mixing water and /or curing media was determined after 28th day of curing as defined in section 3.3.8. Figures 4.20 and 4.21 represent the sorptivity coefficients for the control OPC and PPC with their respective mortars prepared in varied bacteria solutions respectively.

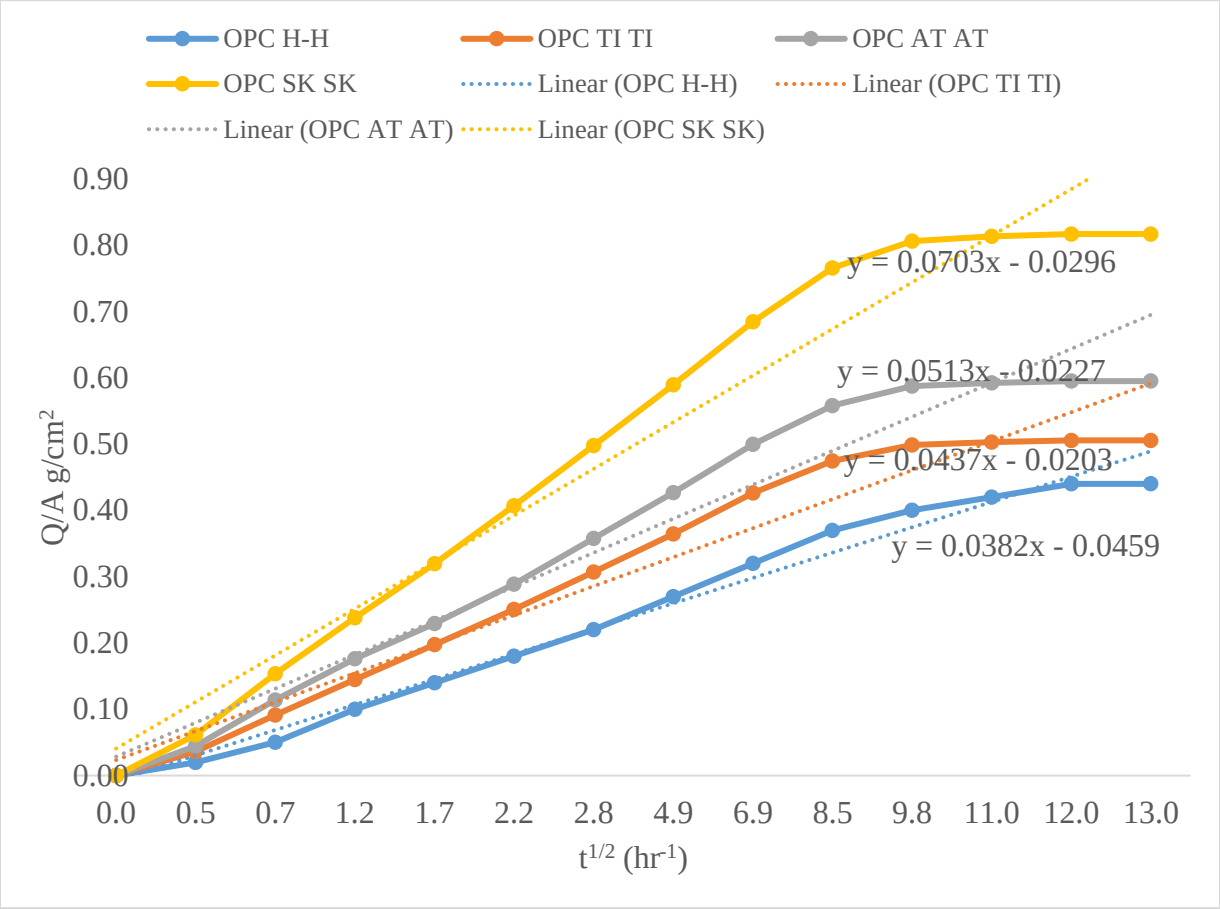

Figure 4.20: Sorptivity coefficients for OPC H-H, OPC TI-TI, OPC AT-AT and OPC SK-SK after 28th day of curing.

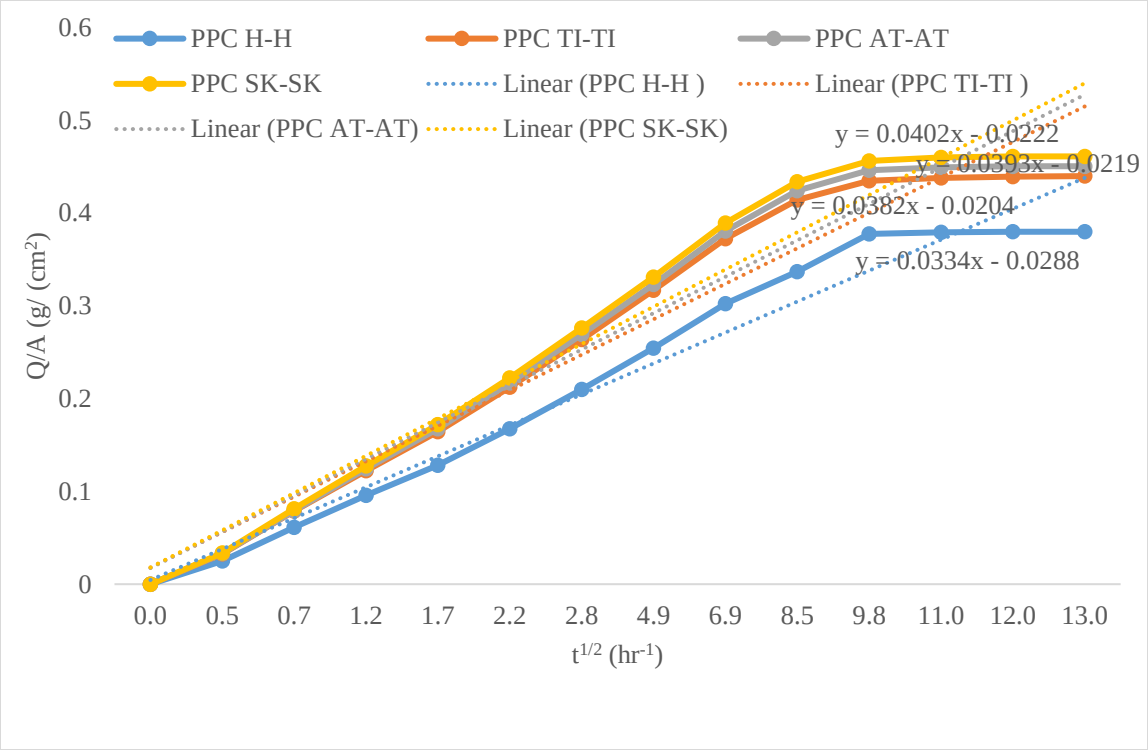

Figure 4.21: Comparative sorptivity coefficients for PPC H-H, PPC TI-TI, PPC AT-AT and PPC SK-SK at 28 days of curing.

Results showed low sorptivity coefficient (k) for OPC H-H and PPC H-H as compared to other mortars of OPC and PPC prepared with the microbial solutions. This observation mirrored the absorptivity results. The high sorptivity coefficients in the OPC and PPC mortars prepared with microbial solutions was attributed to the activities of the bacteria. However, the sorptivity coefficients for the PPC mortars prepared with the microbial solutions was lower compared to the OPC mortars prepared with similar microbial solutions. This was attributed to the pozzolanic activity that leads to densification of the resultant mortar through formation of secondary C-S-H in pozzolana-based cements (Daniel *et al.*, 2019; Walid *et al.*, 2017).

Table 4.14 summarizes the sorptivity coefficient values for both control and mortars of OPC and PPC prepared with microbial solutions at 28 days of curing. As observed, the control OPC (OPC H-H) exhibited higher sorptivity coefficient than control PPC (PPC H-H). This observation agreed with the chemical and phase composition of the test cements as described in table 4.1 and 4.2. OPC has higher CaO and C_3S, C_2S and C_3S phases, which upon hydration has the affinity for higher permeability due to high heat of hydration (Scrivener *et al.,* 2015).

Table 4.14: Sorptivity coefficient values for control and microbial OPC and PPC at 28 days of curing

Cement Type	Mortar Description	Sorptivity Coefficient
OPC	OPC H-H	0.0382
	OPC TI-TI	0.0437
	OPC AT-AT	0.0513
	OPC SK-SK	0.0703
PPC	PPC H-H	0.0334
	PPC TI-TI	0.0382
	PPC AT-AT	0.0393
	PPC SK-SK	0.0402

OPC mortars cast using microbial solutions exhibited higher sorptivity coefficients than the corresponding PPC mortars cast using the same microbial solutions. This was attributed to the massive formation of ettringite on the pore surface of the OPC mortars (Lei *et al.,* 2019). This observation agreed with SEM micrographs where the mortars prepared using microbial solutions showed formation of ettringite crystals. The formation of ettringite (AFt) would cause expansion of exposed mortar leading to formation of micro-cracks within the pore structure (Mari *et al.,*

2021). The formed micro-cracks would form suitable conduits for the ingress of water and/ other external material into the mortar and concrete matrix (Zhenyun *et al.*, 2021).

The sorptivity coefficient results for the mortars prepared with microbial solutions agreed with the mechanical and microstructural test results as reported in previous sections of this work. The test results showed that the selected bacteria increased the sorptivity coefficients of the test mortars. This has a direct negative effect on the durability of such exposed concrete and mortar structures.

4.8 Chloride ingress

4.8.1 Chloride Profiling

Figure 4.22 represent the chloride ion ingress in mortars of PPC H-H and OPC H-H at different penetration depths after 28th day of curing.

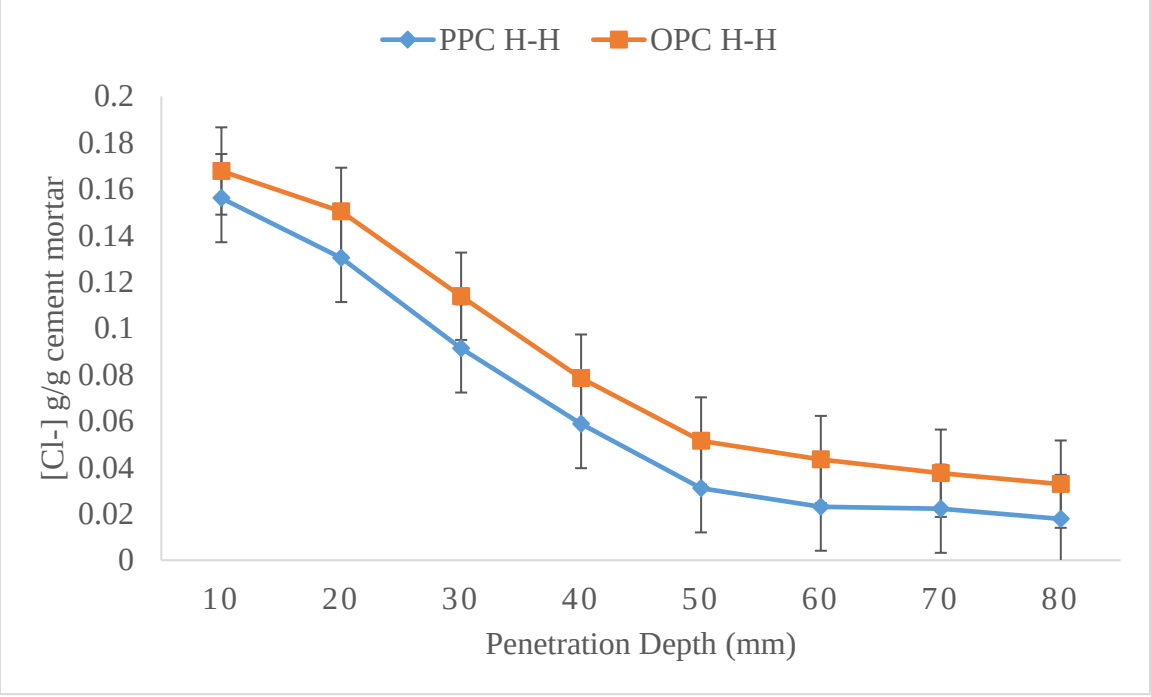

Figure 4.22: Chloride ingress in mortars of PPC H-H and OPC H-H after 28th of curing

The findings of the test analysis indicate that chloride ion intrusion into the cement mortar matrix reduced as the penetration depth increased in both PPC and OPC. This was due to the binding ability of chlorides by the cementitious materials (Chunyu *et al.*, 2019). Cementitious materials have the ability to bind chloride ions (Muralidharan *et al.*, 2005). The binding happens because of adsorption of chloride ions on the calcium silicate hydrate phase (Chunyu *et al.*, 2019). The resultant process leads in formation of Kuzel salt, $Ca_4Al_2(OH)_{12}Cl(SO_4)_{0.5}.5H_2O$ and Friedels salt, $Ca_4Al_2(OH)_{12}Cl.4H_2O$ (Mesbah *et al.*, 2011, Birnin and Glasser, 1998). The binding of some of the chloride ions by the cement material lowers the ingress of the free chloride ions into the pore solution of the cement mortar and/ or concrete and hence minimizing the corrosion of the rebar (Glass and Buenfeld, 2000).

PPC H-H exhibited reduced chloride ingress as compared to OPC H-H. This was attributed to pozzolanic reaction that results in formation of additional C-S-H and C-A-H in pozzolana-based cements (Zornoza *et al.*, 2009). Pozzolanic materials added in cement serve as secondary cementitious materials. These materials are rich with reactive silica and alumina, which takes up the CH from the cement hydration to form additional secondary hydration products. Thomas *et al.* (2012) while studying on the effect of supplementary cementitious materials on chloride binding in hardened cement paste reported that supplementary cementitious materials influence the chloride binding ability. The authors (Thomas *et al.*, 2012) pointed out that the reactive alumina content in supplementary cementitious materials (Fly Ash, natural pozzolans, slag) enhances the formation of Friedels salt. This hinders the ingress of chloride ions in blended cements. Qiao *et al.* (2018), Glass and Buenfeld (2000), and Martin-Perez *et al.* (2000), made similar observations.

Additionally, the decrease in chloride ingress in control PPC was perhaps due to decreased permeability observed in pozzolanic-based cements. This was as reported in water absorptivity test results and SEM morphology for the PPC. Due to pozzolanic activity, the resultant mortar was denser and more packed and hence made the pore structure more compact. Studies done by Zornoza *et al.* (2009) implied that incorporation of spent cracking catalyst (FC3R) on OPC mortars lowered the chloride ingress in OPC mortars. The authors attributed the resistance to pozzolanic reaction of FC3R that resulted in higher proportions of hydrated calcium aluminates and silico-aluminates. According to Zornoza *et al.* (2009), the formation of Friedels salt in pozzolana-based cements improves on the chloride binding capacity. This is as shown in equation 4.12 (Zornoza *et al.,* 2009).

$$CaCl_2 + C_3Al_2O_6.8H_2O + 2H_2O \rightarrow Ca_4Al_2O_6Cl_2.10H_2O \qquad 4.12$$

The higher uptake of chloride ingress in OPC H-H was attributed to phase composition as described in table 4.2. OPC has higher C_3S and C_3A phases, which upon hydration release high heat (Hailong and Le, 2020. The heat generated causes increased pore structure and hence improved permeability (Huawei et *al.,* 2020). This observation agreed with the water absorptivity results. This could perhaps allow the ingress of chloride ions into the mortar matrix. Further, as reported in SEM results, there were extensive formation of CH plates in OPC mortars. CH forms a suitable attack point by chlorides (Kirubajiny *et al.,* 2021).

Figures 4.23 and 4.24 represents the chloride ion ingress in hydrated mortars of PPC and OPC when prepared with *Thiobacillus intermedius*, *Acidithiobacillus thiooxidans* and *Starkeya novella* bacteria medium after 28th day of curing respectively.

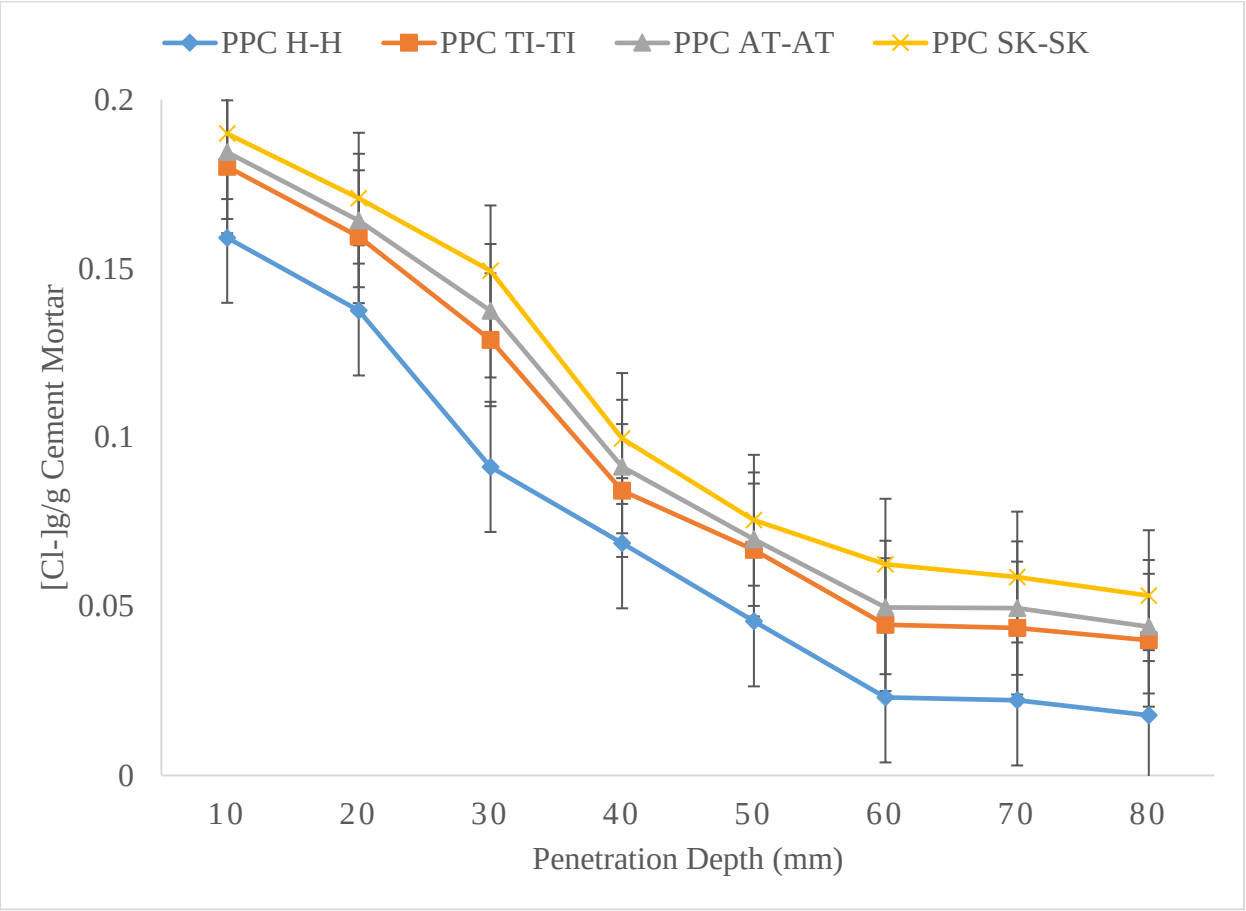

Figure 4.23: Chloride ingress in PPC Mortars Prepared with Selected Bacteria Solutions after 28th day of curing

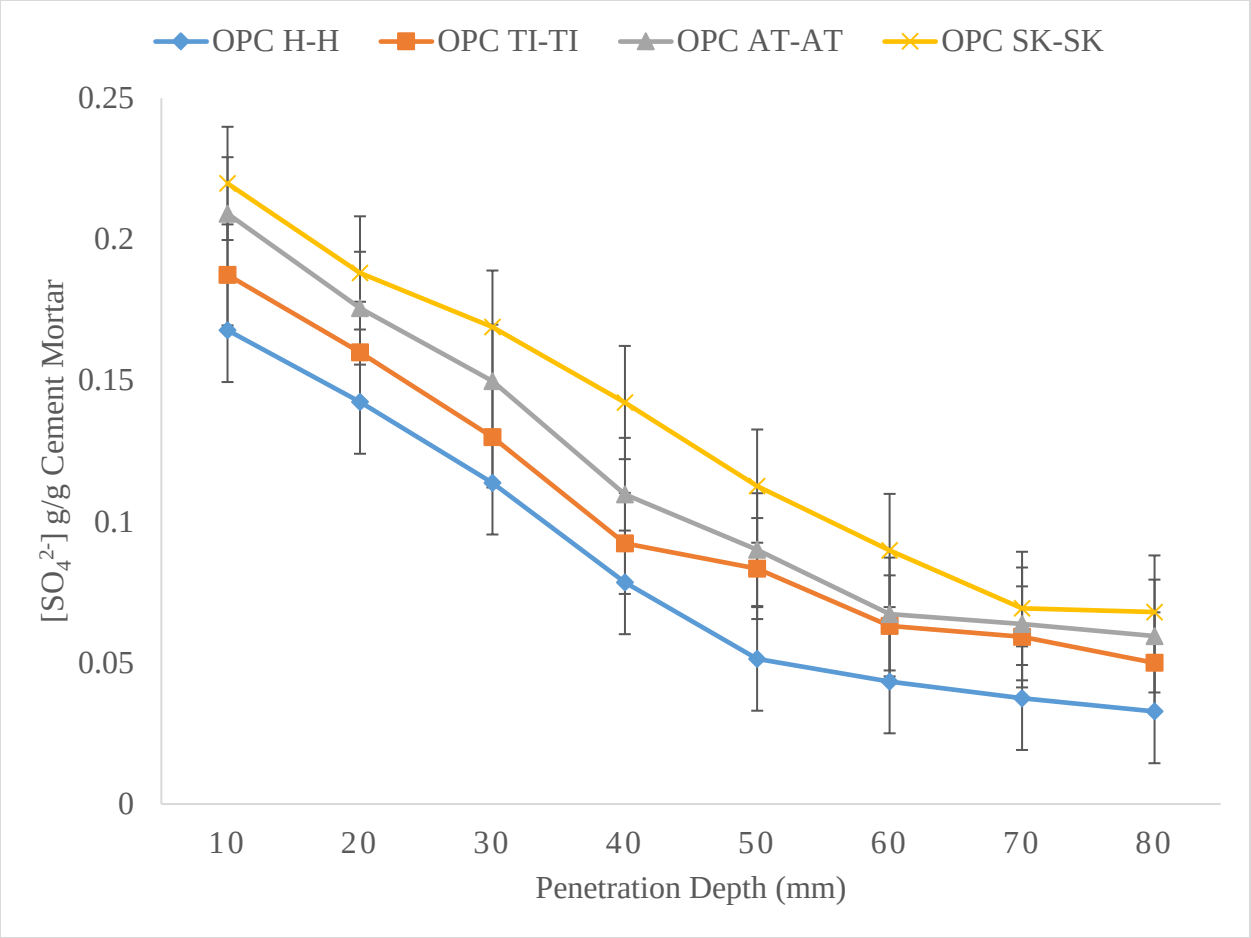

Figure 4.24: Chloride ingress in OPC Mortars Prepared with Selected Bacteria Solutions after 28th day of curing

Figures 4.23 and 4.24 show that the ingress of chloride ions decreased with increase in penetration depth in both test cements. This was as observed in figure 4.22. However, it was observed that the bacteria prepared mortars exhibited increase in chloride ingress across all the penetration depth as compared to the control mortars (PPC H-H and OPC H-H). This was attributed to the attack by aggressive biogenic sulphuric generated by the bacteria activities (Tahereh *et al.*, 2017).

Moreover, the reaction between the generated biogenic sulphuric acid from the bacterial activities and the hydration product (CH) resulted in formation of expansive secondary gypsum and ettringite. This was as confirmed from the SEM analysis results. The formed expansive products would perhaps result in formation of micro- cracks within the pore system of the exposed cement mortar. The formed micro cracks would act as conduit for the ingress of the chloride (Huawei *et al.*, 2020; Munyao *et al.*, 2020a).

Based on the test results, the cement mortars exposed to *Starkeya novella* gave higher chloride ingress as compared to *Thiobacillus intermedius* and *Acidithiobacillus thiooxidans*. This was perhaps due to the ability of *Starkeya novella* to generate higher amounts of biogenic sulphuric acid compared to the other two bacteria within the defined time. The reaction of biogenic acid with the cement constituents would result in formation of expansive secondary ettringite within the pore system. The formed ettringite would enhance formation of micro-cracks hence allowing ingress of chloride ions into the exposed mortar. The performance of *Starkeya novella* on chloride ingress and subsequent degradation of the cement mortars agreed with the other test results such as compressive strength, setting time and absorptivity previously reported in this work.

4.8.2 Chloride Apparent Diffusivity Coefficients

The chloride apparent diffusivity coefficients for the control and microbial PPC and OPC test cements were determined using the error function-fitting curve. Figure 4.25 show the typical chloride error function-fitting curve for PPC SK- SK. Similarly, the apparent chloride diffusion coefficients for the other test mortars were determined using similar error function fitting curves.

The summary of error fitting data for both control and mortars of PPC and PPC prepared with microbial solutions is as tabulated in table 4.15.

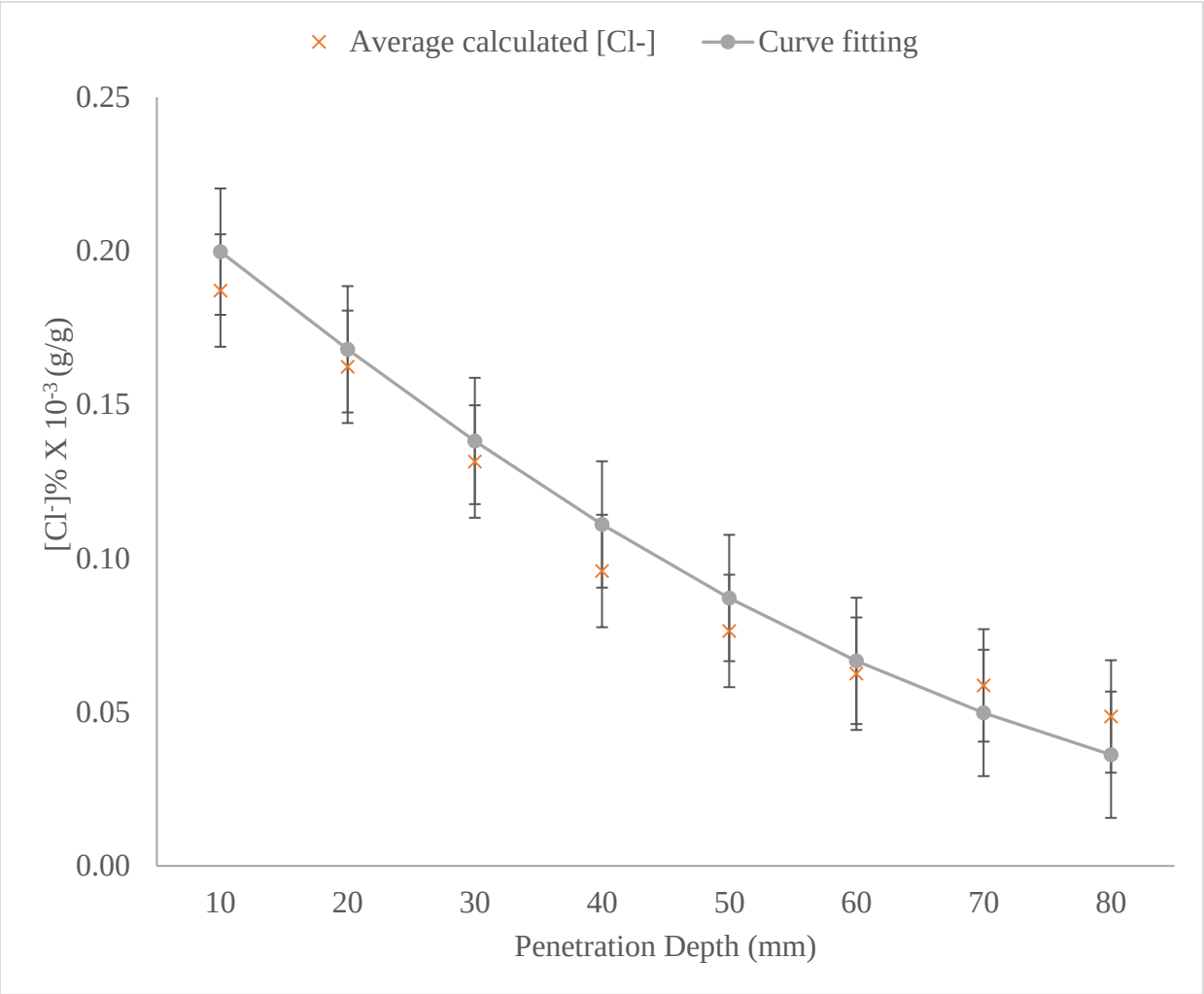

Figure 4.25: Error function fitting curve for PPC SK-SK D_{app} = (6.2077 X 10^{-10} m^2/s, r^2 = 0.9808).

Table 4.15: D_{mig}, D_{app} and r^2 values for control and microbial prepared PPC and OPC Mortars in NaCl

Test Cement Sample	**D_{mig} (m^2/s)**	**D_{app} X $10^{-10} m^2/s$**	**r^2 values**
PPC H-H	6.6016×10^{-9}	3.3484	0.9814
PPC TI-H	7.5956×10^{-9}	3.8526	0.9475
PPC TI-TI	8.5306×10^{-9}	4.3268	0.9513
PPC AT-H	7.4871×10^{-9}	3.7975	0.9509
PPC AT-AT	7.9015×10^{-9}	4.0077	0.9514
PPC SK-H	7.7783×10^{-9}	3.9452	0.9479
PPC SK-SK	1.2239×10^{-8}	6.2077	0.9808
OPC H-H	1.5505×10^{-8}	7.8643	0.9605
OPC TI-H	1.5517×10^{-8}	7.8704	0.9549
OPC TI-TI	1.5617×10^{-8}	7.9211	0.9544
OPC AT-H	1.5542×10^{-8}	7.883	0.9609
OPC AT-AT	1.5621×10^{-8}	7.9231	0.9556
OPC SK-H	1.5552×10^{-8}	7.8881	0.9600
OPC SK-SK	1.6363×10^{-8}	8.2995	0.9542

Generally, mortars prepared with microbial solutions exhibited significantly higher chloride apparent diffusion coefficients as compared to the controls. This was perhaps due to the corrosive activities of the microbes, which increased the pore structure of the exposed cement mortars. Studies conducted by Xiuli *et al.* (2015) revealed that multiscale pores influenced the apparent diffusion coefficient of chloride ions in cement-based materials. The authors argued that the nature

of the pores varied from the gel pores, capillary pores, entrained and entrapped voids. These voids facilitated the transport of chloride within the cement paste matrix.

The chloride apparent diffusion for the PPC mortars prepared with microbial was low compared to that of OPC. This was attributed to the high binding ability of pozzolans. The resultant mortar from PPC is denser and compact due to pozzolanic activity. This lowers the pores sizes of the mortar surface and hence reduced chloride diffusivity. According to Jin *et al.* (2010), virtually all cement made structures operate under complex stress circumstances of compression, torsion and tension. The external mechanical loadings affect the distribution of the pores within the placed concrete and mortar structure. This yields in formation of new micro cracks that forms suitable conduit for diffusivity of aggressive medium into the concrete matrix (Xiuli *et al.,* 2015). The biogenic sulphuric acid generated by the selected bacteria increased the permeability of the exposed microbially prepared cement mortars. This resulted in increase in apparent diffusion coefficients as observed.

OPC SK-SK exhibited higher apparent chloride diffusion coefficient (D_{app} = 8.2995 x 10^{-10} m^2/s). This was due to the pore structure of the OPC SK-SK. The composition of OPC favours the formation of more pores on the surface due to high amount of heat generated by the hydration process (Patel *et al.,* 2016). Huawei *et al.* (2020) while studying on the effect of chloride ion ingress on the pore structure of the connected mortar of recycled coarse aggregate found a strong correlation between chloride permeability and the pore structure of the concrete. The SEM results revealed high formation of expansive ettringite crystals on OPC SK-SK mortars. These could

equally increase the pore structure of the OPC mortar and hence facilitate higher transportation of the chloride ions into the pore matrix.

4.9 Sulphate ingress

4.9.1 Sulphate Profiling

Figures 4.26 show the sulphate ion ingress in OPC H-H and PPC H-H mortars at different penetration depths after 28th day of curing.

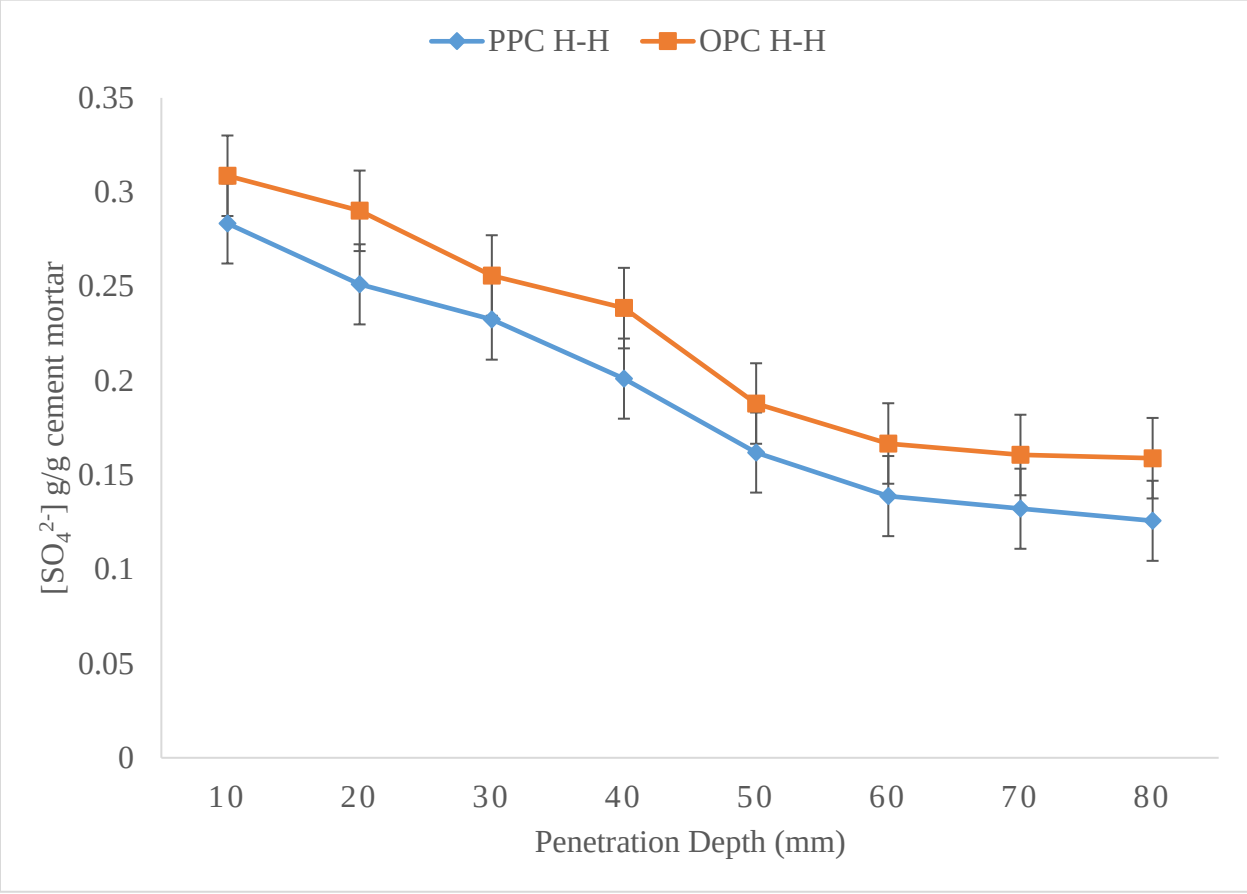

Figure 4.26: Sulphate ingress in mortars of OPC H-H and PPC H-H after 28th day of curing

The analysis results showed that the sulphate ion ingress in cement mortars decreased with increase in penetration depth for both test cements. This was as observed in the case of chloride diffusion test. OPC mortars exhibited higher sulphate ion ingress than PPC across all the penetration depth. This was attributed to the chemical and phase composition of OPC as described in table 4.1 and 4.2. The hydration of OPC results in generation of high amount of heat due to high content of CaO, C_3A and C_3S (Scrivener *et al.*, 2015). The generated heat of hydration in OPC would cause increase in pore size of the placed concrete and mortar. The formed pores would form suitable pathways for the external sulphate to ingress (Tai *et al.*, 2019). As observed from SEM results, OPC exhibited high formation of CH plates within the pore matrix. CH and C_3A act as suitable attack point by sulphates resulting in formation of destructive ettringite crystals as described in equation 4.11 (Fang *et al.*, 2021).

The observed low sulphate ingress in PPC mortars was perhaps due to the pozzolanic activity (Kunther *et al.*, 2015; Yu *et al.*, 2015). Pozzolanic reaction results in formation of additional C-S-H and C-A-H as described in equations 4.3 and 4.4 (Whittaker *et al.*, 2016; Muller *et al.*, 2013). The secondary materials generated improve the density and impermeability of resultant mortar and hence hinders the high rate of sulphate ingress into the mortar matrix of PPC (Michael and Thomas, 2019). Further, Pozzolanic materials have low alkali content due to reduced CaO, Na_2O and K_2O levels as described in table 4.1. Low alkali content in the pore matrix of the PPC mortars would further reduce any possible expansion due to alkali silica reaction (Michael and Thomas, 2019). This results in dense mortars and hence improved pore networks within the matrix. This was as observed in water absorptivity results.

The sulphate ingress results in mortars of OPC and PPC prepared and cured with *Thiobacillus intermedius*, *Acidithiobacillus thiooxidans* and *Starkeya novella* bacteria medium after 28th day of curing are presented in figures 4.27 and 4.28 respectively.

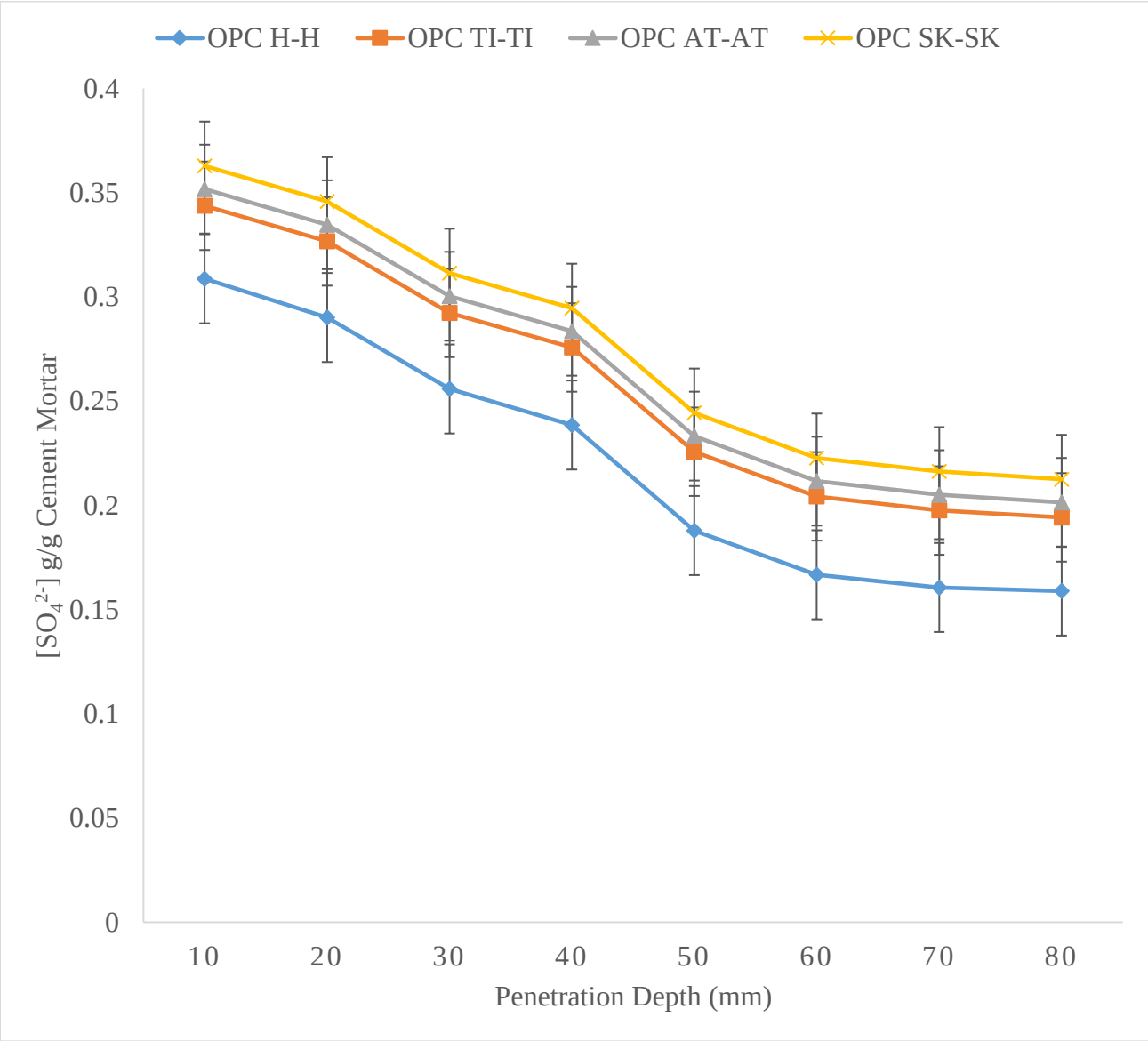

Figure 4.27: Sulphate ingress in OPC Mortars Prepared with Selected Bacteria Solutions after 28th day of curing

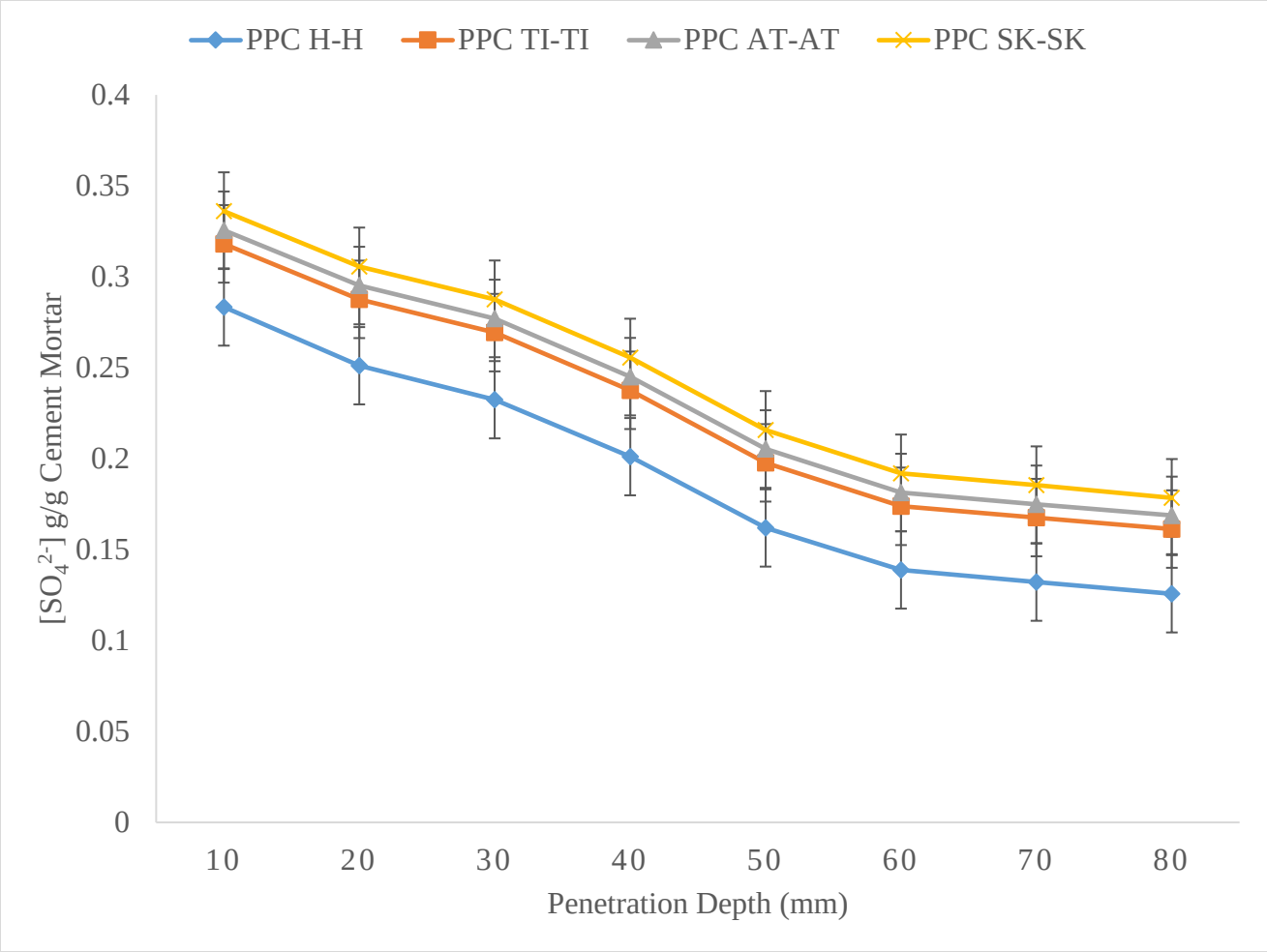

Figure 4.28: Sulphate ingress in PPC Mortars Prepared with Selected Bacteria Solutions after 28th day of curing

The test results as illustrated in figures 4.27 and 4.28 show that the ingress of sulphate ions was more pronounced in the mortars cast using the bacteria solutions in both OPC and PPC test cements. This was attributed to the deleterious effect of biogenic sulphuric acid generated by the test bacteria (Azam *et al.*, 2014). The resultant biogenic acid would attack the soluble constituents of the cement mortar leading to formation of several pores within the matrix of the exposed mortar. The formed pores form pathway for ingress of sulphates into the mortar matrix (Sun, 2015). The

extent of sulphate ingress in cement mortars largely depend on the permeability of the exposed concrete surface (Burak *et al.* 2006).

The reaction of biogenic sulphuric acid generated by the bacteria activities result in formation of gypsum and ettringite as described in equation 4.10 and 4.11. The formed gypsum and ettringite ultimately disrupts the integrity of the hardened concrete and mortar (Fang *et al.,* 2021). The formation of secondary gypsum and ettringite in the pore structure of the hardened mortar or concrete uninterruptedly fills the inner pores of the exposed mortar and concrete resulting in expansion and spalling (Yingwu *et al.,* 2015). The expanded concrete surface causes formation of micro-cracks and hence makes the surface of the concrete and mortar more porous. This allows the transport of other deleterious materials into the pore matrix of the exposed mortar or concrete (Ikumi *et al.*, 2014).

4.9.2 Sulphate Apparent Diffusivity Coefficients

The sulphate apparent diffusivity coefficients for the control and microbial PPC and OPC test cements were determined using the error function fitting curves. Figure 4.29 show the typical error function-fitting curve for PPC SK- SK. Similarly, the apparent sulphate diffusion coefficients for the other test mortars were determined using similar error fitting curves error function-fitting curve. The summary of error fitting data for both control and mortars of PPC and PPC prepared with microbial solutions is as tabulated in table 4.16.

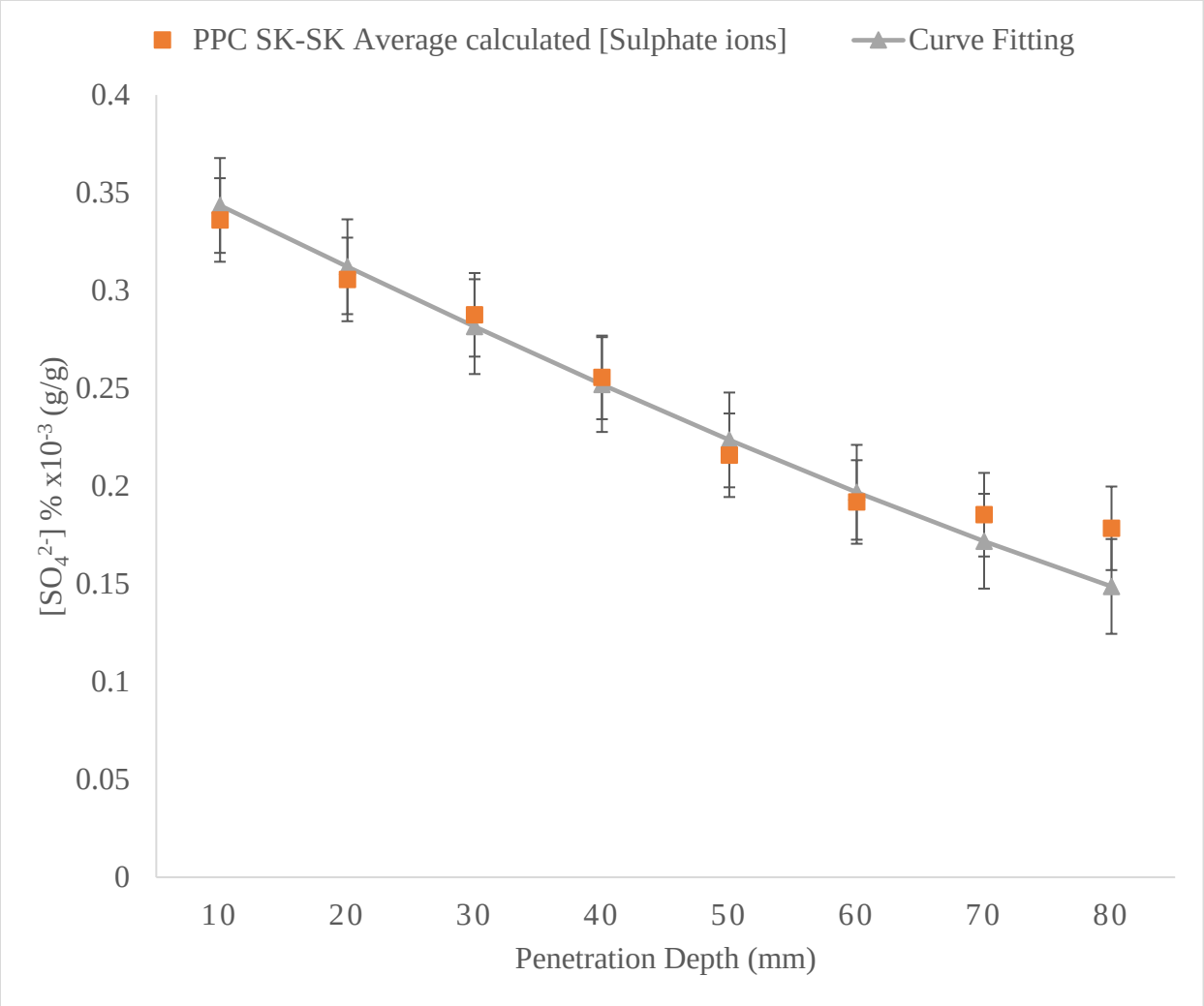

Figure 4.29: Error function fitting curve for PPC SK-SK D_{app} = (8.7043 X 10^{-10} m^2/s, r^2 = 0.9742).

Table 4.16: D_{mig}, D_{app} and r^2 values for control and microbial prepared PPC and OPC Mortars in Na_2SO_4

Test Cement Sample	**D_{mig} X10^{-8} (m^2/s)**	**D_{app}(m^2/s)**	**r^2 values**
PPC H-H	3.2111	8.1434 x 10^{-11}	0.9745
PPC TI-H	3.2615	8.2714 x 10^{-10}	0.9752
PPC TI -TI	3.2666	8.2841 x 10^{-10}	0.9735
PPC AT-H	3.2716	8.2969 x 10^{-10}	0.9741
PPC AT- AT	3.2721	8.2981 x 10^{-10}	0.9736
PPC SK-H	3.4305	8.6999 x 10^{-10}	0.9741
PPC SK -SK	3.4322	8.7043 x 10^{-10}	0.9742
OPC H-H	3.7819	9.5912 x 10^{-11}	0.9789
OPC TI-H	4.2817	1.0859 x 10^{-9}	0.9704
OPC TI -TI	4.5749	1.1602 x 10^{-9}	0.9719
OPC AT-H	4.3085	1.0927 x 10^{-9}	0.9728
OPC AT -AT	4.7336	1.2005 x 10^{-9}	0.9747
OPC SK-H	5.0969	1.2926 x 10^{-9}	0.9793
OPC SK -SK	5.3477	1.3562 x 10^{-9}	0.9797

The test mortars prepared with the selected test bacteria showed higher sulphate apparent diffusion coefficients than the controls. This was as observed in chloride tests. The observed higher sulphate diffusion coefficients for the bacteria prepared mortars was because of the deleterious activities of the bacteria (Yudong *et al.,* 2019).

However, OPC bacteria mortars exhibited higher apparent sulphate diffusion coefficients than PPC. This was due to high C_3A phase in OPC as described in table 4.2 and advanced formation of CH plates in hydrated OPC as observed from SEM morphology. Presence of high C_3A and CH facilitates a suitable attack point by sulphate to form ettringite. Due to the expansive nature of the ettringite crystals, this would perhaps cause multiple micro cracks within the pore structure of the OPC and hence facilitate higher diffusion of sulphate ions (Yingwu *et al.,* 2015).

Presence of ettringite accounts for the formation of discrete cracks that enhances transport of sulphate ions and other deleterious materials into the cement pore matrix (Idiart *et al.,* 2011). Further, studies conducted by Zuo and Sun (2011), showed that the amount of calcium hydroxide in the pore solution influenced the diffusion of sulphate ions. The authors reported that the higher the CH and C_3A, the higher the ettringite formation and subsequently the higher the sulphate diffusivity. The resultant C-S-H gel from the OPC hydration would absorb sulphate and cause decline in structural quality (Fall and Pokharel 2010).

The apparent sulphate diffusion coefficients for the bacteria prepared PPC mortars was not as pronounced as in OPC bacteria mortars. This was attributed to the pozzolanic activity in PPC based cements (Munyao *et al.,* 2020a). Replacement of OPC with pozzolana lowers the resultant CH content, which is the active attack point by the sulphates. Moreover, the reactive silica and alumina in pozzolans reacts with the resultant calcium hydroxide upon hydration to form additional C-S-H and C-A-H as described in equations 4.3 and 4.4. The SEM analysis showed improved C-S-H formation in pozzolanic cement. This perhaps would result in improved pore network within the microstructure of PPC and hence reduced diffusivity by the sulphate ions. Studies conducted by

Ogawa *et al.* (2012) showed that incorporation of slag with higher pozzolanic activity lowered the sulphate diffusion in concrete. Several other authors have reported the ability of pozzolanic cements to resist sulphate diffusivity (Xiancui *et al.*, 2020; Zhenguo *et al.*, 2019; Uysal *et al.*, 2013; Vedalakshmi *et al.*, 2011; Gollop and Taylor, 1996).

CHAPTER FIVE

CONCLUSIONS AND RECOMMENDATIONS

5.1 Conclusions

In consideration of the results and analysis made, the following conclusions were drawn:

i. The chemical and phase composition of the commercial OPC and PPC met the desired requirements as described in KS EAS 18:1-2017

ii. All the physical characteristics (standard consistency, setting time and soundness) of the test cements prepared with distilled water and selected microbial solutions conformed with the KS EAS 18-1 2017 standard. The activity of the test bacteria did not affect the physical characteristics of the test cements.

iii. The selected bacteria significantly decreased the compressive strengths of the commercial OPC and PPC mortars after 28^{th} day of curing. *Starkeya novella* exhibited the highest compressive strength decrease of 27.82 % and 33.50 % for PPC and OPC at 90^{th} day of curing respectively.

iv. The selected bacteria significantly affected the microstructure of the hydrated OPC and PPC mortars. There was enhanced formation of deleterious secondary materials within the pore matrix of the mortars prepared and cured in microbial solutions.

v. The selected bacteria significantly affected the water absorptivity of the commercial OPC and PPC mortars. OPC SK-SK recorded the highest water absorptivity of 72.75% against PPC SK-SK water absorptivity of 25.32%. Chloride and sulphate ion ingress increased significantly on bacteria prepared mortars of PPC and OPC as compared to the controls.

5.2 Recommendations from this research work

The results obtained from this work recommends the following:

i. A method on remediation of concrete and mortar exposed to microbial degradation to be investigated.

ii. Mechanical monitoring to be carried out on *insitu* concrete structures especially in sewer and water collection systems to assess the extent of bacterial deterioration. This will guide in evaluating the service life and durability of such structures and appropriate mitigation measures to be put in place.

iii. A study to monitor the presence of the tested bacteria to be investigated in wastewater collection systems.

5.3 Recommendation for Further work

Based on the research findings of this work, the following are recommendations for further research:

i. Study to investigate the long-term durability of surface treatment on the exposed concrete structures to be carried out.

ii. Need to study the characteristics of other bacteria strains present in sewer collection areas and their contribution to the durability of concrete and cement-based materials.

iii. Study to be carried out on the influence of other microorganisms such as algae and fungi in enhancing the activities of the deleterious bacteria on exposed concrete and mortar structures.

REFERENCES

Aastha, D. (2017). Chapter 4- Fourier Transform Infrared- Spectroscopic methods for Nanomaterials characterization. *Elsevier*. 73-93.

Abo- El-Enein, S.A., Amin, M.S., EL-Hosiny, F.L., Hanafi, S., Elsokkary, T. and Hazem, M.M. (2014). Pozzolanic and hydraulic activity of nano-metakaolin. *HBRC Journal.* ***10,*** 64-72.

Abo-EL-Enein, S.A., El-Kady, G., EL-Sokkary, T.M. and Mahmoud, G. (2015). Physico-Mechanical properties of composite cement paste containing silica fume and Fly ash. *HBRC Journal*. ***11,*** 7-15.

Ahmed, M. S., Khedr, M.H., El-Dek, S.I. and Nabila, S. (2021). Influences of calcium sulfate bearing material and zinc oxide nanoparticles on hydration properties of white cement clinker. *Journal of Materials Research & Technology*. ***11,*** 2003 -2014.

Aiman, Y., Assia, D. and Teddy, F-C. (2019). The effect of the drying temperature on water porosity and gas permeability of recycled sand mortar. *Construction & Building materials.* ***214,*** 677-684.

Aïtcin P-C. and Mindess, S. (2011). Sustainability of Concrete UK: *Spon Press.* 301.

Ali, A. R., Mehrdad, M. and Sajjad, M. (2021). Synergic effect of nano-silica and natural pozzolans on transport and mechanical properties of blended cement mortars. *Journal of Building Engineering.* ***44,*** 102667.

Ali, M. and Mullick, A. (1998). Volume stabilization of high MgO cement: Effect of curing conditions and fly ash addition. *Cement & Concrete Research.* ***28,*** 1585-1594.

Al-Jabiri, T.M. (2002). Concrete strength Development related to MgO and SO_3 contents in cement, MSc. Thesis, University of Baghdad, College of Engineering, Baghdad, Iraq.

Ampadu, K.O. and Tori, K. (2002). Chloride ingress and steel corrosion in cement mortars incorporating low-quality Fly Ashes. *Cement & Concrete Research.* ***32,*** 893-900.

Ann, K.Y. and Song, H.W. (2007). Chloride threshold level for corrosion of steel in concrete. *Corrosion Science.* ***49,*** 4113-4133.

Anu, J., Nivitha, M.R., Murali, J. K. and Robinson, R.G. (2020). Characterization of cement stabilized pond ash using FTIR spectroscopy. *Construction & Building Materials.* ***263,*** 120136.

Aranda, M.A.G., De la Torre, Á.G. and León-Reina, L. (2012). Rietveld quantitative phase analysis of OPC clinkers, cements and hydration products. *Reviews in Mineralogy & Geochemistry.* ***74,*** 169-209.

Ariffin, M.A.A., Bhutta, M.A.R., Hussin, M.W., Tahir, M.M. and Aziah, N. (2013). Sulfuric acid resistance of blended ash geopolymer concrete. *Construction & Building Materials*. ***43****,* 80-86.

Arthur, M. H. (2019). Constitution and specification of Portland cement. Lea's Chemistry of cement and concrete. *Elsevier.* Fifth Edition. 87-155.

ASTM C 1556 - 16. (2016). Standard Test Method for Determining the Apparent Chloride Diffusion Coefficient of Cementitious Mixtures by Bulk Diffusion. ASTM International, West Conshohocken, PA. www.astm.org.

ASTM C 1585-04. (2004). Standard Test Method for measurement of Rate of Absorption of Water by Hydraulic Cement Concretes, ASTM International West Conshohocken, PA. www.astm.org.

ASTM C1723 -16. (2016). Standard Guide for Examination of Hardened Concrete Using Scanning Electron Microscopy, ASTM International, West Conshohocken, PA. www.astm.org.

Aviam, O., Bar-Nes, G., Zeiri, Y. and Sivan, A. (2004). Accelerated biodegradation of cement by sulphur – oxidizing bacteria as a bioassay for evaluating immobilization of low-level radioactive waste. *Applied & Environmental Microbiology.* ***70,*** 6031-6036.

Aye, T. and Oguchi, C.T. (2011). Resistance of plain and blended cement mortars exposed to severe sulfate attacks. *Construction & Building Materials.* ***25,*** 2988-2996.

Azam, Y., Ali, A. and Parisa, H. (2014). Accelerated biodegradation of cured cement paste by *Thiobacillus* species under simulation condition. *International Biodeterioration & Biodegradation.* ***86,*** 317-326.

Bakharev, T. (2005). Resistance of geopolymer materials to acid attack. *Cement & Concrete Research.* ***35,*** 658-670.

Barnett, S.J., Macphee, D.E., Lachowski, E.E. and Crammond, N.J. (2002). XRD, EDX and IR analysis of solid solutions between thaumasite and ettringite. *Cement & Concrete Research.* ***32,*** 719-730.

Bary, B., Leterrier, N., Deville, E. and Le Bescop, P. (2014). Coupled chemo-transport-mechanical modelling and numerical simulation of external sulfate attack in mortar. *Cement & Concrete Research Composites.* ***49,*** pp. 70-83.

Beddoe, R. and Hilbig, H. (2009). Modelling the evolution damage to concrete by acid attack, simulation of Time Dependent Degradation of porous materials: *Final Report on priority program.* ***112,*** 275-293.

Bertron, A. (2014). Understanding interactions between cementitious materials and microorganisms: A key to sustainable and safe concrete structures in various contexts. *Materials & Structures.* ***47***, 1787-1806.

Bettina, H., Herald, H., Mariana, M. M., Jörg, E. D. and Elisabeth, M. (2016). Comparative analysis of biogenic and chemical sulphuric acid attack on hardened cement paste using laser ablation – ICP – MS. *Cement & Concrete Research.* ***87,*** 14-21.

Bhatty, J., Miller, F. and Kosmatka, S. (2004). Innovations in Portland cement manufacturing CD-ROM: SP 400. Portland cement Association Skokie, IL.

Bielefeldt, A., Gutierrez-Padilla, M.G.D., Ovtchinnikov, S., Silverstein, J. and Hernandez, M. (2009). Bacterial kinetics of sulfur oxidizing bacteria and their Biodeterioration rates of concrete sewer pipe samples. *Journal of Environmental Engineering*. ***136***, 731-738.

Birnin-Yauri, U.A. and Glasser, F.P. (1998). Friedel's salt $Ca_2Al(OH)_6$ (Cl, OH).$2H_2O$: Its solid solutions and their roles in chloride binding. *Cement & Concrete Research.* ***28,*** 1713-1723.

Björnström, J., Martinelli, A., Matic, A., Börjesson, L. and Panas, I. (2004). Accelerating effects of colloidal nano-silica for beneficial calcium-silicate-hydrate formation in cement. *Chemical Physics Letters.* ***39,*** 242-248.

Bock, E. and Sand, W. (1993). The microbiology of Masonry Biodeterioration. *Journal of applied Bacteriology*. ***74,*** 503-514.

Bogue, R.H. (1929). Calculation of the Compounds in Portland cement. *Industrial & Engineering Chemistry, Analytical Edition.* ***1,*** 192-197.

Bonen, D. (1993). A microstructural study of the effect produced by magnesium sulfate on plain and silica fume-bearing Portland cement mortars. *Cement & Concrete Research*. ***23,*** 541-553.

Boon, A.G. (1995). Septicity in sewers: causes, consequences and containment. *Water Science & Technology.* ***31,*** 237-253.

Borhan, S., Hesaraki, S. and Ahmadzadeh-ASL, S. (2010). Evaluation of colloidal silica suspension as efficient additive for improving physic chemical and invitro biological properties of calcium sulfate – based nano composite bone cement. *Journal of Materials Science: Materials in Medicine.* ***21,*** 3171-3181.

BS EN 12322 (1999). In vitro diagnostic devices **–** Culture media for microbiology. Performance criteria for culture media. British Standards Institute, London. 21 **–** 23.

BS EN 197-1 (2011). Cement part 1: composition, specifications and conformity criteria for common cements.

Burak, F., Kambiz, R., Kamile, T. and Baris, M. (2006). Sulfate resistances of different types of Turkish Portland cements by selecting the appropriate test methods. Construction & *Building Materials.* ***20***, 819-823.

Cayford, B.I., Dennis, P.G., Keller, J., Tyson, G.W. and Bond, P.L. (2012). High-throughput amplicon sequencing reveals distinct communities within a corroding concrete sewer system. *Applied & Environmental Microbiology*. ***78,*** 7160-7162.

Chen, Y. and Odler, I. (1992). On the origin of Portland cement setting. *Cement & Concrete Research.* ***22,*** 1130-1140.

Cheng, Y., Wei, S. and Karen, S. (2015). Degradation mechanism of slag blended mortars immersed in sodium sulfate solution. *Cement & Concrete Research.* ***72,*** 37-47.

Chunyu, Q., Prannoy, S., Then, N.W.Y., Antara, C. and Jason, W. (2019). Chloride binding of cement pastes with Fly ash exposed to $CaCl_2$ solutions at 5 and 23^0C. *Cement & Concrete Composites.* ***97***, 43-53.

Clifton, J.R. and Ponnersheim, J.M. (1994). Sulfate attack of cementitious materials: Volumetric relations and expansions. NIST IR 5390, Gaithersburg, Maryland.

Collet, G., Crammond, N.J., Swamy, R.N. and Sharp, J.H. (2004). The role of carbon dioxide in the formation of Thaumasite. *Cement & Concrete Research.* ***34***, 599-612.

Crammond, N.J and Halliwell, M. A (1997). Assessment of the conditions required for the Thaumasite form of sulfate attack. *Proceedings of the mechanisms of chemical degradation of cement bases systems, London: E & FN spoon.* 193-200.

Crank, J. (1975). The mathematics of diffusion.2^{nd} Edition, Oxford University Press, London. 69-88.

Crispim, C.A. and GayLarde, C.C. (2005). Cyanobacteria and Biodeterioration of cultural Heritage: A Review. *Microbial Ecology*. ***49,*** 1-9.

Crispim, C.A., Gaylarde, P.M and Gaylarde, C.C. (2003). Algal and Cyanobacterial Biofilms on calcareous Historic Buildings. *Current Microbiology*. ***46,*** 0079-0082.

Cristelo, N., Tavares, P., Lucas, E., Miranda, T. and Oliveria, D. (2016). Quantitative and qualitative assessment of the armphous phase of a class F Fly ash dissolved during alkali activation, solution concentration and temperature. *Cement & Concrete Composites.* ***103***, 1-14.

Cwalina, B. (2008). Biodeterioration of concrete. *Architecture Civil Engineering Environment.* ***1,*** 133-140.

Daniel, H., Caner, T., Mutlu, I., Müslim, M. S. and Semsi, Y. (2019). Compressive strength, water absorption, water sorptivity and surface radar exhalation rate of silica fume and fly ash-based mortar. *Journal of Building Engineering*. ***23,*** 369-376.

Dave, N., Misra, A.K., Srivastava, A. and Kaushik, S.K. (2017). Setting time and standard consistency of quaternary binders: The influence of cementitious material addition and mixing. *International Journal Sustainable Built Environment*. ***6,*** 30–36.

David, T-M., Lucia, F-C. and Sagracio, M-R. (2013). Hydration of calcium aluminates and calcium sulfoaluminates studied by Raman spectroscopy. *Cement & Concrete Research.* ***47,*** 43-50.

Davis, J.L., Nica, D., Shields, K. and Roberts, D.J. (1998). Analysis of concrete from corroded sewer pipes. *International Biodeterioration & Biodegradation.* ***42***, 75-89.

De Belie, N., Monteny, J., Beeldens, A., Vincke, E., Van Gemert, D. and Verstraete, W. (2004). Experimental research and prediction of the effect of chemical and biogenic sulfuric acid on different types of commercially produced concrete sewer pipes. *Cement & Concrete Research*. ***34,*** 2223-2236.

De Muynck, W., Maury, A., De Belie, N. and Verstraete, W. (2009). Evaluation of strategies to prevent algal fouling on white architectural and cellular concrete. *International Biodeterioration & Biodegradation.* ***63,*** 679-689.

De Windt, L. and Devillers, P. (2010). Modeling the degradation of Portland cement pastes by biogenic organic acids. *Cement & Concrete Research.* ***40***, 1165-1174.

Diandian, Z. and Rahil, K. (2021). Hydration and Microstructural development of calcined clay cement paste in the presence of calcium-silicate-hydrate (C-S-H) seed. *Cement & Concrete Composites.* ***122,*** 104162.

Diercks, M., Sand, W. and Bock, E. (1991). Microbial corrosion of concrete. *Experiential.* ***47,*** 514-516.

Dongxing, W., Jiaye, Z. and Ruihong, W. (2021). Assessment of Magnesium Potassium Phosphate for waste sludge solidification: Macro and Micro-analysis. *Journal of Cleaner Production.* ***294,*** 126365.

Ekström, T. (2001). Leaching of concrete report TVBM-3090. Sweden: Lund University, Division of Building Materials.

Emilio, B. A., Mauricio, S.S., Alaa, C. and Moema, R. S. (2008). Coupled reliability model of biodeterioration chloride ingress and cracking for reinforced concrete structures. *Structural Safety.* ***30,*** 110-129.

Escadeillas, G., Bertron, A., Ringot, E., Blanc, P.J. and Dubosc, A. (2007). Accelerated testing of biological stain growth on external concrete walls. Part I: Development of the growth tests. *Materials & Structures.* ***40,*** 1061-1071.

Estokova, A., Harbul'akova, V.O. and Lupta'kova, A. (2012). Study of the deterioration of concrete influenced by biogenic sulphate Attack. *20th International congress of chemical and process Engineering*. Prague, Czech Republic. 25-29.

Fall, M. and Pokharel, M. (2010). Coupled effects of sulphate and temperature on the strength development of cemented tailings backfills: Portland cement paste backfill. *Cement & Concrete Composites.* ***32,*** 819-828.

Fang, L., Zhanping, Y., Abuelkasim, D., Zhuangzhuang, L., Chao, Z. and Shuaicheng, G. (2020). External Sulfate attack on concrete under combined effects of flexural fatigue loading and drying-wetting cycles. *Construction & Building Materials.* ***249,*** 118224.

Fangzhou, R., Chunsheng, Z., Qiang, Z., Zhidong, Z., Ueli, A. and Wei, W. (2021). Quantifying the anomalous water Absorption behavior of cement mortar in view of its physical sensitivity to water. *Cement & Concrete Research.* ***143,*** 106395.

Fernandez -Jimenez, A. and Palomo, A. (2005). Mid-Infrared spectroscopic studies of alkali-activated fly ash structure. *Microporous & Mesoporous Materials.* ***86,*** 207-214.

Firer, D., Friedler, E. and Lahav, O. (2008). Control of sulfide in sewer systems by dosage of iron salts: comparison between theoretical and experimental results and practical implications. *Science of the Total Environment.* ***392***, 145-156.

Flore, M.V.A. and Brouwers, H.J.H. (2012). Chloride related to hydration products: Part 1: Ordinary Portland cement. *Cement & Concrete Research.* ***42***, 282-290.

Franco, Z., Dale, P.B. and Javier, C. (2018). Reducing setting time of blended cement paste containing high SO_3 Fly ash (HSFA) using chemical/ physical accelerators and by fly ash pre-washing. *Cement & Concrete Composites.* ***90,*** 14-26.

Fulin, Q., Wengui, L., Kejin, W., Shishun, Z. and Daichao, S. (2021). Performance deterioration of fly ash / slag-based geopolymer composites subjected to coupled cyclic preloading and sulfuric acid attack. *Journal of Cleaner Production.* ***321***, 128942.

Gao, X.F., Lo, Y., Tam, C.M. and Chung, C.Y. (1999). Analysis of the Infrared Spectrum and the Microstructure of hardened cement paste. *Cement & Concrete Research.* ***29,*** 805-812.

Gardnev, T.J. (2006). Chloride transport through concrete and implications for rapid chloride testing, MSc. Thesis, University of Cape Town, South Africa.

Gartner, E., Young, E.J., Damidot, D. and Jawed, I. (2001). Hydration of Portland cement. In structure and performance of cement, 2nd Edition. Spoon Press. 57-113.

GayLarde, C., M., Ribas S. and Warscheid, T. (2003). Microbial impact on building materials an overview. *Materials & structures.* ***36***, 342-352.

Gaylarde, C., Ribas-Silva, M. and Warscheid, T. (2003). Microbial impact on building materials: an overview. *Materials & structures.* ***36***,342-352.

Geng, Y., Tao, C., Zhen, J., Shaokang, S., Cosmos, A., Jun, Q. and Xianjun, L. (2020). Effect of anhydrite on hydration properties of mechanically activated muscovite in the presence of calcium oxide. *Applied Clay Science*. ***196,*** 105742.

George, R.P., Vishwakarma, V., Samal, S. and Mudali, U.K. (2012). Current understanding and future approaches for controlling microbially influenced concrete corrosion: A review. *Concrete Research Letters* **3.**

George, R.P., Ramya, S., Ramachandran, D. and Mudali, U.K. (2013). Studies on Biodeterioration of normal concrete surface by fungus *Fusarium* species. *Cement & Concrete Research.* ***47,*** 8-13.

Girardi, F. and Maggio, R.D. (2011). Resistance of concrete mixtures to cyclic sulfuric acid exposure and mixed sulfates. Effect of the type of aggregate. *Cement & Concrete Composites.* ***33,*** 276-285.

Glass, G.K. and Buenfeld, N.R. (2000). The influence of chloride binding on the chloride induced corrosion risk in reinforced concrete. *Corrosion Science*. ***42,*** 329 -344.

Glasser, F. P., Nonat, A. and Mutin, J.C. (1992). Hydration and setting of cements. *Spon*. ***16,*** 101.

Gleb, G. M. (2007). Improved cement quality and grinding efficiency by means of closed mill circuit modelling. PhD dissertation, Texas A & M University.

Gollop, R.S. and Taylor, H.F.W. (1996). Microstructural and Micro analytical studies of sulfate attack V. Comparison of different slag blends. *Cement & Concrete Research.* **26,** 1029-1044.

Grengg, C. (2018). Microbial induced acid corrosion in sewer environments. Graz University of technology, PhD thesis.

Grengg, C., Kiliswa, M., Mittermayr, F. and Alexander, M. (2016). Microbially-induced concrete corrosion – A worldwide problem. *International Conference on Cementitious Materials-Microorganisms Interactions.* 1-19.

Grengg, C., Mittermary, F., Koraimann, G., Konrad, F., Szabo, M., Demery, A. and Dietzel, M. (2017). The decisive role of acidophilic bacteria in concrete sewer networks: a new model for fast progressing microbial concrete corrosion. *Cement & Concrete Research.* ***101,*** 93-101.

Grengg, C., Mittermayr, F., Ukrainczyk, N., Koraimann, G., Kienesberger, S. and Dietzel, M. (2018). Advances in concrete materials for sewer systems affected by microbial induced concrete corrosion: a review. *Water Research.* ***134,*** 341-352.

Gu, J.D., Ford, T.E., Berke, N.S. and Mitchell, R. (1998). Biodeterioration of concrete by the fungus *Fusarium*. *International Biodeterioration & Biodegradation.* ***41***, 101-109.

Guadalupe, M. D., Gutierrez, P., Angela, B., Serguei, O., Mark, H. and Joann, S. (2010). Biogenic sulfuric acid attack on different types of commercially produced concrete sewer pipes. *Cement & Concrete Research.* ***40,*** 293-301.

Gutberlet, T., Hilbig, H. and Beddoe, R.E. (2015). Acid attack on hydrated cement – effect of mineral acids on the degradation process. *Cement & Concrete Research.* ***74,*** 35-43.

Hadigheh, S.A., Gravina, R.J., Smith, S.T. (2017). Effect of acid attack on FRP- to- concrete bonded interface. *Construction & Building Materials.* ***152,*** 285-303.

Haile, T., Nakhla, G. and Allouche, E. (2008). Evaluation of the resistance of mortars coated with silver bearing zeolite to bacteria induced corrosion. *Corrosion Science.* ***50****,* 713-720.

Haifen, Y. (2013). Degradation modeling of concrete submitted to biogenic acid attack Universite' Paris - Est, PhD. Thesis.

Haifen, Y., Patrick, D., Patrick, C. and Thierry, C. (2015). Degradation modeling of concrete submitted to biogenic acid attack. *Cement & Concrete Research*. ***70,*** 29-38.

Hailong, Y. and Le, H. (2020). Degradation mechanisms of alkali-activated binders in sulfuric acid: The role of calcium and aluminium availability. *Construction & Building Materials.* ***246,*** 118477.

Hamdy, E., Ahmed, A., Mohammed, H., Mohammed, S. (1999). Effect of Calcium acetate as accelerator and water reducer on the properties of silica fume blended cement. *Ceramics-Silikáty.* ***43,*** 29-33.

Haynes, H., O'Neill, R,. Mehta, P.K. (1996). Concrete deterioration from physical attack by salts. *Concrete International*. ***18,*** 63-68.

Herisson, J., Eric, D. van- H., Moletta-Denat, M., Taquet, P. and Chaussadent, T. (2013). Toward an accelerated Biodeterioration test to understand the behavior of Portland and calcium aluminate cementitious materials in sewer networks. *International Biodeterioration & Biodegradation.* ***84****,* 236- 243.

Herisson, J., Hellebusch, V. E., Gueguen, M., Moletta - Denat, M., Eychenne - Baron, C. and Chaussent, T. (2012). Sulfur cycle in sewer networks and its consequences on cementitious materials. *International Symposium on Microbial Ecology ISME-14*, Denmark.

Hewayde, E., Nehdi, M., Allouche, E. and Nakhla, G. (2007). Effect of mixture design parameters and wetting – drying cycles on resistance of concrete to sulfuric acid attack. *Journal of Materials in Civil Engineering.* ***19***, 155-163.

Hewlett, P.C. (2003). Lea's chemistry of cement and concrete. Oxford: Elsevier.

Haile, T., Nakhla, G. and Allouche, E. (2008). Evaluation of the resistance of mortars coated with silver bearing zeolite to bacteria induced corrosion. *Corrosion Science. **50***, 713-720.

Hime, W.G. and Mather, B. (1999). Sulfate Attack or is it? *Cement & Concrete Research*. ***29,*** 789-791.

Hong, S.Y. and Glasser, F.P. (1999). Alkali Binding in cement pastes part 1: The C-S-H phase. *Cement & concrete Research. **29,*** 1893-1903.

House, M.W. (2013). Using biological and physiochemical test methods to assess the role of concrete mixture design in resistance to microbially induced corrosion. Master's Thesis, Purdue University.

House, M. and Weiss, W. (2014). Review of microbially induced corrosion and comments on needs related to testing procedures: *4th International conference on the durability of concrete structures.* 94-103.

Huang, W., Kazemi-Kamyab, H., Sun, W. and Scrivener, K. (2017). Effect of cement substitution by limestone on the hydration and microstructural development of ultra-performance concrete (UHPC). *Cement & concrete Composites. **77,*** 86-101.

Huawei, L., Chao, L., Guoliang, B. and Chao, Z. (2020). Study on the effect of chloride ion Ingress on the pore structure of the attached mortar of recycled concrete coarse aggregate. *Construction & Building Materials. **263***, 120123

Hughes, T.L., Methven, C.M., Jones, T.G.J., Pelham, S.E., Fletcher, P. and Hall, C. (1995). Determining Cement Composition by Fourier transform Infrared Spectroscopy. *Advanced Cement Based Materials. **2***, 91-94.

Ian, S., John, L. and James, F. (2019). Concrete Aggregates. Lea's Chemistry of cement and concrete. *Elsevier* Fifth Edition.

Idiart, A.E., Lopez, C.M. and Carol, I. (2011). Chemo-mechanical analysis of concrete cracking and degradation due to external sulfate attack. A meso-scale model. *Cement & Concrete Composites. **332,*** 411-423.

Ikumi, T., Cavalaro, S.H.P., Segura, I. and Aguado, A. (2014). Alternative Methodology to consider damage and expansions in external sulfate attack modelling. *Cement & Concrete Research. **63,*** 105-116.

Ikumi, T., Sergio, H.P.C., Ignacio, S. (2019). The role of porosity in external Sulphate attack. *Cement & Concrete Composites. **97,*** 1-12.

Thermo Nicolet Corporation (2001). Introduction to Fourier Transform Infrared Spectrometry.

Irassar, E.F. (2002). Sulphate attack and sulphate resistant cements. In: S.N. Ghosh(Ed.), *Advances in cement Technology:* Chemistry, Manufacture and Testing. 595-629.

Irassar, E.F. (2009). Sulfate attack on cementitious materials containing limestone filler – A review. *Cement & Concrete Research.* ***39,*** 241-254.

Islander, R.L., Devinny, J.S. Mansfield, F., Postyn, A. and Shih, H. (1991). Microbial ecology of crown corrosion in sewers. *Journal of Environmental Engineering*. ***117,*** 751-770.

Ismail, N., Nonaka, T., Noda, S. and Mori, T. (1993). Effect of carbonation on microbial corrosion of concrete. *Journal of construction management and Engineering.* ***20,*** 133-138.

James, B. and Ivan, O. (2019). 5 - Hydration, setting and Hardening of Portland Cement. Lea's Chemistry of Cement and Concrete. Fifth Edition. *Elsevier,* 157-250.

Jamotka, I., Krajci, L., Uhlik, P. and Bacuvcik, M. (2014). Natural and calcined clay diatomite as cement replacement materials: Microstructure and pore structure study. *International Journal of Engineering Research & Technology*. ***3,*** 20-26.

Jana, D. and Lewis, R.A. (2005). Acid attack in a concrete sewer pipe – a petrographic and chemical investigation in: *proceedings of 27th International Conference on Cement Microscopy.*

Jansen, D., Goetz, F.N., Lothenbach, B. and Neubauer, J. (2012). The Early Hydration of ordinary Portland cement (OPC): An approach comparing measured heat flow with calculated heat flow from QXRD. *Cement & concrete Research.* ***42****,* 134-138.

Javad, D. and Mahdi, N. (2020). Compressive and direct tensile behavior of concrete containing Forta-Ferro Fiber and calcium aluminate cement subjected to sulfuric acid attack with optimized design. *Construction & Building Materials.* ***253,*** 118999.

Jean, H., Eric, D. van H., Marina, M-D., Pascal, T. and Thierry, C. (2013). Toward an accelerated biodeterioration test to understand the behaviour of Portland and Calcium aluminate cementitious materials in sewer networks. *International Biodeterioration & Biodegradation*. ***84,*** 236-243.

Jensen, H.S. (2009). Hydrogen Sulfide Induced concrete corrosion of sewer networks, PhD Thesis, Aalborg University.

Jensen, H.S., Nielsen, A.H., Hvitved-Jacobsen, T. and Vollertsen, J. (2008). Hydrogen Sulfide initiated corrosion in concrete sewer – a conceptual approach for prediction. *In proceedings from 11th International Conference of urban drainage. Edinburg.*

Jensen, H.S., Nielsen, A.H., Hvitved-Jacobsen, T. and Vollertsen, J. (2009). Modelling of hydrogen sulfide oxidation in concrete corrosion products from sewer pipes. *Water Environment Research.* ***81,*** 365-373.

Jiang, G. and Yuan, Z. (2014). Inactivation Kinetics of Anaerobic waste water biofilms by free nitrous acid. Applied Microbiology & Biotechnology. ***98***, 1367-1376.

Jiang, G., Melder, D., Keller, J. and Yuan, Z. (2017). Odor emissions from domestic wastewater: a review. *Critical Reviews in Environmental Science & Technology*. ***47,*** 1581-1611.

Jiang, G., Sun, J., Sharma, K.R. and Yuan, Z. (2015). Corrosion and odor management in sewer systems. *Current Opinion in Biotechnology*. ***33,*** 192-197.

Jin, W.L., Yan, Y.D., Wang, H.L. (2010). Research progress on the chloride transportation in stressed concrete. *Journal of the Chinese Ceramic Society*. ***38,*** 2217-2224.

Jorge, F.M., Sanchez-Silva, M. and Johana, H. (2012). Review of reinforced concrete Biodeterioration mechanisms. *VIII International conference on fracture mechanics of concrete and concrete structures.*

Joseph, A.P., Keller, J., Bustamante, H. and Bond, P.L. (2012). Surface neutralization and H_2S oxidation at early stages of sewer corrosion: Influence of temperature relative humidity and H_2S concentration. *Water Research.* ***46,*** 4235-4245.

Joshi, S., S. Goyal, S., Mukherjee, A. and Reddy, M.S. (2019). Protection of concrete structures under sulfate environments by using calcifying bacteria. *Construction & Building Materials*. ***209,*** 156-166.

Juilland, P., Gallucci, E., Flatt, R. and Scrivener, K. (2010). Dissolution theory applied to the induction period in alite hydration. *Cement & Concrete Research.* ***40,*** 831-844.

Karim, M.R., Hossain, M.M., Khan, M.N.N., Zain, M.F.M., Jamil, M., and Lai, F.C. (2014). On the utilization of pozzolanic wastes as an alternative resource of cement. *Materials.* ***7,*** 7809-7827.

Khan, M.U., Ahmad, S. and Al-Gahtani, H.J. (2017). Chloride-induced corrosion of steel in concrete: An overview on chloride diffusion and prediction of corrosion initiation time. *International Journal of corrosion.* Article ID 5819202. 9 pages.

Kim, D.H., Shimura, K. and Horiguchi, T. (2010). Effect of tensile loading on chloride penetration of concrete mixed with granulated blast furnace slag. *Journal of Advanced Concrete Technology.* ***8***, 27-34.

Kledynski. Z., Machowska, A., Pacewska, B., Wilinska, I. (2017). Investigation of hydration products of fly ash - slag paste. *Journal of Thermal Analysis & Calorimetry.* ***130,*** 351-363.

Kong, L., Liu, C., Cao, M. and Fang, J. (2018). Mechanism study of the role of biofilm played in sewer corrosion of mortar. *Construction & Building Materials*. ***169,*** 44-56.

Konstantino, S., Michal, H., Alberto, V., Petra, M., Michal, V. (2021). Physical-chemical-mechanical quantitative assessment of the microstructural evolution in Portland-Limestone cement

pastes exposed to magnesium sulfate attack at low temperature. *Cement & Concrete Research.* ***149,*** 106566.

Kosmatka, S., Kerkhoff, B. and Panarese, W.C. (2002). Design and control of concrete mixtures, 14th Ed. Portland Cement Association, Skokie, IL, USA.

Kraiwood, K., Chai, J., and Jatuphon, T. (2000). Effect of Insoluble residue on properties of Portland cement. *Cement & Concrete Research.* ***30,*** 1209-1214.

Krishnapriya, S., Babu, D.L.V. and Arulraj, G.P. (2015). Isolation and identification of bacteria to improve the strength of concrete. *Microbiological Research.* ***174,*** 48-55.

KS EAS 148-1 (2017). Cement-Test Methods. Part 1: Determination of Strength. Kenya Bureau of Standards. Nairobi-Kenya.

KS EAS 148-2 (2017). Cements – Test methods part 2: Chemical analysis, Kenya Bureau of Standards, Nairobi-Kenya.

KS EAS 148-3 (2017). Cement- Test Methods. Part 3: Determination of setting times and soundness. Kenya Bureau of Standards. Nairobi- Kenya

KS EAS 18-1 (2017) Cement part 1: Composition, Specification and Conformity Criteria for common cements, Kenya Bureau of Standards, Nairobi - Kenya.

Kumar, M.P. and Paulo, J.M. M. (2006). Concrete: Microstructure, Properties and Materials. Department of Civil and Environmental Engineering University of California at Berkeley. 3rd Edition.

Kunther, W., Lothenbach, B. and Skibsted, J. (2015). Influence of the Ca / Si ratio of the C-S-H phase on the interaction with sulfate ions and its impact on the ettringite crystallization pressure. *Cement & Concrete Research.* ***69***, 37-49

Kurokawa, D., Yoshida, H. and Fukuda, K. (2014). Crystallization of belite-melilite clinker minerals in the presence of liquid phase. *Cement & Concrete Research,* ***60,*** 63-67.

Lahav, O., Lu, Y., Shavit, U. and Loewenthal, R., (2004). Modelling hydrogen sulfide emission rates in gravity sewage collection systems. *Journal of Environmental Engineering*. ***11,*** 1382-1389.

Lambert, I. and Clever H. L. (1992). Alkaline earth hydroxides in water and aqueous solutions solubility data series. **52**. Oxford: pergamon press.

Lea, F.M. (1998). The Chemistry of Cement and Concrete. Edward Arnold, London. Fourth Edition. 421 – 424.

Lea, F.M. (2004). Chemistry of cement and concrete. *Elsevier,* Fourth Edition.

Lee, N.K. Lee, H.K. (2016). Influence of the slag content on the chloride and sulfuric acid resistances of alkali-activated fly ash / slag paste. Cement & Concrete Composites. ***72***, 168-179.

Leeman, A. and Holzer, L. (2001). Influence of mica on the properties of mortar and concrete. *https:www.researchgate.net/publication/304181219.*

Lea, F.M. (1998). The Chemistry of Cement and Concrete. Edward Arnold, London. Fourth Edition. 421 – 424.

Lea, F.M. (2004). Chemistry of cement and concrete. *Elsevier*, Fourth Edition.

Lei, G., Terry, B., Philip, V. (2019). Sulphuric acid exposure of conventional concrete and alkali-activated concrete: Assessment of test methodologies. *Construction & Building Materials.* ***197,*** 681-692.

Le Saoůt, G., Kocaba, V. and Scrivener, K. (2011). Application of the Rietveld method to the analysis of anhydrous cement. Cement & Concrete Research. ***41***, 133-148.

Linderolt, O., Wadso, L. and Jansen, D. (2021). Long-term cement hydration studies with isothermal calorimetry. *Cement & Concrete Research.* ***141,*** 106344.

Liu, Y., Lei, S., Lin, M., Li, Y., Ye, Z. and Fan, Y. (2017). Assessment of pozzolanic activity of calcined coal-series kaolin. *Applied Clay Science.* ***143,*** 159-167.

Liu, Z., Cui, X. and Tang, M. (1992). Hydration and setting time of MgO-type expansive cement. *Cement & Concrete Research.* ***22,*** 1-5.

Liu, Z., Schutter, D. G., Deng, D. and Yu, Z. (2012). "Salt weathering" Distress on concrete by sulfates? *Advances in crystallization processes*. ***17,*** 431-464.

Li, X., Jiang, G., Kappler, U. and Bond, P., (2017). The ecology of acidophilic microorganisms in the corroding sewer environment. *Frontiers in Microbiology*. ***8,*** 683.

Lors, C., Chehade, M. and Damidot, D. (2009). pH variations during growth of *Acidithiobacillus thiooxidans* in buffered media designed for an assay to evaluate concrete biodeterioration. *International Biodeterioration & Biodegradation.* ***63,*** 880-883.

Macfadyen, J.D. (2006). Cement and Cement raw materials. *Industrial Minerals & Rocks*, 7th edition. 1121-1136

Macphee, D.E. and Lachowski, E.E. (1998). Cement components and their phase relations. *Lea's chemistry of cement and concrete.* Fourth Edition, *Oxford: Butterworth – Heinemann*, 95-129.

Marchland, J., Odler, I. and Skalmy, J.P. (2003). Sulfate attack on concrete. CRC Press.
Maregesi, G., R. (2021). Mica in concrete. *Advanced Engineering Solutions Journal.* ***1,*** 1-8.

Mari, K., Keisuke, T. and Yuichiro, K. (2021). Physiochemical properties of the Portland Cement- based Mortar exposed to deep seafloor conditions at a depth of 1680 M. *Cement & Concrete Research.* ***142,*** 106335.

Marinescu, M.V.A., and Brouwers, H.J.H. (2009). Chloride binding in OPC hydration products. *In: Proceedings of 17th Ibausil International conference on Building Materials.* Weimar, Germany.

Mark, R. and Hutchnison, P. (1986). On the structure of the Roman Pantheon. *The Art Bulletin.* ***68,*** 24-34.

Martin-Perez, B., Zibara, H., Hooton, R.D. and Thomas, M.D.A. (2000). A study of the effect of chloride binding on service life predictions. *Cement & Concrete Research.* ***30***, 1215-1223.

Matos, J.S. and Aires, C.M. (1995). Mathematical modelling of sulfides and hydrogen sulfide gas build-up in the Costa do Estoril sewage system. *Water Science & Technology.* ***31,*** *255-261.*

Meddah, M.S., Benkari, N., Al-Saadi, S.N. and Al-Maktoumi, Y. (2020). Sarooj Mortar: From a traditional building material to an engineered Pozzolan- Mechanical and thermal properties study. *Journal of Building Engineering.* ***32,*** 101754.

Meisam S. and Mohsen, H. A. R. (2020). Layered Double Hydroxide Polymer Nanocomposites, 2-FTIR characterization of layered double hydroxides and modified layered double hydroxides. *wood head publishing series in composites Science and Engineering*. 77-101.

Mendes, A., Gates, W.P., Sanjayan, J.G. and Collins, F. (2011). NMR, XRD, IR and Synchrotron NEXAFS Spectroscopic Studies of OPC and OPC/slag cement paste hydrates. *Materials structures.* ***44***, 1773-1791.

Mesbah, A., Francois, M., Cau-dit-coumes, C., Frizon, F., Filinchuk, Y., Leroux, F., Ravaux, J. and Renaudin, G. (2011). Crystal structure of Kuzel's salt $3CaO.Al_2O_3.{}^1/_2CaCl_2.11H_2O$ determined by synchroton powder diffraction. *Cement & Concrete Research.* ***41***, 504-509.

Meysam, N., Nader, G. and Mohammadreza, S. (2018). Alkali-activated natural Pozzolan/ slag mortars: A parametric study. *Construction & Building Materials.* ***164,*** 625-643.

Micelli, F. and Nanni, A. (2004). Durability of FRP rods for concrete structures. *Construction & Building Materials.* ***18***, 491-503.

Michael, J. M. and Thomas, D. D. (2019). Pozzolans and Pozzolanic Materials. *Leas' Chemistry of cement and concrete.* Fifth edition. 363-467.

Miller, A., Dionisio, A. and Macedo, M. (2006). Primary bio receptivity: A comparative study of different Portuguese lithotypes. *International Biodeterioration and Biodegradation.* ***57,*** 136-142.

Min, W., Tian, W., Kai, W. and Lili, K. (2020). Microbiologically induced corrosion of concrete in sewer structures: A review of the mechanisms and phenomena. *Construction & Building Materials.* ***239,*** 117813.

Mindess, S., Young, J.F. and Darwin, D. (2003). Concrete. 2nd Edition. Prentice Hall, Upper Saddle River, NJ, 86-87.

Mohammed, S., Elhem, G. and Mekki, B. (2016). Valorization of pozzolanicity of Algerian clay: Optimization of the heat treatment and mechanical characteristics of the involved cement mortars. *Applied clay science.* ***132,*** 711-721.

Mollah, M.Y.A., Kesmez, M. and Cocke, D.L. (2004). An X-ray diffraction (XRD) and Fourier transform Infrared Spectroscopic (FT-IR) Investigation of the Long-term effect of the solidification/ stabilization (s/s) of arsenic (v) in Portland cement type-v. *Science of the Total Environment.* ***325,*** 255-262.

Mollah, M., Yu, W., Schennach, R., Cocke, D.L. (2000). A Fourier transform infrared spectroscopic investigation of the early hydration of Portland cement and the influence of sodium lignosulfonate. *Cement & Concrete Research*. ***30***, 267-273.

Monteiro, P. and Mehta, P. (1993). Concrete: Structure, properties and materials, Prentice-Hall, Englewood cliffs.

Monteny, J., De Belie, E., Vinckie, E., Verstraete, W. and Taerve, L. (2001). Chemical and Microbiological tests to simulate sulfuric acid corrosion of polymer/modified concrete. *Cement & concrete Research.* ***31,*** 1359-1365.

Monteny, J., Vickie, E., Beeldens, A., De Belie, N., Taerwe, L., Van Gemert, D. and Verstraete, W. (2000). Chemical microbiological and in-situ test methods for biogenic sulfuric acid of concrete. *Cement & Concrete Research.* ***30,*** 623-634.

Moradian, M., Shekarchi, M., Pargar, F., Bonakdar, A. and Valipour, M. (2012). Deterioration of concrete caused by complex attack in sewage treatment Plant Environment. *Journal of performance of constructed facilities.* ***26,*** 124-134.

Mori, T., Koga, M., Hikosaka, Y., Nonaka, T., Mishina, F., Sakai, Y., Koizumi. (1991). Microbial corrosion of concrete sewer pipes, H_2S production from sediments and determination of corrosion rate. *Water Science Technology*. ***23***, 1275-1282.

Mori, T., Nonaka, T., Tazaki, K., Koga, M., Hikosaka, Y. and Noda, S. (1992). Interactions of nutrients, moisture and pH on microbial corrosion of concrete sewer pipes. *Water Research.* ***26,*** 29-37.

Moses, W. K. (2016). Composition and microstructure of concrete mixtures subjected to biogenic acid corrosion and their role in corrosion prediction of concrete outfall sewers. PhD Thesis, University of Cape Town.

Mshali, M.L. and Visser, A.T. (2012). Influence of Mica on unconfined compressive strength of cement-treated weathered granite gravel. *Journal of the South African Institution of Civil Engineering*. ***54,*** 71-77.

Muller, W., Beddoe, R.E. and Heinz, D. (2013). Sulfate attack expansion mechanisms. *Cement Concrete Research. **52***, 208-215.

Munyao, O.M. (2015). Effects of surface and subsurface mixing water of Nairobi, Machakos and Kajiado counties on cement mortar performance. Msc Thesis. Department of Chemistry, Kenyatta University, Kenya.

Munyao, O.M., Thiong'o, J.K., Wachira, J.M., Mutitu, D.K., Genson, M. and Romano, M. (2020_a). Chloride ingress in cement mortars exposed to *Acidithiobacillius thiooxidans. Hindawi. Advances* in *Materials Science & Engineering. Article ID 4191806, 10 pages*.

Munyao, O.M., Thiong'o, J.K., Wachira, J.M., Mutitu, D.K. and Romano, M. (2020_b). Influence of *Starkeya novella* on mechanical and microstructural properties of cement mortars. *Hindawi. Journal of chemistry. Article ID 8212396. 9 pages*

Munyao, O.M., Karanja, J.T., Wachira J. M., Mutitu, D. K., Romano, M., Genson, M. and Marangu, J. M. (2020_c). Study on the effect of *Thiobacillus intermedius* bacteria on the on the Physico-Mechanical properties of mortars of ordinary Portland cement. ***Heliyon 6,*** *e03232*.

Munyao, O.M., Thiong'o, J.K., Wachira, J.M., Mutitu, D.K., Romano, M. and Genson, M. (2019). Use of bacillus species bacteria in protecting the concrete structures from sulphate attack- A review. *Journal of Chemical Reviews. **1,*** 287-299.

Muralidharan, S., Vedalakshmi, R., Saraswathi, V., James, J. and Palaniswamy, N. (2005). Studies on the aspects of chloride ion determination in different types of concrete under macro-cell corrosion conditions. *Building and Environment. **40**,* 1275-1281.

Muthengia, J.W. (2009). Effects of selected media on novel Portland pozzolana cement. PhD Thesis, Department of Chemistry, Kenyatta University, Kenya.

Mutitu, D.K. (2013). Diffusivity of chloride and sulphate ions into mortar cubes made using ordinary portland and portland pozzolana cements. Msc Thesis. Department of Chemistry, Kenyatta University, Kenya.

Mutitu, D. K. (2020). Effect of Microbial Biocementation on Physio-Chemical and Mechanical properties of mortar made from Portland cements. University of Embu, Ph.D Thesis.

Negar, R. and Nemkumar, B. (2019). Development of a sustainable coating and repair materials to prevent bio-corrosion in concrete sewer and wastewater pipes. *Cement & Concrete Composites. **100,*** 99-107.

Neville, A.M. (1996). Properties of concrete. Fourth Edition. Pearson Higher Education, Prentice Hall, Englewood Cliffs.

Neville, A.M. (2004). The confused world of sulfate attack on concrete. *Cement & Concrete Research.* ***34,*** 1275-1296.

Neville, A.M. (2011). Properties of concrete. Harlow, England; New York: Pearson.

Neville, AM. (2011). Properties of concrete. Fifth Edition. Essex, UK: Pearson Education Limited.

Newman, J. and Choo, B.S. (2003). Advanced Concrete Technology. *Elsevier.* 95-202.

Nica, D., Davis, J.L., Kirby, L. Zuo, G. and Roberts, D.J. (2000). Isolation and characterization of microorganisms involved in the biodeterioration of concrete in sewers. *International Biodeterioration & Biodegradation.* ***46,*** 61-68.

Nielsen, A.H., Yongsiri, C., Hvitved-Jacobsen, T. and Vollertsen, J. (2005). Simulation of sulfide build-up in waste water and atmosphere of sewer networks. *Water Science & Technology.* ***52,*** 201-208.

Nielsen, E.P. and Geiker, M.R. (2003). Chloride diffusion in partially saturated cementitious material. *Cement & Concrete Research.* ***33****,* 133-138.

Niloofar, P., Davood, M. and Davood, P. (2019). Use of bacteria to improve electrical resistivity and chloride penetration of air entrained concrete. *Construction & Building Material.* ***210,*** 588-595.

Ngui, F.M. (2015). Pozzolanicity, Compressive strength and ingress of selected aggressive ions in Kibwezi bricks based cement. Msc Thesis. Department of Chemistry, Kenyatta University, Kenya.

O'Connell, M., McNally, C. and Richardson, M.G. (2010). Biochemical attack on concrete in waste water applications: a state of the art review. *Cement & Concrete Composite.* ***32****,* 479-485.

Odler, I. (2007). 6 – Hydration, setting and hardening of Portland cement. Leas' Chemistry of cement and concrete. Fourth Edition. 241-297.

Ogawa, S., Nozaki, T., Yamada, K., Hirao, H. and Hooton, R.D. (2012). Improvement on sulfate resistance of blended cement with high alumina slag. *Cement & Concrete Research.* ***42****,* 244-251.

Okabe, S., Odagiri, M., Ito, T. and Satoh, H. (2007). Succession of sulfur-oxidizing bacteria in the microbial community on corroding concrete in sewer systems. *Applied & Environmental Microbiology.* ***73,*** 971-980.

Över, D. (2012). Early heat evolution in natural Pozzolan incorporated cement hydration. Middle East Technical University. MSc. Thesis. Arkansas, USA.

Parande, A., Ramsamy, P., Ethirajan, S., Rao, C. and Palanisamy, N. (2006). Deterioration of reinforced concrete in sewer Environments. In: Proceedings of the Institution of Civil Engineers-*Municipal Engineer. **159,*** 11-20.

Parker, C.D. (1945). The corrosion of concrete. *Australian Journal of Experimental Biology Medical Science. **23***, 81.

Parker, C.D (1951). Mechanics of corrosion of concrete sewers by hydrogen sulfide. *Sewage & Industrial Waste. **23,*** 1477-1485.

Patel, R.A., Phuna, Q.T., Seetharam, S.C., Perko, J., Jacques, D., Maes, N., De Schutter, G., Ye, G. and Van Breugel, K. (2016). Diffusivity of saturated ordinary Portland cement-based materials: A critical review of experimental and analytical modelling approaches. *Cement & Concrete Research. **90,*** 50-72.

Patrick, J., Aditya, K., Emmanuel, G., Robert, J.F. and Karen, L.S. (2012). Effect of mixing on the early hydration of alite and OPC systems. *Sika Technology Press* Zurich, 2-8.

Pedro, C. R. A. A., Fábio, A.C. and Vanderley, M.J. (2020). Efficiency of Portland-Pozzolana cements: Water demand, chemical reactivity and environmental impact. *Construction & Building Materials. **247,*** 118546.

Peter, B. (2003). Theory of XRF.

Peter, C. H. and Martin, L. (2019). Lea's Chemistry of cement and concrete. Fifth Edition. *Elsevier*.

Philip, A. A. (1998). Cement Plant Operations Handbook for Dry process plants. Second Edition. *Trade ship Publication ltd.*

Ping, G., Yan, F. and Beadoin, J.J. (1994). A study of the hydration and setting Behaviour of OPC-HAC pastes. *Cement & Concrete research*. ***24***, 682-694.

Pipilikaki, P., Papageorgiou, D., Teas, C., Chaniotakis, E. and Katsioti, M. (2008). The effect of temperature on Thaumasite formation. *Cement & Concrete Composites. **30,*** 964-969.

Prieto, B., Silva, B., Aira, N. and Alvarez, L. (2006). Toward a definition of a bio receptivity index for granitic rocks: Perception of the change in appearance of the rock. *International Biodeterioration & Biodegradation*. ***58,*** 150-154.

Provis, J.L., Palomo, A. and Shi, C. (2015). Advances in undertaking alkali – activated materials. *Cement & Concrete Research*. ***78****,* 110-125.

Puertas, F., Martinez-Ramirez, S., Alonso, S., Vazquez, T. (2000). Alkali-activated fly ash / slag cements: Strength behavior and hydration products. *Cement & Concrete Research. **30,*** 1625-1632.

Qiao, C., Coyle, A., Isgor, B. and Weiss, J. (2018). Prediction of chloride Ingress in saturated concrete using formation factor and chloride binding Isotherm. *Advances in Civil Engineering Materials.* ***7,*** 206-220.

Qian, G.R., Shi, J., Cao, Y.L., Xu, Y.F. and Chui, P.C. (2008). Properties of MSW Fly ash – Calcium Sulfoaluminate cement Matrix and Stabilization / Solidification on heavy metals. *Journal of Hazardous Materials.* ***152,*** 196-203.

Ragal, A. (2013). The Physico-Mechanical characteristics of pozzolanic cements, MSc. Faculty of Science, Fayoum University.

Ramsamy, P.L. (2006). Deterioration of reinforced concrete in sewer environments. Proceedings of the Institution of civil Engineers. *Municipal Engineer.* ***159***, 11-20.

Redner, J.A, His, R.P. and Esfandi, E.J. (1994). Evaluating coatings for concrete in wastewater facilities: update. *Journal of Protecting Coatings & Linings.* ***11,*** (1994) 51-61.

Renaudin, G., Segni, R., Mentel, D., Nedelec, J.M., Leroux, F., C. and Taviot-Gueho, C. (2007). A Raman study of the sulfated cement hydrates: Ettringite and mono sulfoaluminates. *Advanced Concrete Technology.* ***5,*** 299-312.

Richard, T., Mercury, L., Poulet, F. and D'Hendercourt, L. (2006). Diffuse reflectance Infrared Fourier transform Spectroscopy as a tool to characterize water adsorption/confinement situations. *Journal of Colloid & Interface Science.* ***304,*** 125-136.

Rigby, D.B. (2010). Evaluation of the Technical Basis for Extended Dry storage and transportation of used Nuclear Fuel. *Nuclear Waste Technical Review Board,* USA.

Rigdon, J.H. and Beardsley, C.W. (1958). Corrosion of concrete by autotrophes. *Corrosion.* ***14***, 60-62.

Rikard, E. Y. (2013). Early Hydration of Portland cement – An Infrared Spectroscopy perspective complemented by calorimetry and scanning Electron Microscopy. Thesis for the Degree of Doctor of Technology, Department of chemical and biological Engineering. Haimers University of Technology, Gothenburg, Sweden.

Rikard, Y., UlfJaglid, Britt-Marie, S. and Itai, P. (2009). Early hydration and setting of Portland cement monitored by IR, SEM and Vicat techniques. *Cement & Concrete Research.* ***39,*** 433-439.

Roberts, D.J., Nica, D., Zuo, G. and Davis, J.L. (2002). Quantifying microbially induced deterioration of concrete: Initial studies. *International Biodeterioration & Biodegradation*. ***49***, 227-234.

Rogers, R.D., Hamilton, M.A. and McConnell, J.W. (1996). Microbial Degradation of Low level Radioactive Waste-Final Report, NUREG/CR-6341, U.S. Nuclear Regulatory Commission, Washington DC, USA.

Rootsey, R., Melchers, R., Stuetz, R., Keller, J. and Yuan, Z. (2012). Taking control of odours and corrosion in sewers. *Environmental Science. Article ID 127346257.*

Roy, J.D.M., Jiang, W. and Silsbee, M.R. (2000). Chloride diffusion in Ordinary blended and alkali-activated cement pastes and its relation to other properties. *Cement & Concrete Research.* ***30,*** 1879-1884.

Run-Sheng, L., Xiao-Yong, W., Han-Seung, L. and Hyeong-Kyu, C. (2019). Hydration and microstructure of cement pastes with calcined Hwangtoh clay. *Materials.* ***12,*** 458.

Sanchez-Silva, M. and Rosowsky, D.V (2008). Biodeterioration of construction materials: state of the art and future challenges. *Journal of Materials in Civil Engineering*. ***20,*** 352-365.

Sand, W. and Bock, E. (1984). Concrete Corrosion in the Hamburg Sewer System. *Environmental Technology Letters.* ***5****,* 517-528.

Sand, W. and Bock, E. (1991). Biodeterioration of ceramic materials by biogenic acids. *International Biodeterioration.* ***27,*** 175-183.

Sand, W., Bock, E. and White, D.C. (1987). Biotest system for rapid evaluation of concrete resistance to sulfur-oxidising bacteria. *Materials Performance.* ***26,*** 14-17.

Santa, R.A.A.B., Bernardin, A.M., Riella, H.G. and Kuhnen, N.C. (2013). Geopolymer synthesized from bottom coal ash and calcined paper sludge. *Journal of Clean Production.* ***57****,* 302-307.

Sarfo-Ansah, J., Atiemo, E., Boakaye, K.A., Adjei, D. and Adjaottor, A.A. (2014). Calcined clay pozzolana as an admixture to mitigate the alkali-silica reaction in concrete. *Journal of Materials Science & Chemical Engineering.* ***2,*** 20-26.

Saricimen, H. and Maslehuddin, M. (1987). Case study of deterioration of concrete in sewerage environment in an Arabian gulf country. *Durability of Building Materials*. **5**.

Satoh, H., Odagiri, M., Ito, T. and Okabe, S. (2009). Microbial community structures and Insitu sulfate-reducing and sulphur-oxidizing activities in biofilms developed on mortar specimens in a corroded sewer system. *Water Research.* ***43,*** 4729-4739.

Satoshi, O., Mitsunori, O., Tsukasa, I. and Hitashi, S. (2007). Succession of Sulfur-oxidizing Bacteria in the microbial community on corroding concrete in sewer systems. *Applied & Environmental Microbiology.* ***73,*** 971-980.

Saucier, F. and Herisson, J. (2015). Use of calcium aluminate cement in H_2S biogenic environment. *In: Institute of Concrete Technology.* 67- 80.

Schmidt, T. (2007). Sulfate attack and the role of internal carbonate on the formation of thaumasite Ph.D Thesis. Ecole polytechnique Federale de Lausanne, Switzerland.

Scrivener, K. and De Belie, N. (2013). Bacteriogenic sulfuric acid attack of cementitious materials in sewage systems, in: Rilem state of the Art Report – Performance of cement – based materials in Aggressive Aqueous Environment. *Springer*.305 – 318.

Scrivener, K.L. Juilland, P. and Monteiro, P.J.M. (2015). Advances in understanding hydration of Portland cement. *Cement & Concrete Research.* ***78,*** 38-56.

Scrivener, K., Ouzia, A., Juilland, P. and Mohammed, A. K., (2019). Advances in understanding cement hydration mechanisms. *Cement & Concrete Research.* ***124,*** 105823.

Scrivener, K., Snellings, R. and Lothenbach, B. (2017). A practical guide to microstructural analysis of cementitious materials. First Edition., CRC Press.

Sedaghat, A. (2016). Cement Heat of Hydration and Thermal control. *Cement & concrete Research.* ***85,*** 67-78.

Sharma, K.R., Yuan, Z., De Haas, D., Hamilton, G., Corrie, S. and Keller, J. (2008). Dynamics and dynamic modelling of H_2S production in Sewer System. *Water Research*. ***42,*** 2527-2538.

Shi, C., Jimenez, A.F., Palomo, A. (2011). New cements for 21st century: The pursuit of an alternative to Portland cement. *Cement & Concrete Research.* ***41***, 750-763.

Shi, C. and Stegemann, J. (2000). Acid corrosion resistance of different cementing materials. *Cement & Concrete Research.* ***30,*** 803-808.

Shiping, W., Mauricio, S., David, T. and Chris, G. (2010). Microbial mediated deterioration of reinforced concrete structures. *International Biodeterioration & Biodegradation.* ***64,*** 748-754.

Shiping, W., Zhenglong, J., Hao, L., Dongsheng, Z. and Sanchez-Silva, M. (2013). Microbiologically induced deterioration of concrete. A Review: *Brazilian Journal of microbiology*. ***44,*** 1001-1007.

Shiyu, Z., Yingliang, Z., Hangxing, D., Jingping, Q. and Chen, H. (2021). Effect of Sodium Chloride concentration and pre-curing time on the properties of cemented paste back fill in a sub-zero environment. *Journal of Cleaner Production*. ***283,*** 125310.

Shoukry, H., Kotkata, M.F., Abo-EL-Enein, S.A., Morsy, M.S. and Shebl, S.S (2016). Enhanced physical, mechanical and microstructural properties of lightweight vermiculite cement composites modified with nano metakaolin. *Construction & Building Materials*. ***112***, 276-283.

Shupeng, Z., Xiaoxiao, X., Shzim, A.M., Zhijun, D., Dongxu, L. and Hongzhi, C. (2018). Effect of calcium sulfate type and dosage on properties of calcium aluminate cement-based self levelling mortar. *Construction & Building Materials.* ***167,*** 253-262.

Sidney, M. (2019). Resistance of concrete to destructive agencies. *Lea's chemistry of cement and concrete.* Fifth Edition, *Elsevier.*

Sihem, H., Belkacem, M., Said, K., Carlos, T., Mehmet, S. K. and Andre, G. S.G. (2021). The effect of content and fineness of natural pozzolana on the rheological, mechanical and durability properties of self-compacting mortar. *Journal of Building Engineering.* ***44,*** 103276.

Siline, M. and Omary, S. (2018). Optimization of the SO_3 content of an Algerian Portland Cement: Study on the effect of various amounts of gypsum on cement properties. *Construction & Building Materials.* ***164,*** 362-370.

Silva, D.A., Roman, H. R. and Gleize, P.J.P. (2002). Evidences of chemical interactions between EVA and hydrating Portland cement. *Cement & Concrete Research*. ***32,*** 1383-1390.

Singh, A., Gupta, S. Singh, J. and Singh, N.P. (2017). Hydration mechanism and strength of OPC and Blended OPC with Fly Ash in the presence of metakaolin. *Construction & Building Materials.* ***72,*** 73-82.

Skalny, J., Marchand, J. and Odler, I. (2002). Sulfate attack on concrete. London; New York: *Spon Press.*

Skoog, D.A., Holler, F.J. and Crouch, S.R (2007). Principles of Instrumental Analysis. Belmont, CA: Thomson Brooks/Cole.

Snellings, R., Salze, A. and Scrivener, K.L. (2014). Use of X-ray diffraction to quantify amorphous supplementary cementitious materials in anhydrous and hydrated blended cements. *Cement & Concrete Research* ***64,*** 89-98.

Song, Y., Tian, Y., Li, X., Wei, J., H. Zhang, H., Bond, P.L., Yuan, Z. and Jiang, G. (2019). Distinct microbially induced concrete corrosion at the tidal region of reinforced concrete sewers. *Water Research.* ***150,*** 393-402.

Song, Z., Jiang, L., Zhang, Z. and Xiong, C. (2016). Distance-associated chloride binding capacity of cement paste subjected to natural diffusion. *Construction & Building Materials.* ***112***, 925-932.

Sravanthi, V., Babu, F., Gregory, G., Wilber, P.E., Tyler, L. P.E., Joshua, D. and Ramsey, N. S. (2013). Characterization and mediation of microbial deterioration of concrete bridges. Final Report. Oklahoma Transportation Center.

Sravanthi, V., Babu, Z. F., Gregory, G. W., Elias, S., Seifollah, N., Tyler, M. L., Joshua, D. R. (2015). Isolation of a sulfur-oxidizing *Streptomyces* sp. from deteriorating bridge structure and its role in concrete deterioration. *International Biodeterioration & Biodegradation.* ***97***, 128-134

Sravanthi Vupputuri, B.F., Gregory, W., Seifollah, N., Tyler, l., and Joshra, D. R. (2013). Characterization and mediation of microbial Deterioration of concrete Bridge structures. Oklahoma state University school of Engineering, 423 Engineering Nonit Shilwater, OK 74078

Starkey, R.L. (1935). Isolation of some bacteria which oxidize thiosulfate. *Soil Science.* ***39,*** 197-220.

Stepkowska, E.T., Jose, M. M. B., Real, C., Perez-Rodriguez, J.L (2005). Hydration of products in two aged cement pastes. *Thermal Analysis & Calorimetry*. ***82,*** 731-739.

Steven S. M. (2011). X-ray Fluorescence Spectrometry (XRF) in Geoarchaelogy. *Springer*

Struble, L.J., and Lei, W.G. (1995). Rheological changes associated with setting of cement paste. *Advanced Cement Based Materials*. ***2,*** 244-230.

Stutzman, P., Heckert, A., Tebbe, A. and Leigh, S. (2014). Uncertainty in Bogue – calculated phase composition of hydraulic cements. *Cement & concrete Research*. ***61,*** 40-48.

Suhua, M., Ruben, S., Xuerun, L., Xadong, S., Karen, L. S. (2021). Alite-Ye'elimite clinker: Hydration Kinetics, Products and Microstructure. *Construction & Building materials.* ***266 -Part B,*** 121062.

Sulikowski, J. and Kozubal, J. (2016). The durability of a concrete sewer pipeline under deterioration by sulfate and chloride corrosion. *Procedia Engineering.* ***153,*** 698-705.

Sumit, J., Shweta, G., Abhijit, M. and Sudhakara, M. R. (2019). Protection of concrete structures under sulfate environments by using calcifying bacteria. *Construction & Building Materials.* ***209,*** 156-166.

Sun, H., Li, Z., Bai, J., Memon, S., Dong, B., Fang, Y., Xu, W. and Xing, F. (2015). Properties of chemically combusted calcium carbide residue and its influence on cement properties. *Materials.* ***8,*** 638-651.

Sun, X. (2015). Improving the understanding of concrete sewer corrosion through investigations of the gaseous hydrogen sulfide uptake and transformation processes in the corrosion layer. The University of Queensland, Brisbane, Queensland. Ph.D thesis.

Sun, X., Jiang, G., Chiu, T.H., Zhou, M., Keller, J. and Bond, P.L. (2016). Effect of surface washing on the mitigation of concrete corrosion under sewer conditions. *Cement & Concrete composites*. ***68,*** 88-95.

Tahereh, N., Abhijit, M., Navdeep, D. and So-Ryong, C. (2017). Biogenic deterioration of concrete and its mitigation technologies. *Construction & Building Materials.****149,*** 575-586.

Tang, L. (2008). Engineering Expression of the Clinconc Model for Prediction of Free and Total Chloride ingress in Submerged Marine Concrete. *Cement & Concrete Research*. ***38,***1092-1097.

Tang, S.W., Cai, X.H., He, Z., Zhou, W., Shao, H.Y., Li, Z.J., Wu, T. and Chen, E. (2017). The review of early hydration of cement-based materials by electrical methods. *Construction & Building materials.* ***146,*** 15-29.

Tayeh, B.A., Abu, B. B., Johari, M. and Zeyad, A. (2013). The role of silica fume in the adhesion of concrete restoration systems. *Advanced Materials Research.* ***626,*** 265-269.

Taylor, H.F.W. (1997). Cement chemistry. 2nd Edition. London: Thomas Telford, 187- 217

Taylor, H.F.W. (1999). Cement Chemistry. Taylor and Thomas Telford Services LTD, London, 8-128.

Thaulow, N., Sahu, S. (2004). Mechanism of concrete deterioration due to salt crystallization. *Materials Characterization.* ***53,*** 123-127.

Theodore, C. and Karen, S. (2012). Alkali fixation of CSH in Blended Cement pastes and its Relation to Alkali Silica Reaction, Laboratory of construction materials. *Cement & Concrete Research*. ***42,*** 1042-1054.

Thomas, M.D.A., Hooton, R.D., Scott, A., Zibara, H. (2012). The effect of supplementary cementitious materials on chloride binding on hardened cement paste. *Cement & Concrete Research.* ***42,*** 1-7.

Tironi, A., Trezza, M., Scian, A. and Irassar, E. (1992). Incorporation of calcined clays in mortars: on microbial corrosion of concrete pipes. *Water Research.* ***26,*** 29-37.

Tixier, R., Mobasher, B. (2003). Modelling of damage in cement based materials subjected to external sulfate attack – Part 1: Formulation. *Materials Engineering*. ***15,*** 305-13.

Trevor, S. (2016). The use of Limestone as an extender and its effect on concrete properties. MSc in Advanced Concrete Technology. Queen's University Belfast. Centre for Architecture and Construction Management.

Trezza, M.A. and Lavat, A. E. (2001). Analysis of the system $3CaO.Al_2O_3$-$CaSO_4.2H_2O$-$CaCO_3$-H_2O by FT-IR Spectroscopy. *Cement & Concrete Research*. ***31,*** 869-872.

Yilmaz, K. and Suna, N. (2014). The effect of using Fly Ash on the strength and hydration characteristics of blended cements. *Construction & Building materials*.***73,*** 25-32.

US Environmental Protection Agency (2010). State of technology for rehabilitation of wastewater collection systems, US Environmental Protection Agency, Office of research and Development. EPA/600/R-10/078.

Uysal, M. and Sumer, M. (2013). Performance of self-compacting concrete containing different mineral and mixtures. *KCSE Journal of Civil Engineering.* ***17,*** 465-472.

Valix, M. and Shanmugarajah, K. (2015). Biogenic acids produced on epoxy linings installed in sewer crown and tidal zones. *Water Research.* ***80,*** 217-226.

Van, A.J.H.P. and Visser, S. (1975). Thaumasite formation: a cause of deterioration of Portland cement and related substances in the presence of sulphates. *Cement & Concrete Research.* ***5,*** 225-232.

Veera, H. (2021). Effect of recycled concrete powder on strength, electrical resistivity, and water absorption of self-compacting mortars. *Case Studies in construction Materials.* ***15,*** e00725.

Vendalakshmi, R., Saraswathy, V. and Yong, A.K. (2011). Performance of evaluation of blended cement concretes under $MgSO_4$ attack. *Magazine of Concrete Research.* ***63***, 669-681.

Vimal, N. P. (2009). Sorptivity Testing to assess durability of concrete against Freeze-Thaw Cycling. Msc. Thesis, McGill University, Montreal, Canada.

Vincke, E., Boon, N. and Verstraete, W. (2001). Analysis of microbial communities on corroded concrete sewer pipes a case study. *Applied Microbiology & Biotechnology*. ***57,*** 776-785.

Vineet, S., Karen, S., Bishwajik, B. and Shashank, B. (2018). Changes in microstructure characteristics of cement paste on carbonation. *Cement & Concrete Research.* ***109,*** 184-197.

Vollertsen, J., Nielsen, A.H., Jensen, H.S., Tove, W.A. and Thorkild, H.J. (2008). Corrosion of concrete sewers – the kinetics of hydrogen sulfide oxidation. *Science of the Total Environment*. ***394,*** 162-170.

Walid, D., Nordine, L., Abdelhafid, K., Mohammed, N. O. (2017). Natural pozzolana addition effect on compressive strength and capillary water absorption of mortar. *Energy Procedia.* ***139,*** 689-695.

Wang, J., Basheer, P.M., Nanukuttan, S.V. and Bai, Y. (2014). Influence of compressive loading on chloride ingress through concrete. In: *Proceedings of the Civil Engineering Research Association of Ireland (CERAI).* Queen's University, Belfast.

Wei, S., Sanchez, M., Trejo, D. and Gillis, C. (2010). Microbial deterioration of reinforced concrete structures. *International Biodeterioration & Biodegradation.* ***64,*** 748-754.

Wells, T., Melchers, R.E. and Bond, P. (2009). Factors involved in the long term corrosion of concrete sewers. Australasian corrosion association proceedings of corrosion and prevention, Coffs Harbours, Australia.

Whittaker, M., Zajac, M., Ben, H. M. and Black, L. (2016). The impact of alumina availability on sulfate resistance of slag composite cements. *Construction & Building Materials.* ***119***, 356-369.

Wieslaw, K. (2014). Cement and Concrete chemistry. *Springer.*
Wilson-Jones, M. (2003). Principles of Roman Architecture. New Haven: Yale University press: 284.

Wood, A.P., Woodall, C.A., and Kelly, D.P. (2005). *Halothiobacillus neapolitanus* strain OSWA isolated from "The Old Sulphur Well" at Harrogate (Yorkshire, England). *Systematic & Applied Microbiology.* ***28,*** 746-748.

Wu, L., Hu, C. and Liu, W.V. (2018). The sustainability of concrete in sewer tunnel – A narrative review of acid corrosion in the city of Edmonton, Canada. *Sustainability*. ***10,*** 517.

Xiancui, Y., Linhua, J., Mingzhi, G., YunJie, C., Pengfei, Z., Weizhun, J. and Jie, Z. (2020). Using EDTA-2Na to Inhibit sulfate attack in slag mortar under steam curing. *Construction & Building Materials.* ***265,*** 120324.

Xiuli, D., Liu, J. and Renbo, Z. (2015). Chloride diffusivity in saturated cement paste- subjected to external mechanical loadings. *Ocean Engineering.* ***95,*** 1-10.

Xu, Y., Xiao, Y. W. (2021). Hydration- strength - durability - workability of biochar - cement binary blends. *Journal of Building Engineering.* ***42,*** 103064.

Xuan, L., O'moore, L. Yarong, S., Philip, L. B., Zhiguo, Y., Simeon, W. and Lucija, H., Guangming, J. (2019). The rapid chemically induced corrosion of concrete sewers at high H_2S concentration. *Water Research.* ***162***, 95-104.

Yamanaka, T., Aso, I., Togashi, S., Tanigawa, M., Shoji, K., Watanabe, T., Watanabe, N., Maki, K. and Suzuki, H. (2002). Corrosion by bacteria of concrete in sewage systems and inhibitory effects of formates on their growth. *Water Research.* ***36,*** 2636-2642.

Yan, G., Zhiqi, H., Zuhua, Z., Jun, C., Wanli, B., Chris, R. C., Tingting, Z. (2021). Effect of hydromagnesite addition on the properties and water resistance of magnesium oxysulfate (MOS) cement. *Cement & Concrete Research.* ***143,*** 106387.

Yang, W., Vollertsen, J. and Hvitved-Jacobsen, T. (2005). Anoxic Sulfide oxidation in wastewater of sewer networks. *Water Science &Technology.* ***52,*** 191-199.

Yilmaz, K. (2010). A study on the effect of fly ash and silica fume substituted cement paste and mortars. *Scientific Research & Essays.* ***5,*** 990-998.

Yilmaz, K. and Suna, N. (2014). The effect of using fly ash on the strength and hydration characteristics of blended cement. *Construction & Building Materials.* ***73***, 25-32.

YingJie, C., Aiguo, W., Yingcan, Z., Hao, W., Kaiwei, L., Rui, M., Liping, G. and Daosheng, S. (2021). Enhancing the performance of basic Magnesium Sulphate cement - based coral aggregate concrete through gradient composite design technology. *Composites Part B: Engineering.* ***227,*** 109382.

Yingwu, Z., Hao, T., Hongzhi, C., Feng, X. and Lili, S. (2015). Model for sulfate Diffusion Depth in concrete under complex Aggressive Environments and its Experimental Verification. *Hindawi. Advances in materials Science and Engineering. Article ID 693834, 11 pages.*

YImén, R., Jäglid, U., Steenari, B.M. and Parias, I. (2009). Early hydration and setting of Portland cement monitored by IR, SEM and Vicat techniques. *Cement Concrete Research*. ***39,*** 433-439.

Yongcheng, J., Yail, J. K. and Yanmin, J. (2021). Performance characterization of plain and CFRP-bonded concrete subjected to sulfuric acid. *Materials & Design. **197**,* 109176.

Young, J.F., Tong, H.S. and Berger, R. L. (1997). Composition of solutions in contact with hydrating Tricalcium silicate pastes. *American Ceramic Society. **60,*** 193-198.

Yousefi, A., Allahverdi, A. and Hejazi, P. (2014). Accelerated biodegradation of cured cement paste by Thiobacillus species under simulation condition. *International Biodeterioration & Biodegradation. **86,*** 317-326.

Yu, C., Sun, W. and Scrivener, K. (2015). Degradation mechanisms of slag blended mortars immersed in sodium sulfate solution. *Cement & Concrete Research.**72***, 37-47.

Yu, P., Kirkpatrick, R.J., Poe, B., Mcmillan, P.F. and Cong, X. (1999). Structure of Calcium Silicate Hydrate(C-S-H) Near, - Mid, - and Far-Infrared Spectroscopy. *American Ceramic Society. **82,***742-748.

Yu, Y., Tao, J., Xujian, L., Caiyi, C., Zhengxian, Y. (2018). Biogenic Sulfuric acid corrosion resistance of new artificial reef concrete. *Construction & Building Materials. **158,*** 33-41.

Yuan, H. (2013). Degradation modelling of concrete submitted to biogenic acid attack, Université Paris-Est, Ph.D thesis.

Yuan, H., Dangla, P., Chatellier, P., Chaussadent, T. (2013). Degradation modelling of concrete submitted to sulfuric acid attack. *Cement & Concrete Research*. ***53,*** 267-277.

Yuan, Q., Shi, C.-J., G.D. Shutter, G-De., Katrien, A. and De-Hua, D. (2009). Chloride binding of cement-based materials subjected to external chloride environment – A review. *Construction & Building Materials. **23,*** 1-13.

Yudong, X., Xujian, L., Tao, J., Yongning, L., Weijie, P. (2019). Comparison of corrosion resistance mechanism between ordinary Portland concrete and alkali-activated concrete subjected to biogenic sulfuric acid attack. *Construction & Building Materials. **228,*** 117071.

Yushan, G., Renaud, P. M., Othman, O. M., Teddy, F. C., Patrick, D. (2019). Pore size analyses of cement paste exposed to external sulfate attack and delayed Ettringite formation. *Cement & Concrete Research. **123,*** 105766.

Yuxia, G., Peng, W., Guorui, F., Tingyeoi, X.D. Zehua, W. and Qingdong, L. (2020). Experimental study on Diffusion process of sulfate ion in cemented Backfill material. *Hindawi*. *Advances in Civil Engineering. Article ID 5846397,* 14 pages

Zeinab, A. E. and Tamer, I. A. (2018). Effect of freezing- thawing on concrete behaviour. *Challenge Journal of Concrete Research Letters. **9,*** 21-36.

Zeng, Q., Li, K., Fen-Chong, T. and Dangla. P. (2012). Determination of cement hydration and pozzolanic reaction extents for Fly-ash cement pastes. *Construction & Building Materials.* ***27,*** 560-569.

Zhang, L., De Schryver, P., De Gusseme, B., De Muynck, W., Boon, N. and Verstraete, W. (2008). Chemical and biological technologies for hydrogen sulfide emission control in sewer systems: a review. *Water Research.* ***42,*** 1-12.

Zhang, S.P. and Zong, L. (2014). Evaluation of relationship between water absorption and durability of concrete materials. *Construction & Building Materials.* ***49,*** 33-52.

Zhang, Y. and Napier-Munn, T. (1995). "Effects of particle size distribution, surface area and chemical composition on Portland cement strength. *Powder Technology.* ***83,*** 245-252.

Zhao, J.Q., Kuraoka, S., Baker, T.H.W., Gu, P., Masson, J.F., Boudreau, S. and Brousseau, R.J. (1998). Durability and Performance of Gravity pipes: a state-of-the-art literature review. *National Research Council.* Canada.

Zheng, C., Liyun, W., Vivek, B., Chaofan, Y. (2010). Coupled models to describe combined diffusion - reaction behavior of chloride and sulphate ions in cement - based systems. *Construction & Building Materials.* ***243,*** 118232.

Zhenguo, S., Sergio, F., Barbara, L., Mette, R. G., Wolfgang, K., Josef, K., Duncan, H. Jorgen, S. (2019). Sulfate resistance of calcined clay. Limestone-Portland cements. *Cement & Concrete Research.* ***116***, 238-251.

Zhenyun, Y., Yading, Z., Hengjing, B., Minghao, L. (2021). Synergistic effects of ettringite-based expansive agent and polypropylene fiber on early-age anti-shrinkage and anti-cracking properties of mortars. *Journal of Building & Engineering.* ***39,*** 102275.

Zhu, W., Chen, X., Struble, L.J., Yang, E-H. (2018). Characterization of calcium-containing phases in alkali-activated municipal solid waste incineration bottom ash binder through chemical extraction and deconvoluted Fourier transform infrared spectra. *Journal of Clean Production.* ***192****,* 782-789.

Zilgma, I. and Dagnija, L. (2021). Soluble phosphate salts as setting aids for premixed calcium phosphate bone cement pastes. *Ceramics International.* ***47****,* 24012-24019.

Zornoza, E., Garce's, P., Paya, J. and Climent, M.A. (2009). Improvement of the chloride Ingress resistance of OPC mortars by using spent cracking catalyst. *Cement & Concrete Research.* ***39****,* 126-139.

Zuo, X.B. and Wei, S. (2011). Simulations on sulfate ion diffusivity in concrete column under random excitations. *Advanced Materials Research.* ***261-263,*** 275-279.

APPENDICES

Appendix 1: Publications and Conferences Attended

Publications

1. **Onesmus Mulwa Munyao,** Joseph Karanja Thiong'o, Jackson Muthengia Wachira, Daniel Karanja Mutitu, Genson Murithi and Romano Mwirichia. Chloride ingress in Cement Mortars Exposed to *Acidithiobacillus thiooxidans* Bacteria. Hindawi, Advances in Materials Science and Engineering. Volume 2020, Article ID 4191806, 10 Pages. https://doi.org/10.1155/2020/4191806
2. **Onesmus Mulwa Munyao,** Joseph Karanja Thiong'o, Jackson Muthengia Wachira, Daniel Karanja Mutitu and Romano Mwirichia. Influence of *Starkeya novella* on Mechanical and Microstructural Properties of Cement Mortars. Hindawi, Journal of Chemistry, Volume 2020, Article ID 8212396, 9 pages. https://doi.1155/2020/8212396
3. **Onesmus Mulwa Munyao,** Joseph Karanja Thiong'o, Jackson Muthengia Wachira, Daniel Karanja Mutitu, Romano Mwirichia, Genson Muriithi and Joseph Mwiti Marangu. Study on the effect of *Thiobacillus intermedius* on the physico-mechanical properties of mortars of Ordinary Portland Cement. Elsevier, Heliyon 6 (2020) e03232.
4. **Onesmus Mulwa Munyao,** Joseph Karanja Thiong'o, Jackson Muthengia Wachira, Daniel Karanja Mutitu, Romano Mwirichia and Genson Murithi. Use of *Bacillus Species* Bacteria in Protecting the Concrete Structures from Sulphate Attack- A Review. Journal of Chemical Reviews, 2019, Volume 1, Issue 4, Pages 287-299.
5. Mutitu Daniel Karanja, **Mulwa Onesmus Munyao,** Muthengia Jackson Wachira, Thiong'o Joseph Karanja and Genson Murithi. Microbial effect on water sorptivity and

sulphate ingress by *Bacillus megaterium* on mortars prepared using Portland Pozzolana Cement. Journal of Applied Microbiology ISNN 1364-5072, doi.10.1111/jam.14976

6. Daniel Karanja Mutitu, **Onesmus Mulwa Munyao**, Jackson Muthengia Wachira, Joseph Karanja Thiong'o, Romano Mwirichia and Muriithi Genson. Biocementation Influence on Flexural Strength and Chloride Ingress by *Lysinibacillus sphaericus* and *Bacillus megaterium* in Mortar Structures. Hindawi, Journal of Chemistry. Volume 2020, Article ID 1472923, 13 pages. https://doi.org/10.1155/2020/1472923.
7. Daniel Karanja Mutitu, **Onesmus Mulwa Munyao**, Jackson Muthengia Wachira, Joseph Karanja Thiong'o, Romano Mwirichia and Muriithi Genson. Influence of *Lysinibacillus sphaericus* on Compressive Strength and Water Sorptivity in Microbial Cement Mortar. Elsevier, Heliyon 5(2019) e02881.
8. Karanja Daniel Mutitu, **Mulwa Onesmus Munyao**, Muthengia Jackson Wachira, Romano Mwirichia, Karanja Joseph Thiong'o and Mwiti Joseph Marangu. Effects of Biocementation on Some Properties of Cement Based Material Incorporating *Bacillus Species* Bacteria- A Review. Taylor & Francis. Journal of Sustainable Cement-Based Materials. https://doi.org/10.1080/21650373.2019.1640141.
9. David Munyao Musyoki, **Munyao Onesmus Mulwa,** Joseph Karanja Thiong'o', Jackson Wachira Muthengia, Joanne Ogunah, Daniel Karanja Mutitu, John Kinuthia, Romano Mwirichia and Murithi Genson. Effect of Immobilizing *Bacillus megaterium* on the Compressive Strength and Water Absorption of Mortar. Hindawi, Journal of Chemistry. Volume 2022, Article ID 7752812, 12 pages. https://doi.org/10.1155/2022/7752812.
10. Kelvin Mwangi Wanjiku, **Munyao Onesmus Mulwa,** Joseph Karanja Thiong'o', Jackson Wachira Muthengia, Joanne Ogunah, Daniel Karanja Mutitu, John Kinuthia, Romano

Mwirichia, Murithi Genson, Peter Waithaka and David Munyao Musyoki. Effect of *Lysinibacillus sphaericus* on Physico Mechanical and Chemical Performance of OPC Blended with Natural Tuff and Pulverized Fly Ash. Hindawi, Advances in Materials Science and Engineering. Volume 2022, Article ID 3387928, 15 pages. https://doi.org/10.1155/2022/3387928.

Conference Papers

1. **Onesmus Mulwa Munyao,** Joseph Karanja Thiong'o and Jackson Wachira Muthengia. Microbial Influence on Physico-Mechanical and Microstructural Properties of Cement Mortar. *74th Rilem Annual Week & 40th Cement and Concrete Science Conference.* 31 August - 4 September 2020 at University of Sheffield, Sheffield, United Kingdom.
2. **Onesmus Mulwa Munyao,** Joseph Karanja Thiong'o and Jackson Wachira Muthengia. Effects of Sulphate ions in Mixing water on Cement Mortar Performance. *First Kenya National Dam Conference.* 8th – 9th March 2018 at Flamingo Beach Resort & Spa, Mombasa-Kenya.

Conferences Attended

1. First Kenya National Dam Conference. 8th – 9th March 2018 at Flamingo Beach Resort & Spa, Mombasa-Kenya.
2. Mapei Cement Academy. 6th -8th June 2018 at Mapei Spa-Auditorium, Milan, Italy.
3. LC^3 Doctoral School: "Characterization Methods of Blended Cements". 23rd April – 26th April 2019 at EPFL, Lausanne- Switzerland.
4. 74th Rilem Annual Week & 40th Cement and Concrete Science Conference. 31st August – 4th September 2020 at University of Sheffield, Sheffield, United Kingdom.

Appendix 2: Raw Data for Compressive Strength of OPC Mortars

Curing Period	OPC H- H	OPC AT-H	OPC AT-AT	OPC TI-H	OPC TI-TI	OPC SK-H	OPC SK- SK
	27.40	27.40	26.80	27.20	27.20	27.10	28.00
2 Days	26.00	27.00	27.60	27.20	27.20	27.10	26.00
	28.20	27.20	27.20	27.20	27.20	27.40	27.00
Average	27.20	27.20	27.20	27.20	27.20	27.20	27.00
	40.63	40.64	40.62	40.62	40.58	40.61	40.60
7 Days	40.62	40.63	40.64	40.62	40.65	40.63	40.63
	40.63	40.62	40.62	40.62	40.64	40.64	40.63
Average	40.63	40.63	40.63	40.62	40.62	40.63	40.62
	48.90	39.50	38.90	39.90	39.60	38.60	38.40
28 days	48.70	39.50	38.90	39.90	39.60	38.90	38.70
	49.00	39.50	38.90	39.90	39.60	39.00	38.30
Average	48.87	39.50	38.90	39.90	39.60	38.83	38.47
	49.10	36.70	35.70	39.20	38.70	35.77	34.76
56 days	48.90	36.70	35.90	38.60	38.60	35.77	34.76
	48.60	36.70	35.50	38.70	38.20	35.77	34.76
Average	48.87	36.70	35.70	38.83	38.50	35.77	34.76
	48.90	33.80	32.80	36.20	35.00	33.40	32.50
90 days	48.84	33.80	32.60	35.80	35.20	33.40	32.70
	48.87	33.80	33.00	36.00	35.40	33.40	32.30
Average	48.87	33.80	32.80	36.00	35.20	33.40	32.50

Appendix 3: Statistical Analysis for compressive strength of OPC at varied curing durations

T-Test analysis for OPC H-H and OPC AT-H at 2 days of curing.

	OPC H-H	OPC AT-H
Mean	27.2	27.2
Variance	1.24	0.04
Sample size	3	3
Degree of freedom	4	
t_{cal}	0	
P_{val}	1	
t_{crit}	2.78	

T-Test results for OPC H-H and OPC AT-H at 7 days of curing.

	OPC H-H	OPC AT-H
Mean	40.63	40.63
Variance	0.00	0.00
Sample size	3	3
Degree of freedom	4	
T_{cal}	0.50	
P_{val}	0.64	
T_{crit}	2.78	

T-Test analysis for OPC H-H and OPC AT-H at 28 days of curing.

	OPC H-H	OPC AT-H
Mean	48.87	39.5
Variance	0.02	0
Sample size	3	3
Degree of freedom	4	
T_{cal}	6.21	
P_{val}	0.00	
T_{crit}	2.78	

T-Test analysis for OPC H-H and OPC AT-H at 56 days of curing.

	OPC H-H	OPC AT-H
Mean	48.87	36.7
Variance	0.06	0
Sample size	3	3
Degree of freedom	4	
T_{cal}	13.74	
P_{val}	0.00	
T_{crit}	2.78	

T-Test analysis for OPC H-H and OPC AT-H at 90 days of curing.

	OPC H-H	OPC AT-H
Mean	48.87	33.8
Variance	0.00	0
Sample size	3	3
Degree of freedom	4	
T_{cal}	17.07	
P_{val}	0.00	
T_{crit}	2.78	

T-Test analysis for OPC H-H and OPC AT-AT at 2 days of curing.

	OPC H-H	OPC AT-AT
Mean	27.2	27.2
Variance	1.24	0.16
Sample size	3	3
Degree of freedom	4	
T_{cal}	0.00	
P_{val}	1	
T_{crit}	2.78	

T-Test analysis for OPC H-H and OPC AT-AT at 7 days of curing.

	OPC H-H	OPC AT -AT
Mean	40.63	40.63
Variance	0.00	0.00
Sample size	3	3
Degree of freedom	4	
T_{cal}	0.00	
P_{val}	1	
T_{crit}	2.78	

T-Test analysis for OPC H-H and OPC AT-AT at 28 days of curing

	OPC H-H	OPC AT-AT
Mean	48.87	38.9
Variance	0.02	0
Sample size	3	3
Degree of freedom	4	
T_{cal}	13.01	
P_{val}	0.00	
T_{crit}	2.78	

T-Test analysis for OPC H-H and OPC AT-AT at 56 days of curing

	OPC H-H	OPC AT- AT
Mean	48.87	35.7
Variance	0.06	0.04
Sample size	3	3
Degree of freedom	4	
T_{cal}	12.94	
P_{val}	0.00	
T_{crit}	2.78	

T-Test analysis for OPC H-H and OPC AT-AT at 90 days of curing

	OPC Control	OPC AT (AT)
Mean	48.87	32.80
Variance	0.00	0.04
Sample size	3	3
Degree of freedom	4	
T_{cal}	17.63	
P_{val}	0.00	
T_{crit}	2.78	

T-Test analysis for OPC H-H and OPC TI-H at 2 days of curing

	OPC H-H	OPC TI-H
Mean	27.2	27.2
Variance	1.24	0
Sample size	3	3
Degree of freedom	4	
T_{cal}	0	
P_{val}	1	
T_{crit}	2.78	

T-Test analysis for OPC H-H and OPC TI-H at 7 days of curing

	OPC H-H	OPC TI-H
Mean	40.63	40.62
Variance	0.00	0
Sample size	3	3
Degree of freedom	4	
T_{cal}	2.00	
P_{val}	0.12	
t Critical two-tail	2.78	

T-Test analysis for OPC H-H and OPC TI-H at 28 days of curing

	OPC H-H	OPC TI-H
Mean	48.87	39.9
Variance	0.02	0
Sample size	3	3
Degree of freedom	4	
t_{cal}	11.67	
P_{val}	0.00	
t_{crit}	2.78	

T-Test analysis for OPC H-H and OPC TI-H at 56 days of curing

	OPC H-H	OPC TI-H
Mean	48.87	38.83
Variance	0.06	0.10
Sample size	3	3
Degree of freedom	4	
t_{cal}	12.57	
P_{crit}	0.00	
t_{crit}	2.78	

T-Test analysis for OPC H-H and OPC TI-H at 90 days of curing

	OPC H-H	OPC TI-H
Mean	48.87	36
Variance	0.00	0.04
Sample size	3	3
Degree of freedom	4	
t_{cal}	18.22	
P_{val}	0.00	
t_{crit}	2.78	

T-Test analysis for OPC H-H and OPC TI-TI at 2 days of curing

	OPC H-H	OPC TI-TI
Mean	27.2	27.2
Variance	1.24	0
Sample size	3	3
Degree of freedom	4	
t_{cal}	0.00	
P_{val}	1	
t_{crit}	2.78	

T-Test analysis for OPC H-H and OPC TI-TI at 7 days of curing

	OPC H-H	OPC TI-TI
Mean	40.63	40.62
Variance	0.00	0.00
Sample size	3	3
Degree of freedom	4	
t_{cal}	0.15	
P_{val}	0.89	
t_{crit}	2.78	

T-Test analysis for OPC H-H and OPC TI-TI at 28 days of curing

	OPC H-H	OPC TI-TI
Mean	48.87	39.6
Variance	0.02	0
Sample size	3	3
Degree of freedom	4	
t_{cal}	15.07	
P_{val}	0.00	
t_{crit}	2.78	

T-Test analysis for OPC H-H and OPC TI-TI at 56 days of curing

	OPC H-H	OPC TI-TI
Mean	48.87	38.5
Variance	0.06	0.07
Sample size	3	3
Degree of freedom	4	
t_{cal}	19.17	
P_{val}	0.00	
t_{crit}	2.78	

T-Test analysis for OPC H-H and OPC TI-TI at 90 days of curing

	OPC H-H	OPC TI-TI
Mean	48.87	35.2
Variance	0.00	0.04
Sample size	3	3
Degree of freedom	4	
t_{cal}	17.08	
P_{val}	0.00	
t_{crit}	2.78	

T-Test analysis for OPC H-H and OPC SK-H at 2 days of curing

	OPC H-H	OPC SK-H
Mean	27.2	27.2
Variance	1.24	0.03
Sample size	3	3
Degree of freedom	4	
t_{cal}	0	
P_{val}	1	
t_{crit}	2.78	

T-Test analysis for OPC H-H and OPC SK-H at 7 days of curing

	OPC H-H	OPC SK-H
Mean	40.63	40.63
Variance	0.00	0.00
Sample size	3	3
Degree of freedom	4	
t_{cal}	0.00	
P_{val}	1	
t_{crit}	2.78	

T-Test analysis for OPC H-H and OPC SK-H at 28 days of curing

	OPC H-H	OPC SK-H
Mean	48.87	38.83
Variance	0.02	0.04
Sample size	3	3
Degree of freedom	4	
t_{cal}	17.31	
P_{val}	0.00	
t_{crit}	2.78	

T-Test analysis for OPC H-H and OPC SK-H at 56 days of curing

	OPC H-H	OPC SK-H
Mean	48.87	35.77
Variance	0.06	0
Sample size	3	3
Degree of freedom	4	
t_{cal}	9.14	
P_{val}	0.00	
t_{crit}	2.78	

T-Test analysis for OPC H-H and OPC SK-H at 90 days of curing

	OPC H-H	OPC SK-H
Mean	48.87	33.4
Variance	0.00	0
Sample size	3	3
Degree of freedom	4	
t_{cal}	9.16	
P_{val}	0.00	
t_{crit}	2.78	

T-Test analysis for OPC H-H and OPC SK-SK at 2 days of curing

	OPC H-H	OPC SK - SK
Mean	27.2	27
Variance	1.24	1
Sample size	3	3
Degree of freedom	4	
t_{cal}	0.23	
P_{val}	0.83	
t_{crit}	2.78	

T-Test analysis for OPC H-H and OPC SK-SK at 7 days of curing

	OPC H-H	OPC SK- SK
Mean	40.63	40.62
Variance	0.00	0.00
Sample size	3	3
Degree of freedom	4	
t_{cal}	0.63	
P_{val}	0.56	
t_{crit}	2.78	

T-Test analysis for OPC H-H and OPC SK-SK at 28 days of curing

	OPC H-H	OPC SK - SK
Mean	48.87	38.47
Variance	0.02	0.04
Sample size	3	3
df	4	
t_{cal}	9.77	
P_{val}	0.00	
t_{crit}	2.78	

T-Test analysis for OPC H-H and OPC SK-SK at 56 days of curing

	OPC H-H	OPC SK -SK
Mean	48.87	34.76
Variance	0.06	0.00
Sample size	3	3
Degree of freedom	4	
t_{cal}	9.09	
P_{val}	0.00	
t_{crit}	2.78	

T-Test analysis for OPC H-H and OPC SK-SK at 90 days of curing

	OPC H-H	OPC SK- SK
Mean	48.87	32.50
Variance	0.00	0.04
Sample size	3	3
Degree of freedom	4	
t_{cal}	14.20	
P_{val}	0.00	
t_{crit}	2.78	

Appendix 4: Raw Data for compressive strength of PPC

Curing Period	PPC H-H	PPC AT-H	PPC AT- AT	PPC TI-H	PPC TI -TI	PPC SK-H	PPC SK -SK
2 Days	16.20	16.00	15.80	16.00	16.40	16.00	16.20
	15.80	16.00	16.20	16.00	15.60	16.00	16.40
	16.00	16.00	16.00	16.00	16.00	16.00	15.40
Average	16.00	16.00	16.00	16.00	16.00	16.00	16.00
7 Days	26.10	26.20	26.00	26.20	26.40	26.10	26.10
	26.20	26.20	26.40	26.20	26.10	26.10	26.10
	26.30	26.20	26.20	26.20	26.10	26.10	26.10
Average	26.20	26.20	26.20	26.20	26.20	26.10	26.10
28 days	36.30	33.80	33.40	34.90	34.70	33.20	32.80
	36.60	33.80	33.80	34.90	34.70	33.00	33.00
	36.00	33.80	33.20	34.90	34.70	32.80	32.90
Average	36.30	33.80	33.47	34.90	34.70	33.00	32.90
56 days	39.62	33.00	33.00	33.20	32.90	32.62	32.60
	39.92	32.40	32.80	34.60	34.00	32.62	32.40
	39.89	33.00	32.82	34.60	34.20	32.62	32.20
Average	39.81	32.80	32.87	34.60	33.80	32.62	32.40
90 days	42.50	32.00	31.37	34.00	33.80	31.88	30.70
	42.30	31.80	31.37	33.80	33.80	31.88	30.70
	42.80	32.20	31.37	34.20	33.80	31.88	30.70
Average	42.53	32.00	31.37	34.00	33.80	31.88	30.70

Appendix 5: Raw Data for Setting Times of PPC Pastes

	PPC H-H	PPC AT	PPC TI	PPC SK
Initial Setting Time (Mins)	180	190	190	195
	175	195	180	200
	185	185	170	190
Average	180	190	180	195
Final Setting Time (Mins)	250	250	250	255
	250	255	250	255
	250	245	250	255
Average	250	250	250	255

Appendix 6: Raw Data for Chloride analysis of OPC H-H

Depth (mm)	Chloride concentration in %			Average	Standard
	Sample 1	Sample 2	Sample 3	Calculated	Deviation
10	0.1678	0.1683	0.1673	0.1678	± 0.0004
20	0.1504	0.1507	0.1501	0.1504	± 0.0002
30	0.1134	0.1142	0.1138	0.1138	± 0.0003
40	0.078	0.079	0.0785	0.0785	± 0.0004
50	0.051	0.0518	0.0514	0.0514	± 0.0003
60	0.0434	0.0438	0.043	0.0434	± 0.0003
70	0.0375	0.0377	0.0373	0.0375	± 0.0001
80	0.0326	0.0328	0.033	0.0328	± 0.0001

Appendix 7: Raw Data for Chloride analysis of OPC TI-H

Depth (mm)	Chloride concentration in %			Average	Standard Deviation
	Sample 1	Sample 2	Sample 3	Calculated	
10	0.1846	0.1853	0.1839	0.1846	± 0.0006
20	0.1689	0.17	0.1678	0.1689	± 0.0009
30	0.1282	0.1324	0.1303	0.1303	± 0.0017
40	0.0951	0.0954	0.0948	0.0951	± 0.0002
50	0.0768	0.075	0.0759	0.0759	± 0.0007
60	0.0611	0.0627	0.0619	0.0619	± 0.0007
70	0.0604	0.0609	0.0599	0.0604	± 0.0004
80	0.0569	0.0543	0.0556	0.0556	± 0.0011

Appendix 8: Raw Data for Chloride concentration of OPC TI-TI

Depth (mm)	Chloride concentration in %			Average	Standard
	Sample 1	Sample 2	Sample 3	Calculated	Deviation
10	0.1862	0.1866	0.1864	0.1864	± 0.0002
20	0.1704	0.1707	0.1701	0.1704	± 0.0002
30	0.1313	0.1318	0.1323	0.1318	± 0.0004
40	0.0963	0.0969	0.0957	0.0963	± 0.0005
50	0.0768	0.0774	0.0771	0.0771	± 0.0002
60	0.0631	0.0639	0.0623	0.0631	± 0.0007
70	0.0611	0.0622	0.06	0.0611	± 0.0009
80	0.0571	0.058	0.0562	0.0571	± 0.0007

Appendix 9: Raw Data for Chloride analysis of OPC AT-H

Depth (mm)	Chloride concentration in %			Average	Standard
	Sample 1	Sample 2	Sample 3	Calculated	Deviation
10	0.1889	0.1892	0.1886	0.1889	±0.0002
20	0.1681	0.1685	0.1677	0.1681	±0.0003
30	0.1323	0.1329	0.1317	0.1323	±0.0005
40	0.0969	0.0971	0.0967	0.0969	±0.0002
50	0.0785	0.079	0.078	0.0785	±0.0004
60	0.0634	0.0631	0.0637	0.0634	±0.0002
70	0.0615	0.0618	0.0612	0.0615	±0.0002
80	0.0561	0.0568	0.0554	0.0561	±0.0006

Appendix 10: Raw Data for Chloride analysis of OPC AT-AT

Depth (mm)	Chloride concentration in %			Average Calculated	Standard Deviation
	Sample 1	Sample 2	Sample 3		
10	0.1921	0.1928	0.1914	0.1921	± 0.0005
20	0.1756	0.175	0.1762	0.1756	± 0.0004
30	0.1368	0.136	0.1376	0.1368	± 0.0006
40	0.0994	0.1	0.0997	0.0997	± 0.0002
50	0.0805	0.0797	0.0801	0.0801	± 0.0003
60	0.067	0.0676	0.0673	0.0673	± 0.0002
70	0.064	0.0636	0.0638	0.0638	± 0.0001
80	0.059	0.0595	0.06	0.0595	± 0.0004

Appendix 11: Raw Data for Chloride analysis of OPC SK-H

Depth (mm)	Chloride concentration in %			Average Calculated	Standard Deviation
	Sample 1	Sample 2	Sample 3		
10	0.19	0.1904	0.1902	0.1902	± 0.0001
20	0.1714	0.1708	0.1711	0.1711	± 0.0002
30	0.134	0.1354	0.1347	0.1347	± 0.0005
40	0.098	0.099	0.0985	0.0985	± 0.0004
50	0.0799	0.0801	0.0797	0.0799	± 0.0001
60	0.0648	0.0656	0.0652	0.0652	± 0.0003
70	0.0622	0.0636	0.0629	0.0629	± 0.0005
80	0.0572	0.0582	0.0577	0.0577	± 0.0004

Appendix 12: Raw Data for Chloride analysis of OPC SK-SK

Depth (mm)	Chloride concentration in %			Average Calculated	Standard Deviation
	Sample 1	Sample 2	Sample 3		
10	0.1953	0.1955	0.1957	0.1955	± 0.0001
20	0.1779	0.1783	0.1781	0.1781	± 0.0001
30	0.1393	0.1385	0.1389	0.1389	± 0.0003
40	0.1019	0.1022	0.1025	0.1022	± 0.0002
50	0.082	0.0832	0.0826	0.0826	± 0.0004
60	0.0691	0.0705	0.0698	0.0698	± 0.0005
70	0.0663	0.066	0.0666	0.0663	± 0.0002
80	0.061	0.0628	0.0619	0.0619	± 0.0007

Appendix 13: Raw Data for Chloride analysis of PPC H-H

Depth (mm)	Chloride concentration in %			Average calculated	Standard Deviation
	Sample1	Sample 2	Sample 3		
10	0.1561	0.1572	0.155	0.1561	± 0.0008
20	0.1303	0.1308	0.1298	0.1303	± 0.0004
30	0.0913	0.0915	0.0911	0.0913	± 0.0001
40	0.0587	0.0582	0.0592	0.0587	± 0.0004
50	0.031	0.037	0.025	0.031	± 0.0048
60	0.0228	0.0231	0.0234	0.0231	± 0.0002
70	0.0224	0.022	0.0222	0.0222	± 0.0001
80	0.0178	0.0176	0.018	0.0178	± 0.0001

Appendix 14: Raw Data for Chloride analysis of PPC AT-H

Depth (mm)	Chloride concentration in %			Average calculated	Standard Deviation
	Sample1	Sample 2	Sample 3		
10	0.1839	0.1851	0.1827	0.1839	± 0.0009
20	0.1526	0.1529	0.1523	0.1526	± 0.0002
30	0.0943	0.0953	0.0933	0.0943	± 0.0008
40	0.0726	0.0724	0.0722	0.0724	± 0.0001
50	0.0546	0.054	0.0552	0.0546	± 0.0004
60	0.0423	0.042	0.0426	0.0423	± 0.0002
70	0.0454	0.0461	0.0447	0.0454	± 0.0005
80	0.0396	0.0406	0.0401	0.0401	± 0.0004

Appendix 15: Raw Data for Chloride analysis of PPC AT-AT

Depth (mm)	Chloride concentration in %			Average Calculated	Standard Deviation
	Sample 1	Sample 2	Sample 3		
10	0.1862	0.187	0.1866	0.1866	± 0.0933
20	0.1542	0.1546	0.1538	0.1542	± 0.0162
30	0.0975	0.0972	0.0978	0.0975	± 0.0283
40	0.0771	0.0777	0.0774	0.0774	± 0.0100
50	0.0581	0.0579	0.0577	0.0579	± 0.0097
60	0.0477	0.047	0.0484	0.0477	± 0.0051
70	0.0484	0.0485	0.0486	0.0485	± 0.0005
80	0.0432	0.0433	0.0431	0.0432	± 0.0026

Appendix 16: Raw Data for Chloride analysis of PPC TI-H

Depth (mm)	Chloride concentration in %			Average calculated	Standard Deviation
	Sample1	Sample 2	Sample 3		
10	0.1757	0.1765	0.1761	0.1761	± 0.0003
20	0.1506	0.15	0.1512	0.1506	± 0.0004
30	0.0894	0.0901	0.0908	0.0901	± 0.0005
40	0.069	0.06	0.078	0.069	± 0.0073
50	0.0511	0.0519	0.0503	0.0511	± 0.0006
60	0.0399	0.0397	0.0401	0.0399	± 0.0001
70	0.036	0.048	0.042	0.042	± 0.0048
80	0.0374	0.0371	0.0377	0.0374	± 0.0002

Appendix 17: Raw Data for Chloride analysis of PPC TI-TI

Depth (mm)	Chloride ion concentration g/ g cement			Average calculated	Standard Deviation
	Sample1	Sample 2	Sample 3		
10	0.181	0.1792	0.1801	0.1801	± 0.0007
20	0.1552	0.1538	0.1524	0.1538	± 0.0011
30	0.0975	0.0963	0.0969	0.0969	± 0.0004
40	0.0743	0.0748	0.0738	0.0743	± 0.0004
50	0.0564	0.057	0.0567	0.0567	± 0.0002
60	0.0446	0.0462	0.043	0.0446	± 0.0013
70	0.0468	0.0476	0.0484	0.0476	± 0.0006
80	0.0423	0.0421	0.0425	0.0423	± 0.0001

Appendix 18: Raw Data for Chloride analysis of PPC SK-H

Depth (mm)	Chloride ion concentration in %			Average calculated	Standard Deviation
	Sample1	Sample 2	Sample 3		
10	0.1861	0.1867	0.1864	0.1864	± 0.0002
20	0.1538	0.153	0.1546	0.1538	± 0.0006
30	0.0966	0.0959	0.0952	0.0959	± 0.0005
40	0.0736	0.0731	0.0741	0.0736	± 0.0004
50	0.0555	0.0569	0.0541	0.0555	± 0.0011
60	0.0446	0.045	0.0442	0.0446	± 0.0003
70	0.0452	0.0463	0.0474	0.0463	± 0.0008
80	0.0419	0.0424	0.0414	0.0419	± 0.0004

Appendix 19: Raw Data for Chloride analysis of PPC SK-SK

Depth (mm)	Chloride concentration in %			Average calculated	Standard Deviation
	Sample1	Sample 2	Sample 3		
10	0.185	0.1892	0.1871	0.1871	± 0.0017
20	0.1623	0.1641	0.1605	0.1623	± 0.0014
30	0.13	0.1315	0.133	0.1315	± 0.0012
40	0.0959	0.0972	0.0946	0.0959	± 0.0010
50	0.0757	0.0771	0.0764	0.0764	± 0.0005
60	0.0625	0.0636	0.0614	0.0625	± 0.0008
70	0.0587	0.0607	0.0567	0.0587	± 0.0016
80	0.0481	0.0486	0.0491	0.0486	± 0.0004

Appendix 20: Raw Data for Sulphate analysis of OPC H-H

Depth (mm)	Sulphate Concentration in %			Average Calculated	Standard Deviation
	Sample 1	Sample 2	Sample 3		
10	0.3097	0.3087	0.3077	0.3087	± 0.0008
20	0.2916	0.2886	0.2901	0.2901	± 0.0012
30	0.2578	0.2538	0.2558	0.2558	± 0.0016
40	0.239	0.238	0.2385	0.2385	± 0.0004
50	0.1888	0.187	0.1879	0.1879	± 0.0007
60	0.1673	0.1661	0.1667	0.1667	± 0.0004
70	0.1636	0.1576	0.1606	0.1606	± 0.0024
80	0.1614	0.1589	0.1564	0.1589	± 0.0020

Appendix 21: Raw Data for Sulphate analysis of OPC TI-H

Depth (mm)	Sulphate Concentration in %			Average calculated	Standard Deviation
	Sample1	Sample 2	Sample 3		
10	0.3267	0.3278	0.3256	0.3267	± 0.0008
20	0.3104	0.3086	0.3095	0.3095	± 0.0007
30	0.2758	0.275	0.2766	0.2758	± 0.0006
40	0.259	0.2576	0.2583	0.2583	± 0.0005
50	0.2088	0.2081	0.2095	0.2088	± 0.0005
60	0.1871	0.1861	0.1866	0.1866	± 0.0004
70	0.1802	0.181	0.1806	0.1806	± 0.0003
80	0.178	0.1774	0.1777	0.1777	± 0.0002

Appendix 22: Raw Data for Sulphate analysis of OPC TI-TI

Depth (mm)	Sulphate concentration in %			Average calculated	Standard Deviation
	Sample1	Sample 2	Sample 3		
10	0.3437	0.3426	0.3448	0.3437	± 0.0008
20	0.326	0.3272	0.3266	0.3266	± 0.0004
30	0.292	0.2923	0.2926	0.2923	± 0.0002
40	0.2755	0.2759	0.2757	0.2757	± 0.0001
50	0.225	0.2257	0.2264	0.2257	± 0.0005
60	0.2047	0.2043	0.2039	0.2043	± 0.0003
70	0.197	0.198	0.1975	0.1975	± 0.0004
80	0.1948	0.1936	0.1942	0.1942	± 0.0004

Appendix 23: Raw Data for Sulphate analysis of OPC AT-H

Depth (mm)	Sulphate concentration in %			Average calculated	Standard Deviation
	Sample1	Sample 2	Sample 3		
10	0.3353	0.3331	0.3342	0.3342	± 0.0008
20	0.3183	0.3171	0.3159	0.3171	± 0.0009
30	0.2838	0.2847	0.2829	0.2838	± 0.0007
40	0.267	0.2656	0.2663	0.2663	± 0.0005
50	0.2163	0.2169	0.2157	0.2163	± 0.0004
60	0.1956	0.1946	0.1951	0.1951	± 0.0004
70	0.1887	0.1879	0.1883	0.1883	± 0.0003
80	0.1857	0.1851	0.1854	0.1854	± 0.0002

Appendix 24: Raw Data for Sulphate analysis of OPC AT-AT

Depth (mm)	Sulphate concentration in %			Average calculated	Standard Deviation
	Sample1	Sample 2	Sample 3		
10	0.3524	0.351	0.3517	0.3517	± 0.0005
20	0.3343	0.3349	0.3346	0.3346	± 0.0002
30	0.3014	0.3003	0.2992	0.3003	± 0.0008
40	0.283	0.284	0.2835	0.2835	± 0.0004
50	0.2334	0.2332	0.233	0.2332	± 0.0001
60	0.2122	0.2116	0.211	0.2116	± 0.0004
70	0.206	0.2042	0.2051	0.2051	± 0.0007
80	0.2018	0.201	0.2014	0.2014	± 0.0003

Appendix 25: Raw Data for Sulphate analysis of OPC SK-H

Depth (mm)	Sulphate concentration in %			Average calculated	Standard Deviation
	Sample1	Sample 2	Sample 3		
10	0.3456	0.3453	0.345	0.3453	± 0.0002
20	0.3289	0.3282	0.3275	0.3282	± 0.0005
30	0.2941	0.2957	0.2949	0.2949	± 0.0006
40	0.277	0.2774	0.2778	0.2774	± 0.0003
50	0.2271	0.2274	0.2277	0.2274	± 0.0002
60	0.206	0.2062	0.2064	0.2062	± 0.0001
70	0.1999	0.1989	0.1994	0.1994	± 0.0004
80	0.197	0.196	0.1965	0.1965	± 0.0004

Appendix 26: Raw Data for Sulphate analysis of OPC SK-SK

Depth (mm)	Sulphate concentration in %			Average calculated	Standard Deviation
	Sample1	Sample 2	Sample 3		
10	0.3637	0.3628	0.3619	0.3628	± 0.0007
20	0.345	0.3464	0.3457	0.3457	± 0.0005
30	0.3108	0.312	0.3114	0.3114	± 0.0004
40	0.2941	0.2946	0.2951	0.2946	± 0.0004
50	0.2443	0.244	0.2446	0.2443	± 0.0002
60	0.222	0.2234	0.2227	0.2227	± 0.0005
70	0.216	0.2162	0.2164	0.2162	± 0.0001
80	0.212	0.2125	0.213	0.2125	± 0.0004

Appendix 27: Raw Data for Sulphate analysis of PPC H-H

Depth (mm)	Sulphate concentration in %			Average calculated	Standard Deviation
	Sample1	Sample 2	Sample 3		
10	0.2844	0.2824	0.2834	0.2834	± 0.0008
20	0.2531	0.2491	0.2511	0.2511	± 0.0016
30	0.2306	0.2342	0.2324	0.2324	± 0.0014
40	0.2041	0.1981	0.2011	0.2011	± 0.002
50	0.1634	0.1604	0.1619	0.1619	± 0.0012
60	0.1398	0.1378	0.1388	0.1388	± 0.0008
70	0.131	0.1321	0.1332	0.1321	± 0.0008
80	0.125	0.1264	0.1257	0.1257	± 0.0005

Appendix 28: Raw Data for Sulphate analysis of PPC TI-H

Depth (mm)	Sulphate concentration in %			Average calculated	Standard Deviation
	Sample1	Sample 2	Sample 3		
10	0.3054	0.3051	0.3048	0.3051	± 0.0002
20	0.2741	0.2751	0.2746	0.2746	± 0.0004
30	0.2561	0.2568	0.2554	0.2561	± 0.0005
40	0.224	0.2245	0.225	0.2245	± 0.0004
50	0.1871	0.1862	0.1853	0.1862	± 0.0007
60	0.1613	0.161	0.1616	0.1613	± 0.0002
70	0.1563	0.1571	0.1555	0.1563	± 0.0006
80	0.1487	0.1483	0.1479	0.1483	± 0.0003

Appendix 29: Raw Data for Sulphate analysis of PPC TI-TI

Depth (mm)	Sulphate concentration in %			Average calculated	Standard Deviation
	Sample1	Sample 2	Sample 3		
10	0.3181	0.3195	0.3167	0.3181	± 0.0011
20	0.2883	0.2869	0.2876	0.2876	± 0.0005
30	0.2696	0.269	0.2693	0.2693	± 0.0002
40	0.2376	0.237	0.2382	0.2376	± 0.0004
50	0.1977	0.1972	0.1982	0.1977	± 0.0004
60	0.173	0.1746	0.1738	0.1738	± 0.0006
70	0.1663	0.1689	0.1676	0.1676	± 0.0010
80	0.1613	0.1624	0.1602	0.1613	± 0.0008

Appendix 30: Raw Data for Sulphate analysis of PPC AT-H

Depth (mm)	Sulphate concentration in %			Average calculated	Standard Deviation
	Sample1	Sample 2	Sample 3		
10	0.3126	0.3147	0.3105	0.3126	± 0.0017
20	0.284	0.2821	0.2802	0.2821	± 0.0015
30	0.2654	0.262	0.2637	0.2637	±0.0013
40	0.2321	0.2325	0.2317	0.2321	± 0.0003
50	0.1937	0.193	0.1944	0.1937	± 0.0005
60	0.1688	0.1686	0.1684	0.1686	± 0.0001
70	0.1643	0.169	0.1641	0.1658	± 0.0022
80	0.1559	0.1556	0.1562	0.1559	± 0.0002

Appendix 31: Raw Data for Sulphate analysis of PPC AT-AT

Depth (mm)	Sulphate concentration in %			Average calculated	Standard Deviation
	Sample1	Sample 2	Sample 3		
10	0.3256	0.3286	0.3226	0.3256	± 0.0024
20	0.2952	0.2983	0.2921	0.2952	± 0.0025
30	0.2743	0.2799	0.2771	0.2771	± 0.0022
40	0.2474	0.2451	0.2428	0.2451	± 0.0018
50	0.2053	0.2036	0.207	0.2053	± 0.0013
60	0.1825	0.1803	0.1814	0.1814	± 0.0008
70	0.1749	0.1758	0.174	0.1749	± 0.0007
80	0.1683	0.1693	0.1688	0.1688	± 0.0004

Appendix 32: Raw Data for Sulphate analysis of PPC SK-H

Depth (mm)	Sulphate concentration in %			Average calculated	Standard Deviation
	Sample1	Sample 2	Sample 3		
10	0.3227	0.3239	0.3215	0.3227	± 0.0009
20	0.2932	0.2912	0.2922	0.2922	± 0.0008
30	0.2738	0.2747	0.2729	0.2738	± 0.0007
40	0.2416	0.2428	0.2422	0.2422	± 0.0004
50	0.2033	0.2041	0.2038	0.2037	± 0.0003
60	0.1783	0.1791	0.1787	0.1787	± 0.0003
70	0.1742	0.1745	0.1739	0.1742	± 0.0002
80	0.1658	0.1662	0.1660	0.166	± 0.0001

Appendix 33: Raw Data for Sulphate analysis of PPC SK-SK

Depth (mm)	Sulphate concentration in %			Average calculated	Standard Deviation
	Sample1	Sample 2	Sample 3		
10	0.3394	0.3328	0.3361	0.3361	± 0.0026
20	0.3057	0.3025	0.3089	0.3057	± 0.0026
30	0.2907	0.2845	0.2876	0.2876	± 0.0025
40	0.2585	0.2527	0.2556	0.2556	± 0.0023
50	0.2131	0.2185	0.2158	0.2158	± 0.0022
60	0.1919	0.1942	0.1896	0.1919	± 0.0018
70	0.1836	0.1872	0.1854	0.1854	± 0.0014
80	0.178	0.178	0.1793	0.1784	± 0.0006